Robotically Controlled Jellyfish Swimming Dynamics and Energetics for Ocean Exploration

Thesis by
Simon R. Anuszczyk

In Partial Fulfillment of the Requirements for the
Degree of
Doctor of Philosophy

CALIFORNIA INSTITUTE OF TECHNOLOGY
Pasadena, California

2026
Defended March 31st, 2026

© 2026

Simon R. Anuszczyk
ORCID: 0009-0000-9840-9442

All rights reserved

ACKNOWLEDGEMENTS

I have greatly enjoyed my time at Caltech, largely due to the community of friends, mentors, and colleagues I have found here. Both personally and professionally, this community has pushed me to be the best scientist and member of society I can be.

I would like to thank my advisor, John Dabiri, for welcoming me to his lab group, introducing me to the study of jellies, and providing endless optimism and support. Through each scientific challenge, John has always been encouraging and ready to reframe setbacks positively. His curiosity, interest in experimental details, and constant stream of ideas have made my PhD experience a joy. His openness and mentorship in navigating academia and research have been particularly helpful.

I am deeply grateful to the members of my dissertation committee, Mory Gharib, Michael Dickinson, and Lea Goentoro, who have provided expertise, support, mentorship, and thoughtful feedback throughout this process. Their insight and perspective consistently strengthened this work and pushed me to think more critically about my research.

My friends in the Dabiri lab made the day-to-day experience of research fun and meaningful. Maggie Brown, Malaika Cordeiro, Matt Fu, Roni Goldshmid, Peter Gunnarson, Nina Mohebbi, Kelsi Rutledge, Nathan Wei, and Noa Yoder - thank you for your willingness to discuss ideas and techniques, proofread manuscripts, and lend an extra hand dumping 2000 lbs of salt into the vertical tank.

I have had the pleasure of working with several collaborators during my time at Caltech, including scuba trips with Jack Costello, Sean Colin, Brad Gemmell, Joost Daniels, and Kelly Sutherland. I am also thankful for the mentorship stemming from our work at Friday Harbor Labs of Emily Carrington and Mark Denny. Additionally, I have benefited from many insightful conversations with the founder of this research project, Nicole Xu, as well as Mitchell Ford and Claudia Mills. I had the opportunity to mentor Kyra Phaychanpheng and Giannka Picache.

Behind the scenes, both administrative and lab staff enabled all of this work. GALCIT staff Sarah Pontes, Christine Ramirez, and Jamie Meighen-Sei organized countless research and conference trips, set up department events, and managed purchasing and facilities. Staff in the Office of Laboratory Animal Resources fed and cared for the jellies throughout the last few years of my PhD, taking a massive burden of daily animal husbandry off of my shoulders. This includes Annabel Baltazar, Jeff

Cochrane, Jasmine Garcia, Ivonne Gonzalez, Alex Murillo, Donita Offord, Kelly Poplar, Pedro Zaragoza, as well as veterinarian Alan Avalos and jellyfish expert Olivia Cleek. In addition, Caltech undergrads who assisted with care include Kyra Phaychanpheng, Marissa Till, and Olivia Xu.

In particular, I would like to thank the GALCIT community—especially my first year class, Miya Coimbra, Emma Lenz, Ioannis Mandralis, Sean Mendoza, George Popov, and Divesh Soni. I have appreciated the camaraderie and friendship of too many of my fellow GALCIT students to list, but just to mention a few: Tanner Harms, Miles Chan, Brayden Aller, Michael Stramenga, and Scott Bollt. I would also like to thank everyone I served with on the Galcit Graduate Student Council, the EAS Graduate Student Advisory Board, the Caltech Y Student Activism Speaker Series, and everyone else working to build community on campus.

Outside of research, these past few years have been immeasurably improved by the opportunities to spend time with friends in and around LA. I am especially grateful for my adventure buddies Kristina Andreyeva, Julia Di, and Keenan Albee; climbing trips with Sean Mendoza, Miya Coimbra, Melissa Cronin, and Eugene Gao; and all the friends I've had the pleasure of spending time with during my time at Caltech.

I would especially like to thank my family for their support throughout my long and far-flung academic journey. Throughout many early morning drives to classes and cross-country moves for undergrad and internships, they have visited and supported me. I credit my parents' decision to homeschool me for inspiring my love of learning, books, and exploring and studying nature.

Most of all, thank you to my favorite person, Marni Rosenthal, who has encouraged me throughout this process and made my life so much brighter. Through many practice presentations, soliloquies on jellyfish science, and late nights calling from conferences around the world, I have always been lucky to have your love and support. Thank you and I'm so excited for our next stage in life together.

Lastly, I would like to thank the residents of the Caltech turtle pond for providing endless enjoyment and amusement throughout many walks and study breaks. I am also grateful to the many campus dogs, including but definitely not limited to: Louie, Anna Banana, the dachshund with the wheelchair, that cat walking on a leash, and the many other dogs whose names I was not fortunate enough to learn but whose presence I appreciated.

ABSTRACT

Robotic platforms inspired or enabled by aquatic organisms have the potential to augment conventional technologies for ocean exploration, enabling a more thorough understanding of the impacts of climate change. We present a biohybrid robotic jellyfish that leverages direct stimulation of live *Aurelia aurita* jellyfish muscle tissue via implanted microelectronics. We conduct swimming experiments using a 3D-printed passive mechanical attachment to streamline the jellyfish shape and enhance payload capacity. A six-meter-tall, 13,600-liter saltwater facility was constructed to enable testing of the vertical swimming capabilities of the biohybrid robotic jellyfish. We found that the combination of external swimming control and the addition of the mechanical forebody resulted in an increase in swimming speeds to 4.5 times natural jellyfish locomotion while carrying a payload volume of up to 105% of the jellyfish body volume. In order to measure the energy consumption of free-swimming jellyfish in this facility, we developed a physiological method based on laser-scanned, 3D morphological reconstructions of the animal. Computer vision-based feedback control was used to enable continuous swimming against a flow current for 50 hours without encountering the vertical limits of the tank. Changes in animal volume, measured with reconstructions, were converted to energy consumption using the body chemical composition. Free-swimming, electrically stimulated animals were found to consume 2.5 times more energy than similarly stimulated animals in a constrained environment. Simplified drag models could not fully account for the increased energy consumption. Swimmer biomechanics and energetics cannot be fully understood independently of the surrounding flow field. We experimentally investigated the increased energy consumption using three-dimensional, full velocity field Particle Image Velocimetry to simultaneously study wake energy, momentum, and animal biomechanics. We found electrical stimulation increased posterior wake energy loss by a factor of 2.9 compared to unstimulated jellyfish, primarily due to heightened pulse rates. Stimulation was also found to modify swimming biomechanics by reducing total bell margin movement and relaxation duration. Together, these results demonstrate that biohybrid robotic jellyfish can achieve substantial performance enhancements while revealing the hydrodynamic and energetic tradeoffs associated with electrically controlled swimming. This platform offers a scalable and efficient tool for ocean exploration and provides new insight into the fluid dynamics and energetics of jellyfish locomotion.

PUBLISHED CONTENT AND CONTRIBUTIONS

Anuszczyk, Simon R. and John O. Dabiri (Feb. 2024). "Electromechanical Enhancement of Live Jellyfish for Ocean Exploration". In: *Bioinspiration & Biomimetics* 19.2, p. 026018. ISSN: 1748-3190. DOI: 10.1088/1748-3190/ad277f. URL: https://dx.doi.org/10.1088/1748-3190/ad277f. S.R.A made the primary contributions towards the experiment design, data acquisition, analysis, and writing. J.O.D. contributed to the conceptualization of the study, funding acquisition, analysis and interpretation of the results, and feedback on the manuscript.

Anuszczyk, Simon R., Noa Yoder, et al. (Dec. 2, 2025). "Increasing the Reliability and Versatility of Jellyfish Biohybrid Vehicles via Species Selection and Rhopalia Removal". In: *Biomimetics* 10.12. ISSN: 2313-7673. DOI: 10.3390/biomimetics10120810. Conceptualization, S.R.A., N.Y., J.H.C., J.O.D., B.J.G., K.M.R. and S.P.C.; methodology, S.R.A., N.Y., J.H.C., J.O.D., B.J.G., K.M.R. and S.P.C.; software, S.R.A. and J.O.D.; formal analysis, S.P.C.; investigation, S.R.A., N.Y., J.H.C., J.O.D., B.J.G., K.M.R. and S.P.C.; data curation, S.P.C.; writing—original draft preparation, S.P.C.; writing—review and editing, S.R.A., N.Y., J.H.C., J.O.D., B.J.G., K.M.R. and S.P.C.; visualization, S.P.C.; project administration, J.O.D.; funding acquisition, J.O.D., J.H.C., S.P.C. and B.J.G. All authors have read and agreed to the published version of the manuscript.

TABLE OF CONTENTS

Acknowledgements . . . iii
Abstract . . . v
Published Content and Contributions . . . vi
Table of Contents . . . vii
List of Illustrations . . . x
List of Tables . . . xxi
Chapter I: Introduction . . . 1
1.1 Ocean exploration . . . 1
1.2 Biohybrid robotics . . . 2
1.3 Jellyfish for ocean exploration . . . 3
1.4 Ethics of electrical muscle stimulation . . . 3
1.5 Aims and objectives of this dissertation . . . 4
Chapter II: Electromechanical enhancement of live jellyfish for ocean exploration . . . 6
2.1 Introduction . . . 8
2.2 Methods and Materials . . . 8
Animal husbandry . . . 8
System architecture . . . 8
Components and fabrication . . . 9
Flow visualization experiments . . . 10
Long-distance swimming experiments . . . 11
Kinematics Model . . . 13
2.3 Results . . . 15
Flow visualization experiments . . . 15
Long-distance swimming experiments . . . 16
2.4 Discussion . . . 21
Chapter III: Non-invasive measurement of metabolic rates of free-swimming jellyfish using volumetric laser scanning . . . 26
3.1 Introduction . . . 28
3.2 Materials and Methods . . . 30
Animal husbandry . . . 30
Laser scanning for volumetric reconstruction . . . 30
Validation of volumetric reconstruction . . . 32
Energetic consumption from volumetric changes . . . 32
Carbon content . . . 33
Electrical stimulation for continuous swimming . . . 34
Long duration stimulated free-swimming experiments . . . 35
Basal metabolism . . . 37
Swimming metabolism model . . . 37

3.3 Results . . . 40
Laser scanning technique validation . . . 40
Long duration stimulated free-swimming experiments . . . 41
3.4 Discussion . . . 43
Chapter IV: Wake dynamics and biomechanics of electrically stimulated jellyfish 48
4.1 Introduction . . . 50
Electrical stimulation . . . 51
Experimental plan . . . 51
4.2 Materials and Methods . . . 52
Animal husbandry . . . 52
Electrical stimulation of live jellyfish . . . 52
Laser scanning PIV . . . 53
Post-processing . . . 55
Analytical analysis . . . 55
Biomechanics analysis . . . 62
Statistical Analysis . . . 63
4.3 Results . . . 63
Laser scanning PIV . . . 63
Biomechanics Analysis . . . 68
4.4 Discussion and Conclusion . . . 74
Chapter V: Conclusion . . . 79
5.1 Summary of contributions . . . 79
5.2 Opportunities for future work . . . 80
Quantitative efficiency metrics for jellyfish . . . 80
Directional control of swimming jellyfish . . . 81
Jellyfish swarm dynamics . . . 81
Expanding testing to other species . . . 82
Ocean exploration . . . 82
Bibliography . . . 83
Appendix A: Increasing the reliability and versatility of jellyfish biohybrid vehicles via species selection and rhopalia removal . . . 97
A.1 Introduction . . . 99
A.2 Materials and Methods . . . 102
Animals and care . . . 102
Biohybrid robotic system . . . 102
Field experiments . . . 102
Laboratory experiments . . . 103
Data and statistical analysis . . . 103
A.3 Results . . . 104
Control of bell contraction for excised versus non-excised . . . 104
Control of cubomedusa Alatina alata . . . 105
Comparison of descent rates . . . 105
Contraction frequency limits . . . 105
A.4 Discussion . . . 106
A.5 Conclusions . . . 110

Appendix B: Supplementary material for chapter 4 115

LIST OF ILLUSTRATIONS

Number *Page*

2.1 **Fig 1. Hardware schematic.** (**A**) Biohybrid robot schematic with 5 cm scale bar (horizontal black line). H and D are the height and diameter used to calculate the aspect ratio, $AR = H/D$. 1. Jellyfish bell. 2. Housing with 2.50 ± 0.03 cm diameter containing swim controller and battery. 3. Electrode embedded in muscle tissue. 4. Wooden pin attaching electronics to jellyfish. 5. Polylactic acid 3D printed forebody with $AR_1 = 0.31 \pm 0.01$. 6. Forebody with $AR_2 = 0.66 \pm 0.01$. 7. Forebody with $AR_3 = 1.00 \pm 0.01$. (**B**) Jellyfish biohybrid robot with attached hemi-ellipsoid with AR_3. This image has been digitally manipulated to remove reflections and outline the animal body in black. 9

2.2 **Fig 2. Saltwater vertical tank facility.** The saltwater vertical tank facility used in the long-distance swimming experiments measured 6 m tall by 1.6 m by 1.4 m, or 13,600 liters, shown here with a human for scale. Biohybrid jellyfish swimming trajectories were recorded with a digital camera placed at a height of 1.8 m from the base of the tank and a horizontal distance of 2.1 m from the face of the tank. . . . 12

2.3 **Figure 3. Comparison of flow streamlining with and without passive mechanical forebody.** Jellyfish biohybrid robot with and without attached hemi-ellipsoid forebody. Cyan arrows indicate downward swimming direction of the animals. Yellow arrows highlight areas of flow diversion and demonstrate flow disturbance before (**A**) and after (**B**) addition of streamlined passive mechanical forebody (outlined in red dashed curve). White scale bar in each panel indicates 5 cm. In panel (B), H is the forebody height and D is the maximum forebody diameter. In both panels, the flow visualization was created by superimposing several consecutive images, each shifted spatially so that the jellyfish appears stationary while particles trace pathlines around the animal. 16

2.4 **Figure 4. Example swimming speed measurements of biohybrid robot.** (**A**) Contraction and relaxation cycles show example 30-second swimming speed trace (i.e., swimming distance of 6.2 body diameters) of biohybrid robot with 18 cm animal and attached forebody AR_3. (**B**) Frequency spectrum analysis confirms animal response to external stimulation at 0.5 Hz. Semi-transparent band represents a tracking error of ±5 pixels. 17

2.5 **Figure 5. Measurements of swimming speed in six-meter vertical saltwater facility.** Sample biohybrid robot trajectories at 6.67-s intervals for the biohybrid robot without mechanical forebody (**A**) and with mechanical forebody AR_3 (**B**). Larger spacing between robot images in panel (**B**) qualitatively illustrates faster swimming speed. Zoomed-in image shows middle one-third of height of facility. Orange dropline is marked every 1.5 m. White scale bar indicates 20 cm. (**C**) Normalized biohybrid robot speed increases with streamlining coefficient (S) demonstrating impact of streamlined forebodies. Each color represents one animal with diameters listed in the legend; transparent band represents ± 1 standard deviation, calculated based on the three trials at each point. (**D**) Enhancement factor compares swimming performance of biohybrid robot to same stimulated jellyfish without mechanical forebody. Maximum enhancement factor corresponds to 61% increase in swimming speeds or a combined increase from electrical and mechanical enhancement to 4.5 times typical unstimulated jellyfish locomotion. 18

2.6 **Figure 6. Intracycle swimming speed range and forebody inertia versus streamlining coefficient.** (**A**) Intracycle swimming speed range decreases with streamlining coefficient S due to increased inertia of the hemi-ellipsoid forebody. Error bars indicate ± 1 standard deviation of intracycle speed throughout each trial. A small, random variability is added to the x-axis to help distinguish each of the data points. (**B**) Forebody mass increases with streamlining coefficient S. The largest tested forebody weighed $m_3 = 271.00 \pm .05$ grams in air. . 20

2.7 **Figure 7. Validation of theoretical model of biohybrid robot performance.** (**A**) Model prediction (blue) and empirical measurement (orange) of biohybrid robot swimming speed for AR_3 forebody over 5 body contraction cycles. (**B**) Model prediction (blue) and empirical measurements (orange) of decrease in intracycle swimming speed range with increased forebody mass. Error bars indicate ± 1 standard deviation of the 3 trials at each point. (**C**) Terminal velocity plateau model prediction (blue) matches empirical measurements (orange) of average swimming speeds over all animals and all trials for each forebody configuration. Error bars indicate ± 1 standard deviation of all trials. 21

2.8 **Figure 8. Utilizing biohybrid robotic jellyfish payload capacity for ocean science.** Demonstrated payload mass and volume capacity (i.e., blue boundaries) can be utilized for a variety of ocean science and exploration applications. COTS wildlife trackers with a variety of sensors are shown in red; power sources with approximate duration powering current electronics in yellow; CTD sensors shown in purple; and chemical probes in green. Filling the forebody with a lithium metal battery could power the biohybrid robot for more than 22 weeks. 23

3.1 **Laser scanning system for volumetric reconstructions.** (A) Diagram of laser scanning system with laser, galvanometer rotating at 10 Hz, 250 mm diameter condenser lens to redirect the laser normal to the scanning direction, cylindrical glass rod to form the laser beam into a thin sheet, water tank, and jellyfish. As the laser scanned across the jellyfish, a high speed camera recorded an image stack, or "volume", of 600 slices every 0.1 s. (B) A representative 3D volumetric reconstruction of a live jellyfish. (C) Closed system respirometry setup used to validate laser scanning technique. Jellyfish oxygen consumption was measured using an O_2 probe and temperature probe over time in a sealed chamber. Figure adapted with permission from M. K. Fu, Houghton, and John O. Dabiri (2021). 31

3.2 **Body composition over time.** (A) Measured carbon content of 9 jellyfish with 3 each at 0, 25, and 50 hours of starvation shows no statistically significant change in these variables. (B) Measured nitrogen content also shows no change. 34

3.3 **Jellyfish with embedded electronics for electrical stimulation at constant pulse rate.** (A) Diagram of electronics with swim controller housing TinyLily microprocessor with 250 mAH battery, two electrodes embedded in bell margin stimulating at 0.5 Hz, plastic rod to connect components, ballasting cap to passively maintain downward vertical swimming, and 1 cm scale bar. (B) Electronics embedded in live jellyfish during continuous swimming experiment with 5 cm scale bar. This Figure was adapted from Anuszczyk and Dabiri, 2024. 35

3.4 **Free-swimming tank for long-duration experiments.** (A) Diagram of 6 m by 1.6 m artificial seawater vertical tank facility. Water pumps in the recirculation area on the left generated flow (shown with red arrows), which opposed free-swimming jellyfish. A computer vision camera tracked the swimming animal. (B) The view from the computer vision camera of the middle section of the tank as a jellyfish, circled in yellow, swam downward. As the jellyfish descends, the camera ran a PID control loop interfacing with the water pumps to control the flow, keeping the animal in view of the camera. 36

3.5 **Validation of laser scanning technique for energy measurements.** (A) Linear relationship between wet weight (WW) and laser scanned weight (LSW) of $WW = 0.63LSW - 17.66$ for 10 animals. (B) A sample 1 hour closed system respirometry experiment with linear fit and R-squared value of $R^2 = 0.9921$. This high R-squared value confirms the linearity of jellyfish oxygen consumption over 1 hour. (C) Literature values for natural animals compared with simultaneous closed system respirometry and laser scanning. There is no statistical difference between the oxygen consumption rates found with the two different techniques. Oxygen consumption is given in terms of ml O_2 per hour per g wet weight. (D) We deployed this technique to measure free-swimming metabolism during 50 hour experiments for 3 jellyfish. The jellyfish lost 36% ± 8.4% of their mass on average over the course of this experiment. All error bars represent 1 standard deviation. 40

3.6 **Free-swimming energy consumption and metabolism model.** Total metabolism, shown in blue, in enclosed configurations here was measured using closed respirometry; free-swimming total metabolism was measured using the laser scanning technique. Stimulated free-swimming jellyfish consume 2.5 times as much energy as stimulated enclosed animals. Diagrams represent jellyfish in each configuration. We measured basal metabolism, shown in purple, by excising rhopalia as 42% ± 10% of jellyfish natural swimming energy consumption. The wake metabolism model, in yellow, representing the energy to set water in the wake into motion, underestimates energy consumption. Adding a steady drag metabolism term, in red, for the free-swimming jellyfish continues to underestimate the energy consumption. Oxygen consumption given in terms of ml O_2 per hour per g wet weight. 42

3.7 **Cost of Transport of stimulated jellyfish compared to other animals.** While natural jellyfish are the most efficient metazoans (Gemmell, Costello, et al., 2013), the increase in energy consumption found with the laser scanning technique increases the COT. Thus, these jellyfish have a COT comparable to swimming fish, as shown with the orange x. This COT is more than an order of magnitude smaller than a representative autonomous underwater vehicle (AUV), the REMUS 100. Figure adapted with permission from Gemmell, Costello, et al. (2013). 44

4.1 **Diagram of experimental plan.** This study consists of short timescale measurements of swimming jellyfish on the order of individual pulses. We will utilize three-dimensional, three-component PIV to measure and compare stimulated and unstimulated free-swimming jellyfish. . 52

4.2 **Jellyfish stimulation** (A) Schematic of stimulated jellyfish with jellyfish oriented downwards. Consists of two electrodes, a swim controller containing the electronics and battery (not visible), and a plastic rod embedded in the jellyfish tissue with a small threaded nut on the exumbrellar side to keep rod secure. (B) Photo of electronics embedded in live jellyfish during swimming experiment with additional forebody for payload. Figure adapted from Chapter 3. . . . 53

4.3 **Laser scanning system for 3D-3C PIV.** (A) Diagram of laser scanning system with laser, galvanometer rotating at 10 Hz, 250 mm diameter condenser lens to redirect the laser normal to the scanning direction, cylindrical glass rod to form the laser beam into a thin sheet, water tank, and jellyfish. As the laser scans across the jellyfish, a high speed camera records an image stack, or "volume", of 800 slices every 0.1 s. Figure adapted from Chapter 3. 54

4.4 **Energy volume diagram** (A) Volumetric reconstruction of swimming jellyfish used to mask out pixels in the image stack before analysis. These masks were fed into the PIV code to ensure no spurious velocity vectors were generated inside swimming animal. (B) A wake energy volume was defined behind the swimming jellyfish inside which kinetic energy was analyzed. Instantaneous measurements of kinetic energy inside this volume served as a proxy measurement of energy expended into this region of the wake by the swimming animal. The dimensions of the volume were defined as a width of one diameter D and height including the entire animal as well as extending into the posterior wake by $\frac{D}{2}$ from the vertical center of the animal. 56

4.5 **Contracted jellyfish PIV flow visualization.** (A) Out-of-plane 2D vorticity visualization with overlaid velocity vector field. Jellyfish cartoon mask is shown for illustration. Color bar shows regions of positive and negative vorticity and vorticity cores are visible at margin of jellyfish bell and in the wake. (B) Vorticity with same color scale overlaid on raw image of jellyfish at center plane illuminated by laser. Regions of low magnitude vorticity are filtered out. (C) Kinetic energy density map illustrates regions of high energy in wake with fully contracted jellyfish. Energy density in units of joules/m^3. Cartoon jellyfish mask is shown for illustration and color bar is in log scale. (D) Kinetic energy density map with the same color scale overlaid on raw image of jellyfish at center plane illuminated by laser. Regions of low energy density are filtered out for visualization. . . . 64

4.6 **Relaxed jellyfish PIV flow visualization** (A) Out-of-plane 2D vorticity visualization with overlaid velocity vector field. Jellyfish cartoon mask is shown for illustration. Color bar shows regions of positive and negative vorticity and vorticity cores are visible at margin of jellyfish bell and in the wake. (B) Vorticity with same color scale overlaid on raw image of jellyfish at center plane illuminated by laser. Regions of low magnitude vorticity are filtered out. (C) Kinetic energy density map illustrates regions of high energy in wake with fully relaxed jellyfish. Energy density in units of joules/m^3. Cartoon jellyfish mask is shown for illustration and color bar is in log scale. (D) Kinetic energy density map with the same color scale overlaid on raw image of jellyfish at center plane illuminated by laser. Regions of low energy density are filtered out for visualization. 65

4.7 **Normalized wake energy.** (A) Instantaneous mass-specific net downstream momentum, equation 4.6, transported during each pulse for an unstimulated (gray) and stimulated (purple) animal over the course of 10 second experiments. This trace shows two unstimulated pulses and five stimulated pulses indicated at the bottom of the plot by the colored gradient from light to dark where light represents the beginning of the contraction. (B) Pulse-specific normalized energy $E_{\text{ratio, pulse}}$ given by eq. 4.11. Blue, red, and green points represent animal means for each condition and shaded boxes denote the 95% confidence interval of the pooled pulse mean for each condition. Gray and purple points represent individual pulses. Statistical comparisons were performed on trial-level means using paired t-tests, pairing unstimulated (US) and stimulated (ST) trials from the same animals. No significant difference in energy released per pulse was observed between conditions ($p = 0.91$). (C) Time-specific normalized energy $P_{\text{ratio, time}}$ defined by equation 4.12. Stimulated jellyfish release 2.9 ±1.2 times more energy per second to the near wake than unstimulated animals ($p = 0.047$). Points and shaded boxes are as in panel B. 67

4.8 **Sensitivity of normalized wake energy to control-volume height.** Sensitivity of the pulse-averaged wake energy ratio to the height of the cylindrical control volume. Panels show results for control volume heights of (A) $H = \frac{D}{4}$, (B) $H = \frac{D}{2}$, and (C) $H = D$, where D is the bell diameter. Grey and purple points denote individual pulses for unstimulated (US) and stimulated (ST) trials, respectively. Colored symbols connected by lines indicate animal means. Shaded boxes show the 95% confidence interval of the pooled pulse mean for each condition. The primary analysis uses the $H = \frac{D}{2}$ control volume shown in panel (B). 69

4.9 **Time-resolved momentum transport** (A) Unstimulated mass-specific net downstream momentum shown across a normalized pulse time starting and ending at subsequent points of maximum bell relaxation. Light gray lines represent animal average across individual trials, dark gray line represents mean average across animals, and shaded region is ± 1 standard deviation. (B) Stimulated mass-specific net downstream momentum shown across a normalized pulse time, lines defined same as in (A). 70

4.10 **Average momentum transport in the wake** (A) Mass-specific net downstream momentum, equation 4.5, transported during each pulse. Points represent individual pulses and colored markers denote animal means for unstimulated (US) and stimulated (ST) trials connected by lines for each animal. Shaded boxes indicate the 95% confidence interval of the pooled pulse mean for each condition. (B) Partitioning of momentum between downstream and radial components. Points represent individual pulses and large markers show animal means. Radial momentum is expressed as a percentage of total transported momentum magnitude, while downstream momentum is the signed fraction indicating net downstream transport. 70

4.11 **Vortex ring analysis** (A) Circulation trends downward with stimulation using equation 4.15. Lines connect individual animals, black bars show mean, and statistics use paired t-test for each animal ($p = 0.062$). (B) Impulse also trends downward with stimulation using equation 4.16 ($p = 0.15$). (C) Peak vorticity measured within the vortex core measured using equation 4.14. Decreases for animals 2 and 3 but increases for animal 1, resulting in no change on average. 71

4.12 **Margin movement** (A)-(C) Margin movement between fully relaxed and contracted states for three jellyfish with diameters of 15±0.1 cm, 19±0.1 cm, and 27±0.1 cm respectively, measured at full relaxation. "US", "PE", and "ST" refer to unstimulated, unstimulated with embedded onboard passive electronics, and stimulated experiments. Stimulation reduces margin movement with a p-value of 0.035, while there is no statistically significant difference between the other experiments. (D) Average margin movement across (A)-(C). Stimulation reduces bell margin movement by 36.5±5.4% with a p-value of 0.035. 72

4.13 **Bell kinematics.** (A)-(B) Contraction and relaxation duration measurements for 6 jellyfish. Stimulation decreases relaxation duration by 24±9.7%. (C)-(D) Contraction and relaxation speed for 6 jellyfish show no statistically significant change with stimulation. Bars show mean ± SD across trials (one value per trial). P-values are from Welch's two-sample *t*-test comparing trial-level means between conditions. 73

A.1 Fig. 1. Jellyfish species used for biohybrid robots swimming in the natural water column. A) Non-excised and B) excised Aurelia aurita. C) Non-excised and D) excised Cassiopea xamachana. E) Cubomedusa Alatina alata without swim controller. F) A. alata with swim controller. 101

A.2 Fig. 2. Timing of bell contractions versus stimulation signals from the swim controller for individual jelly-fish. The fineness ratio (or aspect ratio) illustrates when the jellyfish bells are in their completely re-laxed, expanded state (minimum fineness ratio) or in their contracted state (maximum fineness ratio). A swim cycle begins when the jellyfish in the relaxed state initiates muscle contractions that cause the bell to contract thus increasing the fineness ratio. The orange vertical lines indicate the timing of the stimulation from the swim controller. 104

A.3 Fig. 3. Comparison of stimulation frequency to jellyfish pulse frequency and delay. When the swim control-ler was able to manipulate pulses, the stimulation and pulse frequencies were the same. Asterisk indicates when the stimulation and the pulse frequencies were significantly different (*t*-test, $p < 0.05$). E) Time delay between when the jellyfish received the stimulation and the bell began to contract to start a swim cycle. Species with the same letters were not significantly different from each other while species with different delay times were indicated with different letter (Student-Newman-Keuls Pair-wise comparison, $P < 0.05$). 106

A.4 Fig. 4. Swimming speeds of the different species. A) Depth versus time for the different species. For Cassiopea spp. and Aurelia aurita we had profiles for animals with their rhopalia intact (unexcised, blue) and with their rhopalia removed (excised, green). B) Relationship between jellyfish bell contraction frequency and the speed that the jellyfish descended. 107

A.5 Fig. 5. Relationship between stimulation frequency and jellyfish bell pulse frequency. Dotted line shows where the 1:1 relationship falls on the plot. 107

B.1 **Normalized bow wave energy.** (A) A bow-wave control volume defined ahead of the swimming jellyfish within which kinetic energy was analyzed. Instantaneous measurements of kinetic energy inside this volume served as a proxy for energy transferred into the bow-wave region of the wake by the swimming animal. The dimensions of the volume were defined as a width of one bell diameter D and a height of $\frac{D}{2}$. (B) Pulse-specific normalized energy $E_{\text{bow ratio, pulse}}$ given by eq. B.1. Blue, red, and green points represent animal means for each condition and shaded boxes denote the 95% confidence interval of the pooled pulse mean for each condition. Gray and purple points represent individual pulses. Statistical comparisons were performed on trial-level means using paired t-tests, pairing unstimulated (US) and stimulated (ST) trials from the same animals. No statistically significant difference in energy released per pulse was observed between conditions ($p = 0.67$). (C) Time-specific normalized energy $E_{\text{bow ratio, time}}$. Points and shaded boxes are as in panel B. While stimulated jellyfish animal-level means increased, the increase in time-normalized bow-wave energy was not statistically significant ($p = 0.11$). 116

LIST OF TABLES

Number *Page*

4.1 **Volumetric PIV acquisition and processing parameters.** 57

Chapter 1

INTRODUCTION

1.1 Ocean exploration

The ocean contains the majority of the habitable volume on earth, and many of its habitats and species remain largely unexplored (Ramirez-Llodra et al., 2010). The acceleration of climate change is leading to increasing ocean warming, acidification, and deoxygenation, which poses a danger to biodiversity and associated ocean resources (Levin and Le Bris, 2015). Recognizing these impacts, the United Nations has declared 2021-2030 the “United Nations Decade of Ocean Science for Sustainable Development" in an effort to galvanize ocean exploration (Ryabinin et al., 2019). Less than 80% of the ocean has been explored, with basic properties such as depth known for only 18% of the ocean at a resolution of 1 km (Wölfl et al., 2019). These knowledge gaps motivate more comprehensive ocean exploration at timescales relevant to climate change (Benway et al., 2019).

A variety of robotic technologies for ocean exploration have resulted in significant advances in ocean science (Yuh, Marani, and Blidberg, 2011; Zereik et al., 2018). For example, remote sensing platforms such as uncrewed aerial vehicles and satellites have been used to produce high resolution maps of sensitive marine habitats (Ventura et al., 2018) and to study important physical characteristics such as salinity (Reul et al., 2014) and temperature (Parker, Folland, and Jackson, 1995). However, these technologies are limited in the achievable depth of observations by water turbidity and solar illumination (Kavanaugh et al., 2021). Deep-sea tools, including gliders (Rudnick, 2016), seafloor-mounted buoys (Favali and Beranzoli, 2006), and autonomous underwater vehicles, (Sahoo, Dwivedy, and Robi, 2019) can explore to significant depths, but mission duration is often limited by battery capacity. The sheer size of the ocean, comprising more than 1.3 billion cubic kilometers (Charette and W. H. F. Smith, 2015), challenges the cost-effective scaling of these technologies for comprehensive ocean coverage (Zereik et al., 2018).

Robotic vehicles comprised entirely of mechanical components have increasingly been inspired by the demonstrated performance of aquatic animals, with the goal of improving robotic vehicle propulsive efficiency and range. For example, an acoustically controlled soft robotic fish was developed to observe aquatic animal

behavior with minimal disruption (Katzschmann et al., 2018). However, this robot required an accompanying human diver, thereby limiting operating depths to those safe for human diving. A benthic walking robot demonstrated locomotion along the seafloor and geological sediment sampling using a shovel (Picardi et al., 2020). While valuable for benthic exploration, this and similar robots are limited to the seafloor due to their inability to swim. A soft snailfish-inspired robot demonstrated swimming locomotion at a depth of 10,900 m (G. Li et al., 2021). This work presented a novel method for electronics hardening by distributing the electronics in a polymeric matrix, but power consumption limited swimming to 45 minutes. Each of the aforementioned examples demonstrates the emerging capabilities of robotic mimics of aquatic organisms; however, the performance envelope of live aquatic animals in the ocean has not yet been realized by these approaches.

A different strategy, biologging, embeds sensor tags on live animals such as pinnipeds (Carter et al., 2016), sea turtles (Cuevas et al., 2008), and jellyfish (Mooney et al., 2015; Fossette et al., 2016) and records measurements of the aquatic environment as the animals locomote naturally through the ocean. Biologgers can be used to study ocean characteristics such as salinity, temperature, and oxygen distribution using conductivity-temperature-depth instruments, oxygen probes, hydrophones, and other sensors (Chung, J. Lee, and W. Y. Lee, 2021). However, the timing and locations of the measurements are uncontrolled and limited to the path of the tagged animal.

1.2 Biohybrid robotics

Biohybrid robots have the potential to combine the control of fully mechanical robotic platforms and the swimming performance envelope of live aquatic animals to achieve the goal of comprehensive ocean exploration. Proof-of-concept of biohybrid robotic control has been achieved in a variety of organisms, including beetles (Sato et al., 2009), cockroaches (Sanchez et al., 2015), hawkmoths (Bozkurt, F Gilmour, and Lal, 2009), tissue-engineered rays (S.-J. Park et al., 2016), and jellyfish (Nawroth et al., 2012). Some biohybrid robots have also made use of biofuel cells to power onboard electronics (Matic et al., 2014; Shoji et al., 2016) and to do sensing for insect swarms (Romano, 2023). By utilizing biological locomotion, biohybrid robotics can potentially capitalize on the efficiency and adaptability of existing biological organisms. Biohybrid robotics have significant potential but so far have largely been confined to proof-of-concept and have not yet been deployed as platforms for science.

This thesis investigates jellyfish as a platform for biohybrid robotic sensors that can access the full ocean, including its deepest regions. Jellyfish are naturally occurring in a diverse range of oceanic environments, including tropical (Jennifer E. Purcell, 2012) and polar regions (Jennifer E. Purcell et al., 2010), and span depths from surface level to those exceeding 10,800 meters (Gallo et al., 2015). They are also tolerant to hypoxic conditions below 1 mg O_2 per liter (J. E. Purcell, 2007), in contrast to fish, who avoid levels below 2 to 3 mg O_2 per liter. In terms of locomotion, jellyfish are the most energy efficient of all known metazoans, with a cost of transport 3.5-fold lower than even efficiently swimming fish such as salmon (Gemmell, Costello, et al., 2013). We focus primarily on the jellyfish species *Aurelia aurita* (Linnaeus, 1758).

1.3 Jellyfish for ocean exploration

Jellyfish have previously been used as biologgers to investigate their ecology and behavior (Mooney et al., 2015; Fossette et al., 2016). Previous work has also demonstrated that live jellyfish swimming can be controlled by external electrical stimulation from an implanted microelectronic device (Nicole W. Xu and John O. Dabiri, 2020). When swimming contractions were stimulated at approximately 0.6 Hz, jellyfish were observed to swim up to 2.8 times the baseline swimming speed without the swim controller. These increased speeds required only an estimated twofold increase in energy expenditure, implying a concomitant increase in propulsive efficiency during external swimming control.

Although previous work demonstrated the feasibility of external control of jellyfish swimming frequency and quantified associated performance gains (Nicole W. Xu and John O. Dabiri, 2020; Nicole W. Xu, Townsend, et al., 2020a), key gaps remain in the development of the biohybrid jellyfish robot as a research platform for ocean science. As the most efficient metazoan (Gemmell, Costello, et al., 2013), studying the locomotion strategies of jellyfish for use in ocean exploration can also illuminate new insights into fluid dynamics and biomechanics.

1.4 Ethics of electrical muscle stimulation

In consideration of the ethics of the aforementioned robotic manipulations, the authors of that work collaborated with bioethicists to establish a framework for responsible implementation of these techniques (Nicole W Xu, Lenczewska, S. Wieten, et al., 2020; Nicole W Xu, Lenczewska, S. E. Wieten, et al., 2025; Nicole W Xu and John O Dabiri, 2024). This framework suggests consideration of the

4 "Rs" of reduction, replacement, refinement, and reproducibility, which we have utilized in this thesis. It is important to note that the jellyfish genus that is the focus of this work, *Aurelia*, lacks a central nervous system and nociceptors, and therefore lacks the capacity to sense pain (E. S. J. Smith and Lewin, 2009). While they have a known mucosal stress response, this was not observed to occur in any prior experiments using external swimming control.

1.5 Aims and objectives of this dissertation

This thesis addresses several key scientific questions underlying the large-scale deployment of biohybrid robotic systems for ocean exploration. We utilize a variety of experimental techniques and computational methods to investigate both the limits of the biohybrid system and the physics, fluids, and physiology of jellyfish.

Chapter 2 investigates the ability of biohybrid robotic jellyfish to carry scientific payloads and the possibility of strategically placing these payloads to reduce drag on the swimming animals. The ability to carry scientific sensors is vital to the practicability of using biohybrid jellyfish as ocean-going sensors. *Aurelia aurita* jellyfish are oblate species with flat exumbrellar surfaces. This chapter investigates how changing the shape of the exumbrellar surface affects swimming performance. In previous work, assessment of swimming performance was limited to tests either in a 2-meter-tall laboratory water tank (Nicole W. Xu and John O. Dabiri, 2020) or in a coastal marine environment (Nicole W. Xu, Townsend, et al., 2020a). Swimming performance over longer vertical distances consistent with the envisioned deep ocean measurements has not been characterized. Finally, while natural jellyfish boast a low cost of transport (Gemmell, Costello, et al., 2013), this performance is achieved despite a body shape that is not naturally streamlined.

Long duration swimming at high speeds could enable biohybrid jellyfish to traverse large areas of the ocean as well as swim to the depths of the abyssal region. Chapter 3 describes the development of a 13.6 m^3 vertical water treadmill for continuous swimming experiments. This facility is utilized for swimming experiments where jellyfish swim for more than two km over the course of two days. Simultaneous measurements using a new laser-scanning technique enable physiological energy consumption measurements throughout these experiments.

Chapter 4 investigates the origin of the change in energy consumption observed during the free-swimming experiments in Chapter 3. A single camera system for three-dimensional, three-component Particle Image Velocimetry is deployed

for simultaneous swimming kinematics measurements. These experiments seek to understand the impact of pulse rate and onboard electronics on hydrodynamics and energy consumption while advancing our understanding of the capabilities of biohybrid robotic jellyfish.

Chapter 2

ELECTROMECHANICAL ENHANCEMENT OF LIVE JELLYFISH FOR OCEAN EXPLORATION

The contents of this chapter have been adapted from Anuszczyk & Dabiri (2024), published in *Bioinspiration and Biomimetics* under the title "Electromechanical enhancement of live jellyfish for ocean exploration". As the first author, Simon Anuszczyk made the primary contributions towards the experiment design, data acquisition, analysis, and writing. Co-author John Dabiri contributed to the conceptualization of the study, funding acquisition, analysis and interpretation of the results, and feedback on the manuscript.

Abstract

The vast majority of the ocean's volume remains unexplored, in part because of limitations on the vertical range and measurement duration of existing robotic platforms. In light of the accelerating rate of climate change impacts on the physics and biogeochemistry of the ocean, the need for new tools that can measure more of the ocean on faster timescales is becoming pressing. Robotic platforms inspired or enabled by aquatic organisms have the potential to augment conventional technologies for ocean exploration. Recent work demonstrated the feasibility of directly stimulating the muscle tissue of live jellyfish via implanted microelectronics. We present a biohybrid robotic jellyfish that leverages this external electrical swimming control, while also using a 3D printed passive mechanical attachment to streamline the jellyfish shape, increase swimming performance, and significantly enhance payload capacity. A six-meter-tall, 13,600-liter saltwater facility was constructed to enable testing of the vertical swimming capabilities of the biohybrid robotic jellyfish over distances exceeding 35 body diameters. We found that the combination of external swimming control and the addition of the mechanical forebody resulted in an increase in swimming speeds to 4.5 times natural jellyfish locomotion. Moreover, the biohybrid jellyfish were capable of carrying a payload volume up to 105% of the jellyfish body volume. The added payload decreased the intracycle acceleration of the biohybrid robots relative to natural jellyfish, which could also facilitate more precise measurements by onboard sensors that depend on consistent platform motion. While many robotic exploration tools are limited by cost, energy expenditure, and varying oceanic environmental conditions, this platform is inexpensive, highly efficient, and benefits from the widespread natural habitats of jellyfish. The demonstrated performance of these biohybrid robots suggests an opportunity to expand the set of robotic tools for comprehensive monitoring of the changing ocean.

2.1 Introduction

We investigate for the first time the feasibility of simultaneous electrical and mechanical modification of live jellyfish as biohybrid robotic platforms. The mechanical modification comprises the addition of a passive forebody to streamline the natural jellyfish body shape while also facilitating a significant payload capacity. The performance of the electromechanically modified jellyfish is tested in a specially constructed six-meter-tall, 13,600-liter saltwater facility where the jellyfish can be observed swimming over distances up to 35 body diameters. These measurements, combined with an analytical model of the swimming dynamics, enable optimization of the design of the biohybrid jellyfish robots.

2.2 Methods and Materials

Animal husbandry

We conducted long-distance swimming experiments with $N = 3$ jellyfish of diameters $d_1 = 16.0 \pm 0.5$ cm, $d_2 = 16.5 \pm 0.5$ cm, and $d_3 = 18.0 \pm 0.5$ cm and flow visualization experiments with 1 jellyfish of diameter $d_4 = 19.0 \pm 0.5$ cm. Utilizing jellyfish of varying geometries allowed us to draw broader conclusions about the applicability of this study to a range of animals. *Aurelia aurita* were obtained from Cabrillo Marine Aquarium (San Pedro, CA, USA) and housed in a 453-liter pseudokreisel tank (Jelliquarium 360, Midwater Systems, Thousand Oaks, CA, USA). The tank was filled with artificial seawater made from sea salt (Instant Ocean Sea Salt, Spectrum Brands, Blacksburg, VA, USA) and deionized water balanced at 35 parts per thousand (ppt) and kept at 21°C. The jellyfish were hand-fed twice daily with live *Artemia franciscana* brine shrimp (Hatching Shell-Free Brine Shrimp Eggs E-Z Egg, Brine Shrimp Direct, Ogden, UT, USA). Brine shrimp were hatched every other day in aerated hatchery cones of artificial seawater heated to 28°C for 24 hours, then transferred to beakers at 21°C. Brine shrimp were fed PHYTO-Feast (Reef Nutrition, Reed Mariculture Inc., Campbell, CA) and enriched with SELCO (Self-Emulsifying Lipid Concentrate, Brine Shrimp Direct, Ogden, UT, USA). The animals' care was in accordance with institutional guidelines.

System architecture

Figure 1(a) shows the biohybrid robot electronics schematic and all components. The aspect ratio of the forebodies is defined as $AR = H/D$, where H is the forebody height and D is the maximum forebody diameter. The system comprises the jellyfish bell (1), the 3D-printed 2.50 ± 0.03 cm diameter electronics housing containing the

swim controller and battery (2), the two electrodes embedded in the jellyfish muscle tissue (3), a wooden pin attaching the electronics to the jellyfish (4), a 3D-printed hemi-ellipsoid with $AR_1 = 0.31 \pm 0.01$ (5), a hemi-ellipsoid with $AR_2 = 0.66 \pm 0.01$ (6), and a hemi-ellipsoid with $AR_3 = 1.00 \pm 0.01$ (7). Figure 1(b) is a sample image of a jellyfish biohybrid robot with an attached AR_3 forebody swimming in a lab saltwater tank.

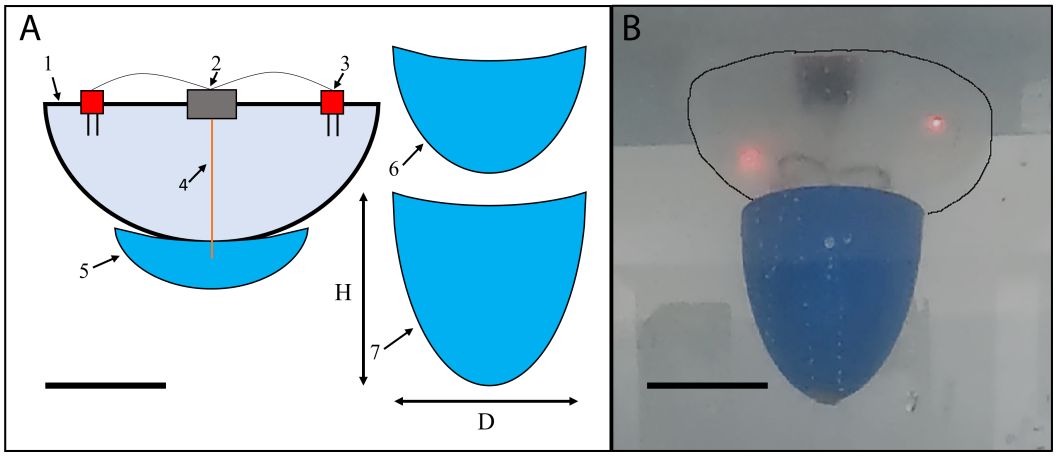

Figure 2.1: Fig 1. Hardware schematic.
(**A**) Biohybrid robot schematic with 5 cm scale bar (horizontal black line). H and D are the height and diameter used to calculate the aspect ratio, $AR = H/D$. 1. Jellyfish bell. 2. Housing with 2.50 ± 0.03 cm diameter containing swim controller and battery. 3. Electrode embedded in muscle tissue. 4. Wooden pin attaching electronics to jellyfish. 5. Polylactic acid 3D printed forebody with $AR_1 = 0.31 \pm 0.01$. 6. Forebody with $AR_2 = 0.66 \pm 0.01$. 7. Forebody with $AR_3 = 1.00 \pm 0.01$. (**B**) Jellyfish biohybrid robot with attached hemi-ellipsoid with AR_3. This image has been digitally manipulated to remove reflections and outline the animal body in black.

Components and fabrication

The electronics were based on previous work (Nicole W. Xu and John O. Dabiri, 2020) and consisted of a TinyLily processor (TinyCircuits, Akron, OH, USA) and a 15 mAH lithium-polymer battery cell (PGEB181118, PowerStream Technology Inc., Orem, UT, USA) enclosed in a custom 2.50 ± 0.03 cm diameter 3D printed housing printed on a resin printer for waterproofing at high pressure (Form 3, Formlabs, Somerville, Massachusetts). The housing utilized a male threaded base and a female threaded cap compressing a face-sealed soft Buna-N O-ring with food-safe O-ring grease. Silver wire coated in perfluoroalkoxy was threaded through small holes in the housing and connected to platinum rods (A-M Systems, Sequim,

WA, USA) embedded in the animal muscle tissue to create two electrodes. The holes were sealed with adhesive, and an LED was connected in series to each electrode to provide visual confirmation of stimulation as shown in Figure 1(b).

Hemi-ellipsoid forebodies were designed with a density gradient such that the anterior portion, the bottom as shown in Figure 1(b), was more dense than the posterior portion. Perturbations from vertical swimming, either due to endogenous swimming contractions by the animal or external fluid disturbances, were resisted by the passive restoring torque created by the position of the center of gravity below the center of buoyancy. Hence, the biohybrid robot was constrained to swim in the vertical direction, as envisioned for vertical ocean profiling. Concavity at the forebody-animal interface created a close fit against the exumbrellar bell surface. The forebodies were 3D printed out of PLA (Polylactic Acid) on an X1 Carbon printer (Bambulab, Shenzhen, China) and coated with 2-part epoxy resin for waterproofing. After drying, a hole was drilled into the forebody at the interface with the animal to create a press fit for the wooden rod as shown in Figure 1(a) item 4. The forebodies were ballasted to maintain 0.01 ± 0.01 grams positive buoyancy in saltwater at 35 ppt.

Flow visualization experiments

Flow visualization experiments to observe the effect of the forebody streamlining were conducted in a 1.2 m by 0.5 m by 0.5 m tank filled with artificial seawater at 35 ppt and seeded with 13 micron silver-coated hollow glass particles (SH400S20, Potters Industries, Carlstadt, NJ, USA). The biohybrid robot swam down through a laser sheet generated by a 671 nm continuous wave laser (5-Watt LRS0671 DPSS Laser System, Laserglow Technologies, North York, Ontario, Canada) shone through a 250 mm diameter condenser lens and a sheet forming optic. A high speed camera normal to the laser sheet recorded at 125 frames per second with a shutter speed of $1/200$ seconds, a resolution of 1024x1024 pixels (FASTCAM SA-Z, Photron USA Inc., San Diego, CA, USA), and a fixed focal length macro lens (Micro-NIKKOR 105 mm with a 36 mm extension tube, Nikon, Tokyo, Japan). The images were processed in MATLAB (MathWorks, Natick, MA, USA) by stacking every third frame for 50 frames. In each frame, the biohybrid robot was translated to the location in the previous frame such that the biohybrid robot was motionless. This manipulation transformed the video into the biohybrid robot frame of reference, and consequently, the observed particles traced out pathlines as in a long exposure image. This process was repeated for the biohybrid robot without the forebody and

with the AR_3 forebody configuration to compare the streamlining effects.

Long-distance swimming experiments

A 6 m tall, 13,600 liter saltwater facility was constructed for testing jellyfish biohybrid robot swimming performance. This 6 m by 1.6 m by 1.4 m, or 13.4 m^3, vertical tank was filled with artificial seawater balanced at 35 ppt and held at 21°C (figure 2). The facility has a 151 liter per minute continuous filtration pump, which turns over the entire system water volume every 90 minutes. This pump was turned off at least 2 hours before beginning experiments to allow residual currents to dissipate. The facility has three acrylic windows on each of three sides, spanning the width of the tank. A digital camera (GoPro HERO9 Black, GoPro Inc., San Mateo, CA) recording at a resolution of 3840x2160 pixels was used to record videos of the jellyfish biohybrid robot swimming trials. The camera was centered horizontally at a height of 1.8 m from the base of the tank and set back 2.1 m from the front. A 100 watt LED floodlight illuminated the tank from below through a porthole on the bottom of the tank.

While salinity and temperature were carefully matched between the pseudokreisel and this facility, the jellyfish were also acclimated by slowly introducing water from this facility to the jellyfish for 30 minutes in a 5 gallon bucket. Each jellyfish was then transferred to a glass bowl and equipped with the electronics by inserting the wooden pin through the stomach of the jellyfish and embedding both electrodes into the muscle tissue on opposite sides of the bell margin. The jellyfish was transferred into the saltwater facility, and the appropriate forebody was mounted to complete the biohybrid robot. A slack polymer string with a 0.3 mm diameter was tied onto the electronics housing to facilitate recovery. The biohybrid robot was positioned horizontally in the center of the tank to avoid contacting the walls and released to begin swimming. Swimming data from the middle 2 m section of the tank was used in order to ensure the animal had reached a constant average swimming speed, and to avoid the hydrodynamic impact of the tank bottom. Post-processing of the measurements confirmed that the biohybrid robot reached a constant average swimming speed for all forebody configurations before entering the region of interest in the middle 2 m section of the tank. The sequence of forebody aspect ratio tests was randomized to minimize any systematic biases associated with a drift in animal swimming performance over the course of the swimming trials. Each forebody configuration was tested 3 times for a total of 12 trials per biohybrid robot. Between each trial, the biohybrid robot was retrieved using the polymer string, and the tank

was allowed to return to quiescence for 10 minutes before beginning the next trial. Experiments were conducted with all 3 jellyfish over 2 days.

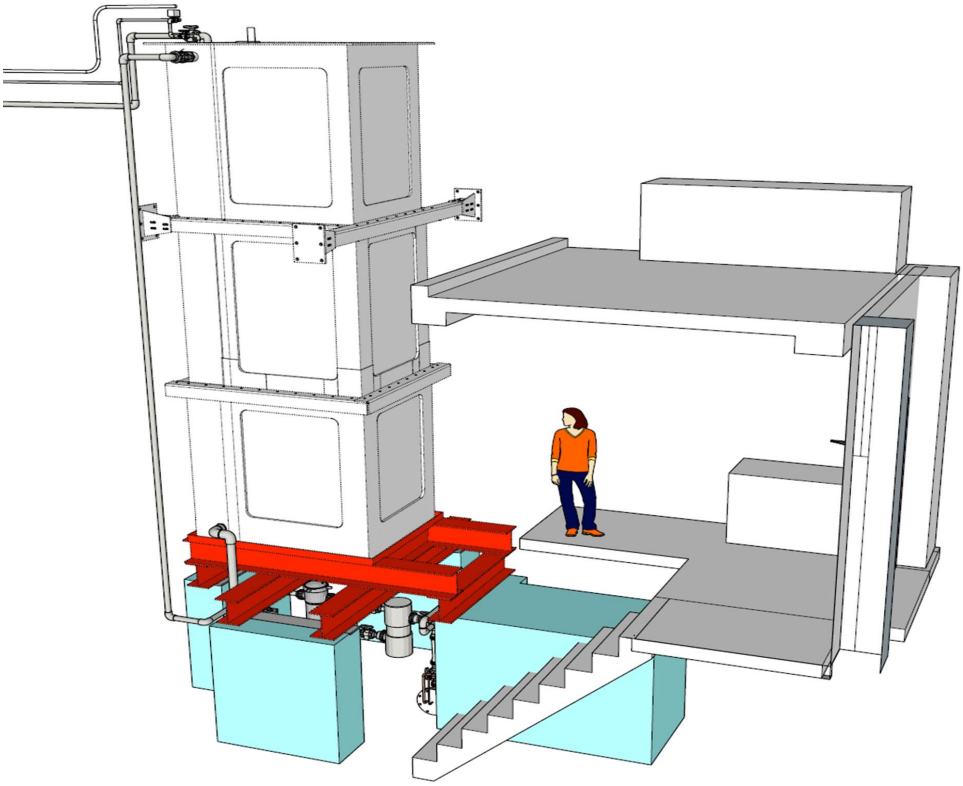

Figure 2.2: Fig 2. Saltwater vertical tank facility.
The saltwater vertical tank facility used in the long-distance swimming experiments measured 6 m tall by 1.6 m by 1.4 m, or 13,600 liters, shown here with a human for scale. Biohybrid jellyfish swimming trajectories were recorded with a digital camera placed at a height of 1.8 m from the base of the tank and a horizontal distance of 2.1 m from the face of the tank.

Post-processing used a combination of a custom MATLAB tracking program and a commercial motion tracking software (Blender Foundation, Amsterdam, Netherlands) to track the jellyfish. The MATLAB tracking program assigned a tracking box around the biohybrid robot and used the centroid of the box to calculate biohybrid robot swimming speeds. The average swimming speed per trial was computed based on the slope of a linear regression of the measured swimming distance versus time. The best-fit line exhibited an R-square value of 0.9894 ± 0.0141, indicating the appropriateness of a linear regression. To determine instantaneous velocities during each trial, Blender was used to track the location of a point chosen near the centroid of the biohybrid robot. This tracking method better reproduced the intracycle speed changes as the jellyfish biohybrid robot contracted and relaxed

but was not able to track the jellyfish without a forebody. Blender position data was imported into MATLAB, where velocities were calculated as finite differences. Horizontal velocities were assumed as proxies for out-of-plane velocities, and all 3 components were taken into account for all calculations. Intracycle speed changes were found with a program in MATLAB that identified peaks and valleys in the speed trace and calculated the difference from a peak to the closest valley. Average speeds for both programs were the same. The steady-state swimming speed for each trial was characterized by a drag coefficient C_D, corresponding to the measured terminal velocity with scaling coefficients, $u = 0.1417 + 0.0225\sqrt{1/C_D}$ where u is the observed speed.

The forebody drag coefficients C_D, used in calculating the streamlining coefficient, $S = -log(C_D)$, were found by conducting drop tests of the forebodies. Forebodies of the same form factor as those used in our experiments but at a higher infill density were printed out of PLA such that they were negatively buoyant. These forebodies were attached to a slack polymer string with a 0.3 mm diameter for ease of recovery, submerged at the top of the vertical tank, and released to sink at terminal velocity. These experiments were recorded using the same GoPro camera setup and post-processing methods as described above. The coefficients of drag C_D were found using the drag equation (Batchelor, 2000) which after accounting for buoyancy, becomes

$$C_D = \frac{2g(m_f - V_f\rho_w)}{\rho_w S_f u^2} \tag{2.1}$$

where g is the acceleration of gravity, m_f is the mass of the forebody, V_f is the volume of the forebody, ρ_w is the density of saltwater, S_f is the frontal surface area of the forebody impacting the flow, and u is the terminal velocity at which the forebody falls. Each forebody was tested three times, and the average velocity was used to calculate $C_{D,1} = 0.93 \pm 0.05$, $C_{D,2} = 0.52 \pm 0.03$, and $C_{D,3} = 0.17 \pm 0.01$ where the error is the standard deviation of all three trials. The drag on the jellyfish without a forebody was approximated as a flat plate with $C_{D,0} = 1.12$ (Hoerner, 1967).

Kinematics Model

We derived a first-principles physics-based kinematics model for our biohybrid robot by extending previous models (Daniel, 1983; McHenry and Jed, 2003; Nicole W. Xu and John O. Dabiri, 2020) to predict the performance of biohybrid robots with

various payload and animal geometries. Starting with a force balance from Newton's second law

$$\sum F = m_R \frac{\partial u}{\partial t} \tag{2.2}$$

where $\sum F$ is the sum of the forces, m_R is the combined mass of the biohybrid robot, u is the swimming speed, and t is time. The thrust of the biohybrid robot T is assumed to oppose drag D and the unsteady acceleration reaction Ac

$$T - D - Ac = m_R \frac{\partial u}{\partial t} \tag{2.3}$$

with the forces given as

$$T = \frac{\rho_w}{A_{sub}} (\frac{dV_R}{dt})^2 \tag{2.4}$$

$$D = \frac{1}{2} C_D \rho_w S_R u^2 \tag{2.5}$$

$$Ac = \alpha m_R \frac{\partial u}{\partial t} \tag{2.6}$$

where $\rho_w = 1.024$ g/cm^3 is the density of saltwater at 35 ppt and 21°C, A_{sub} is the subumbrellar opening area of the jellyfish, V_R is the instantaneous volume of the biohybrid robot, C_D is the coefficient of drag calculated above, S_R is the instantaneous frontal surface area of the biohybrid robot, and $\alpha = (h/r)^{1/4}$ is the added mass coefficient where h is the bell height and r is the bell radius. We define

$$V_R = V_f + V_0 + \frac{dv}{dt} t \tag{2.7}$$

$$S_R = S_f + S_0 + \frac{3}{2h} \frac{dv}{dt} t \tag{2.8}$$

where V_f is the volume of the forebody, S_f is the frontal surface area of the forebody, the relaxed volume of the jellyfish $V_0 = 2/3\pi h r^2$, the relaxed frontal surface area of the jellyfish $S_0 = \pi r^2$, the change in volume $dv = V_{ex} V_0$ with a constant volume exchange of V_{ex}, change in time $dt = t_c$ during contraction and $dt = t_r$ during relaxation. Substituting these equations back into the force balance leads to

$$\frac{\rho_w}{A_{sub}}(\frac{dV_R}{dt})^2 = \frac{1}{2}C_D\rho_w S_R u^2 + (1+\alpha)m_R\frac{\partial u}{\partial t} \tag{2.9}$$

which was solved for u in MATLAB using the ODE45 function. Jellyfish geometry was measured to experimentally determine h and r for each jellyfish, and video analysis led to approximate contraction and relaxation times of $t_c = 0.5$ and $t_r = 1.5$ respectively.

2.3 Results

We modified the shape of the exumbrellar surface of the natural jellyfish by attaching additively manufactured hemi-ellipsoids of various aspect ratios to the apex of the animals (see Methods). As in prior work (Nicole W. Xu and John O. Dabiri, 2020), the jellyfish swim muscles, which are located on the subumbrellar surface, were stimulated with two electrodes to produce regular contractions at 0.5 Hz with a 3.7-volt, 10-ms square wave. The biohybrid robot is ballasted to create a slight positive buoyancy and a horizontal restoring torque, constraining the animals to swimming in the vertical direction. This positive ballasting ensured that the observed downward swimming could be attributed only to the active animal swimming and not to the passive dynamics of the attached mechanical forebodies.

Flow visualization experiments

We first studied the hydrodynamics of the biohybrid robot in a 1.2-m tall, 300 liter saltwater tank to investigate the hydrodynamic impacts of the mechanical forebodies on the local flow around the jellyfish. Time-lapse images of 13 micron, neutrally buoyant tracer particles showed that the addition of hemi-ellipsoids of increasing aspect ratios streamlines the flow around the biohybrid robots (figure 3; see also Supplementary Movies 1 and 2). Specifically, comparison of the tracer particle pathlines illustrated the reduction in flow re-direction at the apex of the biohybrid robots relative to the natural jellyfish (yellow arrows). While the total lateral diversion of flow is the same in the two cases, i.e., directing flow around the maximum body width at the bell margin, the passive forebody achieves this diversion in a more gradual fashion. It was anticipated that the larger lateral diversion of flow at the apex of the natural jellyfish shape would lead to greater drag than on the streamlined forebodies.

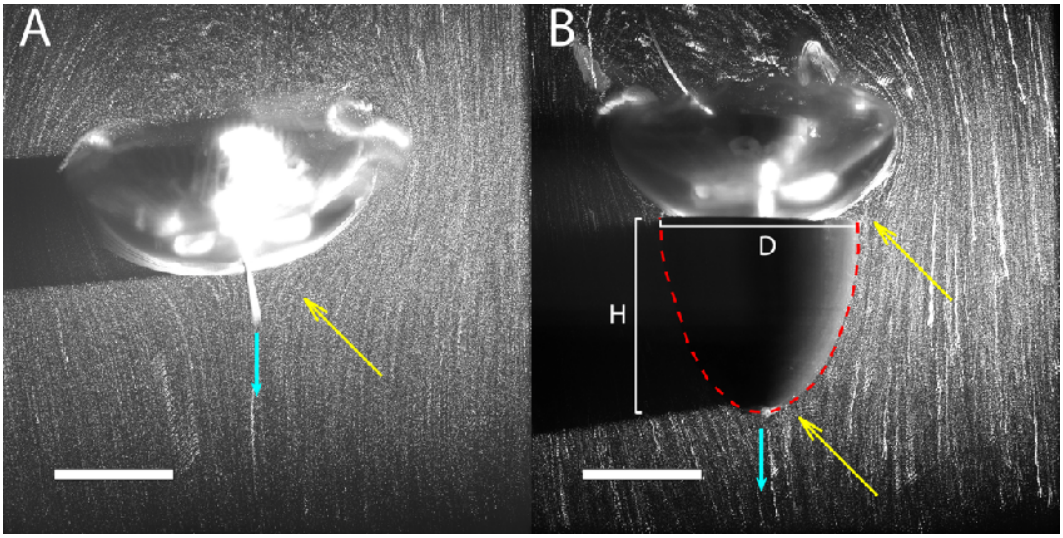

Figure 2.3: Figure 3. Comparison of flow streamlining with and without passive mechanical forebody.
Jellyfish biohybrid robot with and without attached hemi-ellipsoid forebody. Cyan arrows indicate downward swimming direction of the animals. Yellow arrows highlight areas of flow diversion and demonstrate flow disturbance before (**A**) and after (**B**) addition of streamlined passive mechanical forebody (outlined in red dashed curve). White scale bar in each panel indicates 5 cm. In panel (B), H is the forebody height and D is the maximum forebody diameter. In both panels, the flow visualization was created by superimposing several consecutive images, each shifted spatially so that the jellyfish appears stationary while particles trace pathlines around the animal.

Long-distance swimming experiments

To test the impact of the streamlining on swimming performance, the natural jellyfish and biohybrid robots were tested in a new 6 m tall, 13,600 liter saltwater facility built for free-swimming experiments (see Methods for facility description). Figure 4(a) shows a 30-second swimming speed trace (i.e., swimming distance of 6.2 body diameters) of the swimming biohybrid robot showing speed peaks during the jellyfish bell contraction phase and troughs during bell relaxation. The swimming speed oscillated with each contraction and relaxation, and eventually reached a steady state average swimming speed. A spectral analysis of the swimming speed trace shows that the animal responded to external electrical stimulation by contracting at the 0.5 Hz stimulation frequency (figure 4(b)). Figure 4(a-b) was made using the Blender tracking program.

We tested the stimulated jellyfish biohybrid robot without a forebody and with the addition of three different hemi-ellipsoid forebodies of increasing aspect ratio (see

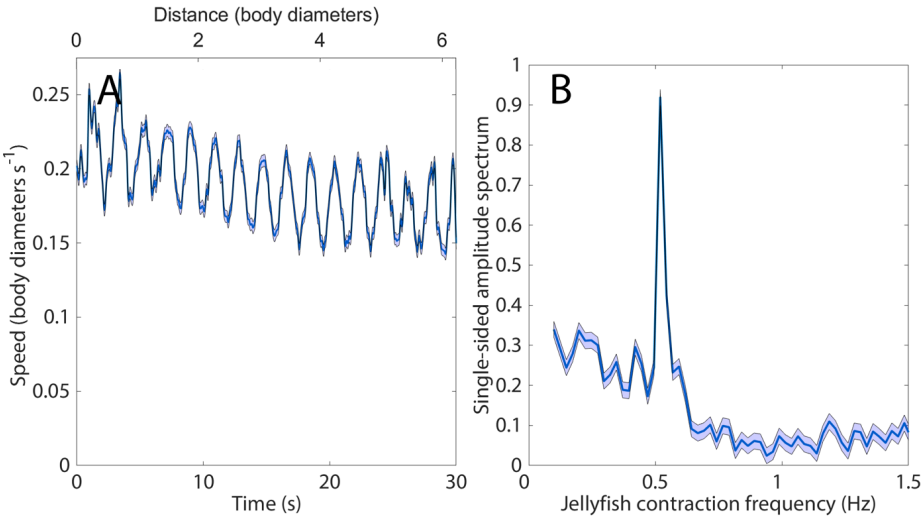

Figure 2.4: Figure 4. Example swimming speed measurements of biohybrid robot.
(**A**) Contraction and relaxation cycles show example 30-second swimming speed trace (i.e., swimming distance of 6.2 body diameters) of biohybrid robot with 18 cm animal and attached forebody AR_3. (**B**) Frequency spectrum analysis confirms animal response to external stimulation at 0.5 Hz. Semi-transparent band represents a tracking error of ±5 pixels.

Methods). A total of $N = 3$ different animals were tested with bell diameters of $d_1 = 16.0 \pm 0.5$ cm, $d_2 = 16.5 \pm 0.5$ cm, and $d_3 = 18.0 \pm 0.5$ cm. Each forebody configuration was tested 3 times in a randomized order to ensure that trends in forebody performance were not affected by any drift in animal performance over time. Sample biohybrid robot trajectories with and without the addition of a hemi-ellipsoid forebody AR_3 are shown in Figures 5(a) and 5(b), respectively (see also Supplementary Movies 3 and 4). The images in Figure 5 are equally spaced at intervals of 6.67 seconds and show a zoomed-in view of the middle one-third of the total height of the facility. An orange scaling dropline was marked every 1.5 meters to provide a reference length scale. The spatial intervals between images of the animal in Figure 5(b) are larger than those in Figure 5(a), qualitatively illustrating the faster swimming speed of the biohybrid robot with the addition of the streamlined mechanical forebody.

The biohybrid robot swimming speed was found to increase with the aspect ratio of the forebody, with the largest increase occurring between AR_0 (i.e., no forebody) and AR_1. Figure 5(c) plots the normalized biohybrid robot swimming speed (in body diameters per second) versus streamlining coefficient, S (see Methods). Swimming

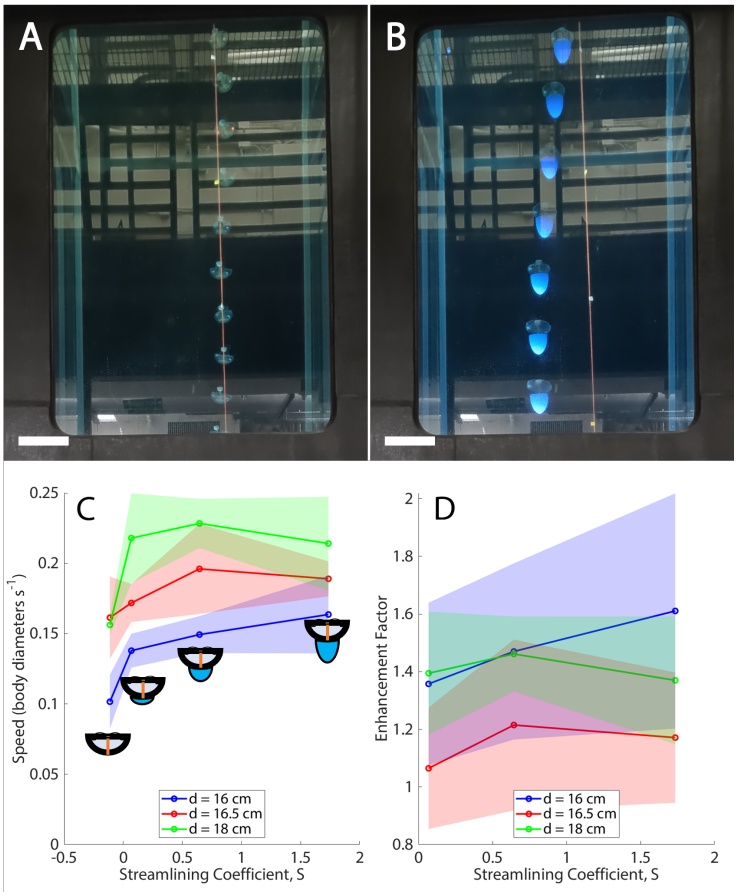

Figure 2.5: Figure 5. Measurements of swimming speed in six-meter vertical saltwater facility.
Sample biohybrid robot trajectories at 6.67-s intervals for the biohybrid robot without mechanical forebody (**A**) and with mechanical forebody AR_3 (**B**). Larger spacing between robot images in panel (**B**) qualitatively illustrates faster swimming speed. Zoomed-in image shows middle one-third of height of facility. Orange dropline is marked every 1.5 m. White scale bar indicates 20 cm. (**C**) Normalized biohybrid robot speed increases with streamlining coefficient (S) demonstrating impact of streamlined forebodies. Each color represents one animal with diameters listed in the legend; transparent band represents ± 1 standard deviation, calculated based on the three trials at each point. (**D**) Enhancement factor compares swimming performance of biohybrid robot to same stimulated jellyfish without mechanical forebody. Maximum enhancement factor corresponds to 61% increase in swimming speeds or a combined increase from electrical and mechanical enhancement to 4.5 times typical unstimulated jellyfish locomotion.

speeds increased in direct proportion to the streamlining coefficient, reaching a plateau for the most streamlined forebodies. This plateau is likely due to the counteracting impacts of increased streamlining, inertia, and unsteady added mass.

While larger forebodies have smaller C_D values, they also displace significantly more mass and limit the ability of the biohybrid jellyfish robot to accelerate during the contraction phase. Diameter-normalized swimming speeds were observed to be larger for the larger jellyfish, likely reflecting a greater propulsive capacity to translate the mechanical forebodies downward against their positive buoyancy.

We also compared the swimming performance of each biohybrid robot to the same jellyfish without a mechanical forebody (figure 5(d)). The maximum enhancement factor (i.e., performance ratio relative to swimming without a forebody), which occurred for the mechanical forebody with the largest streamlining coefficient, i.e., AR_3, corresponded to an increase in swimming speeds of up to 61%. Across all cases, we observed an average increase in swimming speed of 38% ± 22%. The performance plateau observed in Figure 5(c) for the most streamlined forebodies persists here, and the change in enhancement factor between forebodies AR_2 and AR_3 is not statistically significant. In light of prior work demonstrating an increase of up to 2.8 times the swimming speed of natural jellyfish (Nicole W. Xu and John O. Dabiri, 2020), the present results suggest that the combined electromechanical enhancement could enable an overall increase in swimming speeds to more than 4.5 times natural, unstimulated jellyfish locomotion. Figure 5(c-d) was made using the MATLAB tracking program.

The addition of mechanical forebodies adds inertia to the biohybrid robotic system proportional to the volume of displaced water. The largest forebody corresponds to an increase in the mass by $m_3 = 271.04 \pm .05$ grams of payload and a volume of 105% ± 1% of the animal body volume. Figure 6(a) plots the intracycle swimming speed range in body diameters per second vs S of all 24 trials of the biohybrid robot with the three forebodies. With increasing streamlining coefficient S, the intracycle swimming speed range of the biohybrid robot decreased. Figure 6(b) illustrates that the forebody mass increased in direct proportion to the streamlining coefficient, which explains the concurrent reduction in intracycle swimming speed range. Specifically, because the biohybrid robot swam in a highly unsteady motion as shown in Figure 6(a), the additional inertia changed the swimming dynamics. Figure 6(a) was made using the Blender tracking program.

We developed a theoretical model of the biohybrid robot swimming dynamics to further investigate the dependence of the swimming performance on the forebody geometry and properties as well as the animal swimming behavior (see Methods). Figure 7(a) compares an example predicted swimming speed trace (blue) and mea-

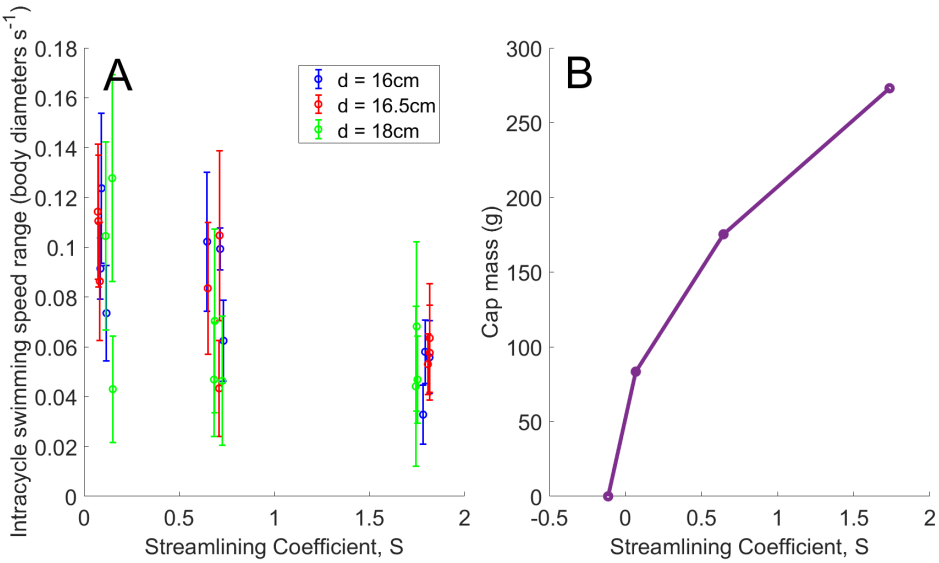

Figure 2.6: Figure 6. Intracycle swimming speed range and forebody inertia versus streamlining coefficient.
(**A**) Intracycle swimming speed range decreases with streamlining coefficient S due to increased inertia of the hemi-ellipsoid forebody. Error bars indicate ± 1 standard deviation of intracycle speed throughout each trial. A small, random variability is added to the x-axis to help distinguish each of the data points. (**B**) Forebody mass increases with streamlining coefficient S. The largest tested forebody weighed $m_3 = 271.00 \pm .05$ grams in air.

surements from swimming tests using the mechanical forebody AR_3 over 5 body contraction cycles. The model generally captures the trends in both swimming speed and intracycle speed range versus forebody mass (figure 7(b)). The overlayed data in Figure 7(a-b) was made using the Blender tracking program. While the model predicted a decrease in the intracycle swimming speed range with increasing forebody mass, it underestimated the quantitative decrease observed between the AR_2 and AR_3 cases. We speculate that this might be due to a change in the effective coefficient of drag of the combined biohybrid robotic system with the AR_3 forebody, given its smaller absolute drag coefficient.

Pooling the measurements from all 3 animals tested in these experiments, we observed a plateau in the average speed between the AR_2 and AR_3 cases. This plateau is qualitatively consistent with a scaled version of the terminal velocity equation, i.e., it indicates that performance at high swimming speeds is likely limited by the terminal velocity of the mechanical forebody. In sum, the model generally captures the biohybrid robot dynamics and may therefore be used to extrapolate to larger jellyfish and different forebody geometries in the future.

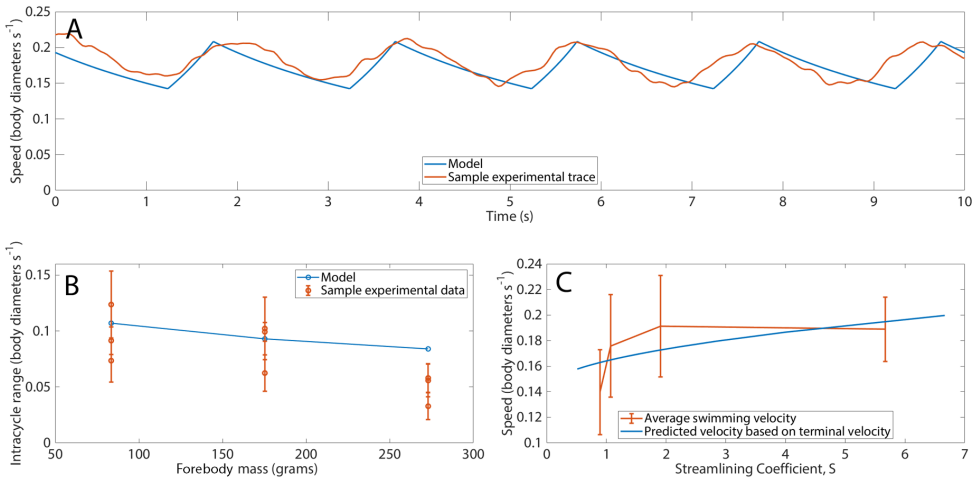

Figure 2.7: Figure 7. Validation of theoretical model of biohybrid robot performance.
(**A**) Model prediction (blue) and empirical measurement (orange) of biohybrid robot swimming speed for AR_3 forebody over 5 body contraction cycles. (**B**) Model prediction (blue) and empirical measurements (orange) of decrease in intracycle swimming speed range with increased forebody mass. Error bars indicate ± 1 standard deviation of the 3 trials at each point. (**C**) Terminal velocity plateau model prediction (blue) matches empirical measurements (orange) of average swimming speeds over all animals and all trials for each forebody configuration. Error bars indicate ± 1 standard deviation of all trials.

2.4 Discussion

We have presented the electromechanical enhancement of a biohybrid jellyfish robot for ocean exploration through the addition of streamlined, passive forebodies. We demonstrated the ability to travel at speeds up to 4.5 times baseline jellyfish swimming speeds while carrying a payload of more than 270 grams in a volume of 105% of the jellyfish volume. The flow around the biohybrid robot was examined using time-lapse pathline visualization to demonstrate local streamlining effects, and biohybrid robot swimming performance was investigated in a custom 6 m tall saltwater facility that enabled testing of swimming over distances significantly longer than prior studies. The addition of a payload was found to decrease intracycle acceleration, which may facilitate more precise onboard measurements in cases where unsteady platform motion should be minimized. By utilizing live animals and their ability to extract chemical energy from the water column via feeding, this approach has the potential to eliminate most of the battery power typically required for underwater propulsion, instead leveraging and controlling the jellyfish

locomotion. This suggests an opportunity to expand the set of biohybrid robotic tools for ocean exploration.

While this work has focused on maximizing the swimming speed of the biohybrid jellyfish robots, it has not considered the associated metabolic costs of this increased performance. Previous work investigated the metabolic costs of natural jellyfish and found low muscle mass of less than 1% of body mass, resulting in low metabolic rates and a cost of transport lower than other animals (Gemmell, Costello, et al., 2013). Previous work on biohybrid jellyfish also found that increased swimming performance was not penalized by proportional increases in energy expenditure; in fact, the externally stimulated biohybrid jellyfish swam more efficiently than their natural counterparts (Nicole W. Xu and John O. Dabiri, 2020). However, energy expenditure experiments have not been conducted for freely swimming biohybrid robotic jellyfish due to the challenges presented by the animals low respiratory rates combined with large volumes of water required for free-swimming, resulting in imperceptible changes in oxygen concentration. Understanding the metabolic costs of the biohybrid jellyfish robot is important to developing a complete understanding of the increased performance. Future work will aim to address this knowledge gap using a combination of flow measurements and respirometry. Longer-term experiments on timescales relevant to ocean exploration (i.e., weeks to months in duration) will be necessary to confirm the sustainability of the performance observed here, while continuing to ensure the long-term well-being of the jellyfish. Finally, jellyfish in these experiments swam vertically to focus on vertical profiling applications in the ocean. Future work will extend the maneuverability of the biohybrid robotic jellyfish to enable three-dimensional exploration.

The demonstrated ability to carry payloads could be utilized to investigate a variety of ocean science questions. Figure 8 explores some of the ways in which the mass and volume of the largest AR_3 hemi-ellipsoid forebody could be used to further ocean exploration. Several commercial off-the-shelf (COTS) wildlife trackers are shown in red, which include different combinations of sensors for parameters such as temperature, depth, light, and accelerometers for motion tracking (ORI400, Little Leonardo, Tokyo, Japan; MINIPAT, Wildlife Computers Inc, WA, USA; Daily Diary, Wildbyte Technologies Ltd, Swansea, United Kingdom). The forebody could instead be utilized as a large battery (power sources shown in orange), which could power the biohybrid robot for up to 22 weeks using a disposable 101.6 watt-hour lithium-metal battery (Bradley et al., 2001) or from 11 to 22 weeks using other

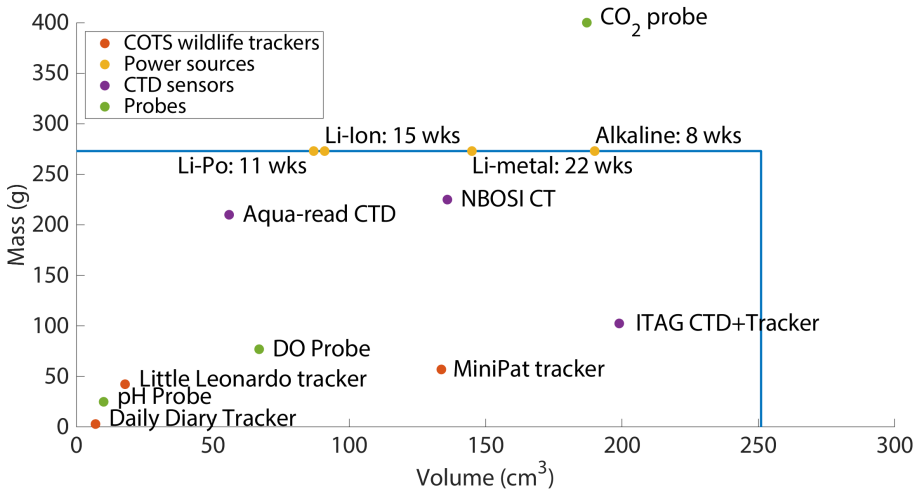

Figure 2.8: Figure 8. Utilizing biohybrid robotic jellyfish payload capacity for ocean science.
Demonstrated payload mass and volume capacity (i.e., blue boundaries) can be utilized for a variety of ocean science and exploration applications. COTS wildlife trackers with a variety of sensors are shown in red; power sources with approximate duration powering current electronics in yellow; CTD sensors shown in purple; and chemical probes in green. Filling the forebody with a lithium metal battery could power the biohybrid robot for more than 22 weeks.

battery types (Bradley et al., 2001; Manthiram, 2017). The relatively high energy density of lithium batteries could be exploited to preserve additional volume for less dense scientific payloads. For example, an onboard conductivity-temperature-depth (CTD) sensor, such as those shown in purple, could provide salinity and temperature measurements to inform ocean science models. Several COTS CTDs (LeveLine-MINI, AQUAREAD, Broadstairs, England; NBOSI CT, Neil Brown Ocean Sensors Inc., East Falmouth, MA, USA) could be accommodated within the forebody volume, as could a custom CTD with tracker from previous work (Mooney et al., 2015). The biohybrid robot could also be used for ocean chemistry profiling (shown in green) by embedding a dissolved oxygen (DO) probe (Kit-103DX, Atlas Scientific, Long Island City, NY, USA), or to study ocean chemical plumes using a pH probe (ENV-20-pH, Atlas Scientific, Long Island City, NY, USA). While currently too large to fit into the forebody volumes tested in this work, a CO_2 probe to aid in the understanding of carbon distribution in the ocean may fit in a future forebody design (CO_2 probe, Aquams, Maxeville, France). Deploying a combination of a larger battery and embedded sensors could power the biohybrid jellyfish robot for several weeks of exploration while recording using onboard sensors. Future work will

continue to optimize this platform for longer deployment durations and additional scientific sensors. This versatility enables a wide variety of possible ocean science and exploration initiatives, including improving ocean science models, investigating the concentrations of dissolved carbon dioxide, and studying the distribution of marine life in the ocean.

Future work could also investigate jellyfish behavior while undergoing stimulation. This could include studying potential changes in feeding behavior with embedded electronics, as well as probing for changes after stimulation terminates, and studying tissue healing around embedded electrodes over long time scales. There also exists an opportunity to study biohybrid robot jellyfish interactions with wild jellyfish through the field of animal-robot interactions (Romano et al., 2019).

This biohybrid robot itself can be fabricated for approximately $20 plus the cost of the jellyfish, which can be procured from local aquaria or collected from the ocean. Fabrication of the robot utilizes consumer-grade 3D printers and manufacturing methods without specialized equipment. Production and deployment of these robots can be easily scaled. This accessibility of the technology can democratize ocean exploration and make it feasible to deploy swarms of biohybrid robots for comprehensive ocean exploration on timescales commensurate with a changing ocean.

Acknowledgments

The authors would like to thank Cabrillo Marine Aquarium for providing the jellyfish used in these experiments.

Funding:

This work was supported by the National Science Foundation Alan T. Waterman Award and NSF Graduate Research Fellowship grant number DGE-1745301.

Author contributions:

S.R.A. and J.O.D. conceived of project, S.R.A. conducted experiments, S.R.A. and J.O.D. analyzed results and wrote paper.

Competing interests:

The authors declare that they have no competing financial interests.

Data and materials availability:

Contact J.O.D. for data and source code.

Chapter 3

NON-INVASIVE MEASUREMENT OF METABOLIC RATES OF FREE-SWIMMING JELLYFISH USING VOLUMETRIC LASER SCANNING

Abstract

Measuring energy consumption of marine organisms often requires enclosing the animal in a sealed chamber of similar volume to quantify changes in oxygen concentration of the surrounding water. This method limits measurements of free-swimming organisms without boundary effects or movement restrictions. We present energy consumption measurements of free-swimming jellyfish based on 3D morphological reconstructions of the animal during the process of catabolysis utilizing a non-invasive technique. We used a 6-meter tall, 13,600 liter water tank for swimming experiments without food present in the water column. To study continuous swimming, we implemented an onboard microelectronic swim controller that externally stimulated jellyfish swimming for 50 hours. Computer vision-based feedback control was used to enable continuous swimming against a flow current without encountering the vertical limits of the tank over a distance of 2.55 km or 15,000 body lengths. Using a 3D laser scanning system, we created morphological reconstructions of the jellyfish before, during, and after swimming experiments. Changes in animal volume were converted to energy consumption using the body chemical composition determined with elemental analysis. Free-swimming, electrically stimulated animals were found to consume 2.5 times more energy than similarly stimulated animals in a constrained environment, likely due in part to additional hydrodynamic drag associated with free-swimming. Simplified drag models could not fully account for the increased energy consumption. This highlights the need for hydrodynamic models that more effectively capture these dynamics. These measurements suggest that this technique could be applied more broadly to measuring free-swimming metabolic rates of other gelatinous invertebrates.

3.1 Introduction

Energy sourcing, consumption, and allocation are vital to maintaining life. Measuring energy consumption enables the prediction of an organism's performance and contributes to the characterization of survival, fitness, and phenology (Groot, Trueman, and Bates, 2024). Thus, accurate energy consumption measurements are important not only for understanding physiology but also organismal biology more broadly. A variety of techniques have been developed to measure the metabolism of marine organisms. The most common of these techniques, respirometry, measures the respiratory rate, which is a metabolic measurement of oxygen consumption commonly used as a proxy for energy consumption. Respirometry comprises three main techniques, each with associated benefits and drawbacks (Svendsen, Bushnell, and Steffensen, 2016). Closed system respirometry encloses the animal in a tank, generally of a similar size as the animal, and measures the decreasing oxygen concentration in the water as the animal respires (Keys, 1930). These systems are simple and ubiquitous, but avoiding hypoxic effects and the buildup of organic waste in the chamber limits experimental duration. Flow-through respirometry instead provides a continuous flow of water through the chamber and measures the difference in oxygen concentration at the inlet and outlet to calculate oxygen consumption. While this technique minimizes hypoxic effects, concerns of sensor issues, mixing, and waste buildup due to imperfect mixing persist. Finally, intermittent-flow respirometry combines periods of closed system respirometry with flushes of the chamber to eliminate both hypoxic effects and the buildup of waste (Svendsen, Bushnell, and Steffensen, 2016). However, all of these methods rely on changes in oxygen consumption measurable above background noise. In practice, each requires comparatively small experimental chambers, which introduce other confounding variables such as movement restriction and accompanying animal stress (Ikeda et al., 2000).

Other techniques attempt to avoid the limitations of small experimental chambers by studying animal energy consumption in situ. Doubly labeled water is the standard technique for terrestrial organisms and involves introducing hydrogen and oxygen isotopes to the animal whose elimination rates are then measured. However, this technique is not applicable to marine organisms due to high body water turnover rates making elimination rate measurements infeasible (Treberg et al., 2016). Biotelemetry, including electromyogram sensors and accelerometry, has been used to indirectly estimate energy consumption. These techniques are most applicable to large fish due to tag size and generally do not control for different types of activity. Like doubly

labeled water, isotopic trace turnover methods such as carbon isotopes consumed through feeding are valuable for energy consumption measurements. However, these techniques require extensive validation before application to measure decay curves for each species (Treberg et al., 2016). Vertebrates have calcium carbonate structures known as otoliths as part of the vestibular system. As the otolith grows with the animal, mineral layers are deposited in accordance with both environmental conditions and metabolic conditions. In bony fishes, the otolith-isotope method can identify metabolic rates through animal dissection and analysis. This method usually involves euthanizing the animal, limiting ongoing studies; gelatinous zooplankton have no similar structures for analysis (Groot, Trueman, and Bates, 2024). Although these techniques enable energetic measurements in more realistic free-swimming environments, their accompanying limitations make them unsuitable for gelatinous zooplankton.

Here, we develop, characterize, and implement a non-invasive technique that overcomes these limitations by inferring the energy consumption of free-swimming *Aurelia aurita* jellyfish medusae based on changes in body volume due to catabolysis. Catabolysis is the process by which an organism breaks down tissue when deprived of nutrients. Decreases in size during periods of catabolysis have been documented in many marine organisms, including fishes (Gingerich, Philipp, and Suski, 2010; Einen, Waagan, and Thomassen, 1998; Simpkins et al., 2003), flatworms (Gambino et al., 2024), and jellyfish (Lilley et al., 2014; Arai, 1986; Ishii and Båmstedt, 1998; Z. Fu et al., 2014). Previous work has shown starving *Aurelia aurita* jellyfish mass decreases by up to 13.4% per day (Ishii and Båmstedt, 1998), and some work predicts a derived respiratory carbon demand of more than 17% per day (Bondyale-Juez et al., 2022). One study inferred metabolic rates from average mass changes of *Aurelia aurita* ephyrae to estimate the respirometry rate. However, this study relied on euthanasia as part of their protocol for measuring animal mass, limiting the applicability of this technique (Z. Fu et al., 2014). Recent developments in volumetric (3D) laser scanning enable detailed 3D reconstructions of gelatinous zooplankton (M. K. Fu, Houghton, and John O. Dabiri, 2021; Daniels, Sainz, and Katija, 2023). This allows for measurements of changing body size due to catabolysis while in situ, which can be converted to energetic consumption rates (Harris, 1999).

One important confounding variable in energetics is the activity level of the animal. Jellyfish pulse rate, and thus metabolism, varies significantly based on environmental

conditions and animal morphology (Tills et al., 2016; Dillon, 1977; McHenry and Jed, 2003). In order to control this variable, we utilized onboard electrical stimulation (Nicole W. Xu and John O. Dabiri, 2020) to fix the animal pulse rate at a defined frequency across animals and throughout the duration of the test.

In this paper, we first describe the calibration and validation of the volumetric measurements obtained from the 3D laser scanning technique with wet weight measurements. Volumetric changes due to catabolysis detected by the laser scanning system were related to respiratory rate using established relationships in the literature and verified against closed-system respirometry measurements for both naturally swimming and electrically stimulated swimming. We conducted body composition measurements to inform this relationship. This technique was then utilized for free-swimming measurements of electrically stimulated jellyfish. Testing over swimming durations greater than 15,000 body lengths enabled assessment of long-term changes in metabolism during catabolysis. We compared these measurements against predictions from a physics-based energetics model and basal metabolism experiments.

3.2 Materials and Methods

Animal husbandry

Aurelia aurita medusae were obtained from Cabrillo Marine Aquarium (San Pedro, CA, USA) and Aquarium of the Pacific (Long Beach, CA). They were housed in a 453 liter pseudokreisel tank (Jelliquarium 360, Midwater Systems, Thousand Oaks, CA, USA). The tank was filled with artificial seawater mixed with sea salt (Instant Ocean Sea Salt, Spectrum Brands, Blacksburg, VA, USA) and deionized water at 35 parts per thousand (ppt) and kept at 21°C. The jellyfish were hand-fed twice daily with live *Artemia franciscana* brine shrimp (Hatching Shell-Free Brine Shrimp Eggs E-Z Egg, Brine Shrimp Direct, Ogden, UT, USA). Brine shrimp were hatched every other day in aerated hatchery cones of artificial seawater heated to 28°C for 24 hours, then transferred to beakers at 21°C. Brine shrimp were fed PHYTO-Feast (Reef Nutrition, Reed Mariculture Inc., Campbell, CA) and enriched with SELCO (Self-Emulsifying Lipid Concentrate, Brine Shrimp Direct, Ogden, UT, USA).

Laser scanning for volumetric reconstruction

Volumetric reconstructions of the jellyfish were created using a single-camera laser scanning system (Fig. 1A). This system used a 671 nm continuous laser (5 W Laserglow LRS0671 DPSS Laser System) and a series of optics to generate a

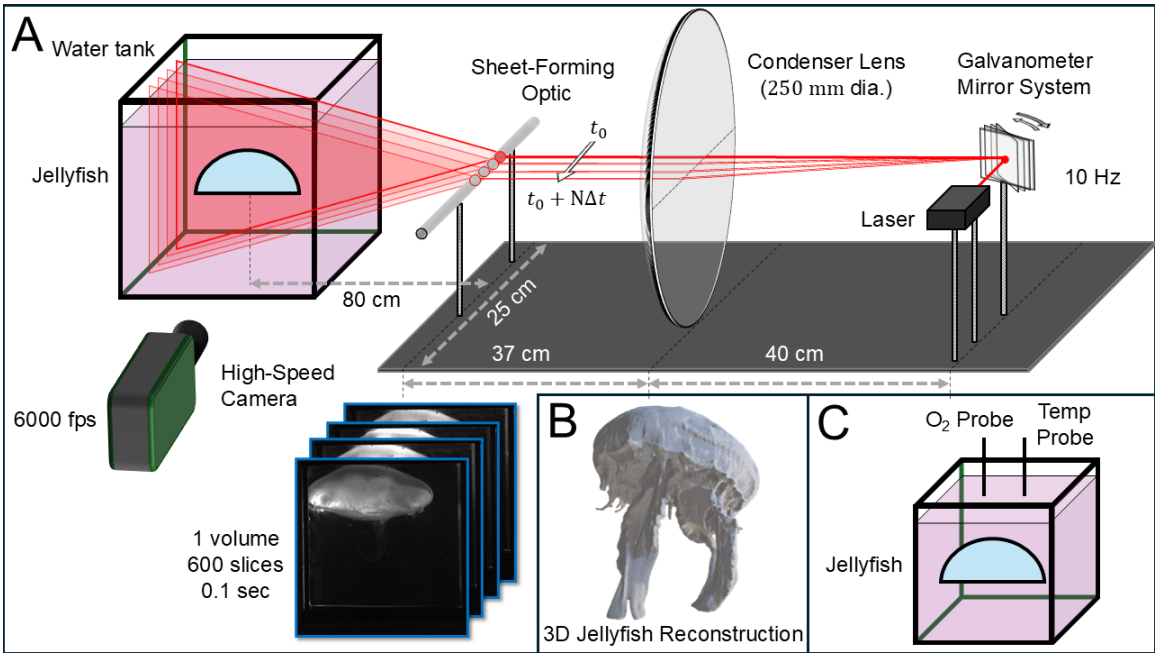

Figure 3.1: Laser scanning system for volumetric reconstructions. (A) Diagram of laser scanning system with laser, galvanometer rotating at 10 Hz, 250 mm diameter condenser lens to redirect the laser normal to the scanning direction, cylindrical glass rod to form the laser beam into a thin sheet, water tank, and jellyfish. As the laser scanned across the jellyfish, a high speed camera recorded an image stack, or "volume", of 600 slices every 0.1 s. (B) A representative 3D volumetric reconstruction of a live jellyfish. (C) Closed system respirometry setup used to validate laser scanning technique. Jellyfish oxygen consumption was measured using an O_2 probe and temperature probe over time in a sealed chamber. Figure adapted with permission from M. K. Fu, Houghton, and John O. Dabiri (2021).

scanning laser sheet. The optics consisted of a mirror mounted on a rotating galvanometer (Thorlabs GVS211/M, 10 kHz bandwidth) controlled with an arbitrary function generator (Tektronix AFG3011C) to sweep across the volume of inquiry at 10 Hz; a 25 cm diameter condenser lens to redirect the laser normal to the scanning direction; and a cylindrical, 16-mm diameter glass rod used to form the laser beam into a thin sheet. The laser sheet was set to sweep normal to its plane across a distance of 11.7 cm. A high-speed camera recording at 6000 fps (Photron FASTCAM SA-Z) thus captured 600 1024 x 850 pixel or 22.5 x 18.7 cm 2D images for each scan. A custom MATLAB code was written to reconstruct the jellyfish from these image stacks. The code identified the jellyfish and performed binarization, thresholding, and morphological opening and closing operations to create a detailed reconstruction (Fig. 1B).

Validation of volumetric reconstruction

Experiments were performed to characterize the accuracy and precision of the laser scanning technique. To measure the relationship between volumetric reconstructions and wet weight of jellyfish, 10 jellyfish were scanned and weighed to compare wet weight (WW) and laser scanned weight (LSW). Each jellyfish was first scanned using the procedure described in this section. Then, they were carefully removed from the tank, patted dry to remove additional water, and weighed on an electric balance (Eosphorus Sf-400C, 600 g range, 0.01 g precision).

Energetic consumption from volumetric changes

This laser scanning technique used repeated laser scans and volumetric reconstructions over several hours to convert a change in volume due to catabolysis to an average energy consumption rate for each jellyfish. In order to validate this conversion, simultaneous laser scanning and closed system respirometry experiments were performed. The jellyfish was scanned and reconstructed using the procedure described in this section and immediately transferred to a 15.1 liter closed respirometry chamber filled with artificial seawater at 35 ppt (Fig. 1C). An oxygen probe (OPTO-430, Unisense, Denmark) and temperature sensor (TEMP-UNIAMP-7, Unisense, Denmark) were used to continuously measure the oxygen concentration at a sampling frequency of 0.1 Hz. After 24 hours, the animal was removed, scanned, and the artificial seawater in the respirometry chamber was flushed and replaced. The animal was returned to the respirometry chamber for a second 24 hour respirometry measurement. Finally, at 48 hours from experiment initiation, the animal was removed, scanned, and the experiment was completed. The respirometry chamber was chosen to be large enough that the animal avoided hypoxic conditions over the course of the experiment. This experiment was repeated for 3 animals. Oxygen consumption in an empty respirometry chamber was measured, and background oxygen consumption was subtracted from experimental results. A linear fit to the data was used as the average respiratory rate (RR). These values were compared with literature values for *Aurelia aurita* wet weight (WW) given by

$$RR = 0.0765 WW^{1.038} \tag{3.1}$$

(S. Uye and Shimauchi, 2005).

The method to convert the measured change in laser-reconstructed animal size to

an energetic rate was based on earlier animal physiology work (Ikeda et al., 2000). The respiratory rate is defined as

$$RR = \frac{\Delta V \rho C}{RQa} \tag{3.2}$$

in terms of the change in volume of the animal ΔV, tissue density ρ, tissue carbon content C, respiratory quotient RQ, and a unit conversion term a. The change in volume ΔV was measured using the laser scanning method described in this section. Since jellyfish are neutrally buoyant and approximately 96% water (S. Uye and Shimauchi, 2005), ρ was assumed to be equal to the density of seawater $\rho = 1024$ kg m^{-3} at 35 ppt and 21°C. We experimentally measured the tissue carbon content C of 9 *Aurelia aurita* as described in the following section. The respiratory quotient RQ depends on the type of tissue metabolized and represents the ratio of carbon dioxide produced to oxygen consumed. For jellyfish, we used a range $RQ = 0.8-0.9$ since they metabolize primarily protein (S. Uye and Shimauchi, 2005; Ikeda et al., 2000). Uncertainty in these input parameters was propagated to provide error bounds for metabolic estimates. Previous work reports that the weight specific respiratory rate of *Aurelia aurita* does not change with starvation state, (Frandsen and Riisgård, 1997) suggesting equation 3.2 does not need to be corrected for starvation state. We normalize all RR by animal WW in grams to allow comparisons across animal morphology.

Carbon content

Tissue carbon content, C, was experimentally measured for 9 animals to measure body composition changes while undergoing catabolysis (figure 3.2). The animals were transferred to a clean 108 liter artificial seawater tank without food. Three animals were randomly selected for removal at each timestep of 0 hours, 25 hours, and 50 hours after the experiment start. Each animal was patted dry, WW measured on an electric balance, and transferred to an electric oven where they were dried at 60-65°C until a constant weight was achieved. Dried samples were pulverized in a mortar and pestle and weighed. Samples were then analyzed for carbon and nitrogen content on an elemental analyzer (Santa Barbara Marine Science Institute Analytical Lab, CEC 440HA, Control Equipment Corp., MA, USA). These experiments did not show statistically significant changes in carbon content over 50 hours without feeding. We found an average carbon content of 0.105% ± 0.026% of WW, which is not statistically different from the 0.13% ± 0.06% reported in the literature (S.

Uye and Shimauchi, 2005). We used the value measured in the present experiments for the laser scanning method calculations. Analysis showed an average carbon-to-nitrogen ratio of 3.64 ± 1.26 which is not statistically different from the literature value of 3.71 ± 1.63 (S. Uye and Shimauchi, 2005).

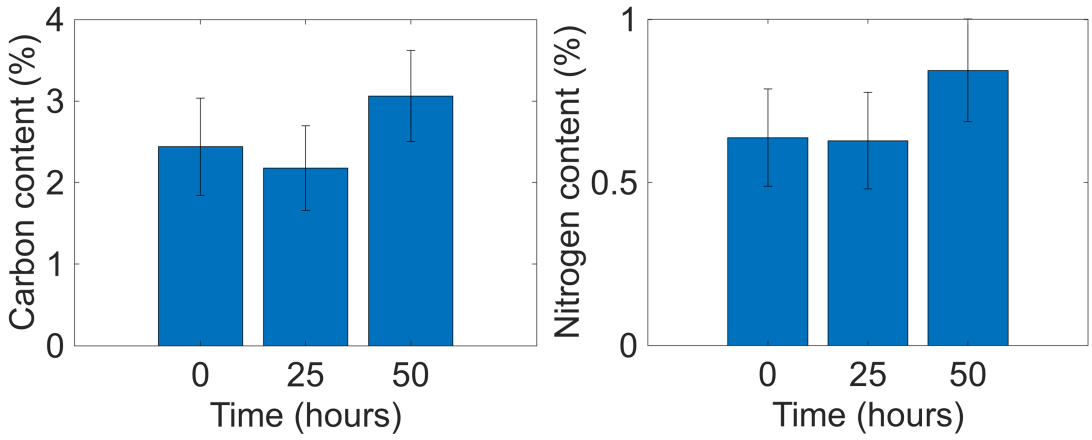

Figure 3.2: Body composition over time. (A) Measured carbon content of 9 jellyfish with 3 each at 0, 25, and 50 hours of starvation shows no statistically significant change in these variables. (B) Measured nitrogen content also shows no change.

Electrical stimulation for continuous swimming

Figure 3.3A shows the electronics for onboard electrical stimulation embedded in a model jellyfish. The system consists of a swim controller enclosed in a custom 5.10 ± 0.03 cm diameter electronics housing, two electrodes embedded in the jellyfish muscle tissue, a threaded plastic rod, and a ballasting cap. The swim controller includes a small processor (TinyLily, TinyCircuits, Akron, OH, USA) and a 250 mAH lithium-polymer battery cell (GM602025-PCB, PowerStream Technology Inc., Orem, UT, USA). All parts of the electronics housing and ballast were fabricated via stereolithography (Form 3 Color Base Resin) on a Form 3+ resin printer (Formlabs, Somerville, Massachusetts). The swim controller housing utilized a threaded cap with two O-rings for waterproofing at high pressure. Wire coated in perfluoroalkoxy was threaded through small holes in the housing and connected to platinum rods (A-M Systems, Sequim, WA, USA) embedded in the animal muscle tissue. The pass-throughs were sealed with epoxy, and an LED was connected in series to each electrode to provide visual confirmation of stimulation. The ballasting cap passively maintains vertical downward swimming and could house future sen-

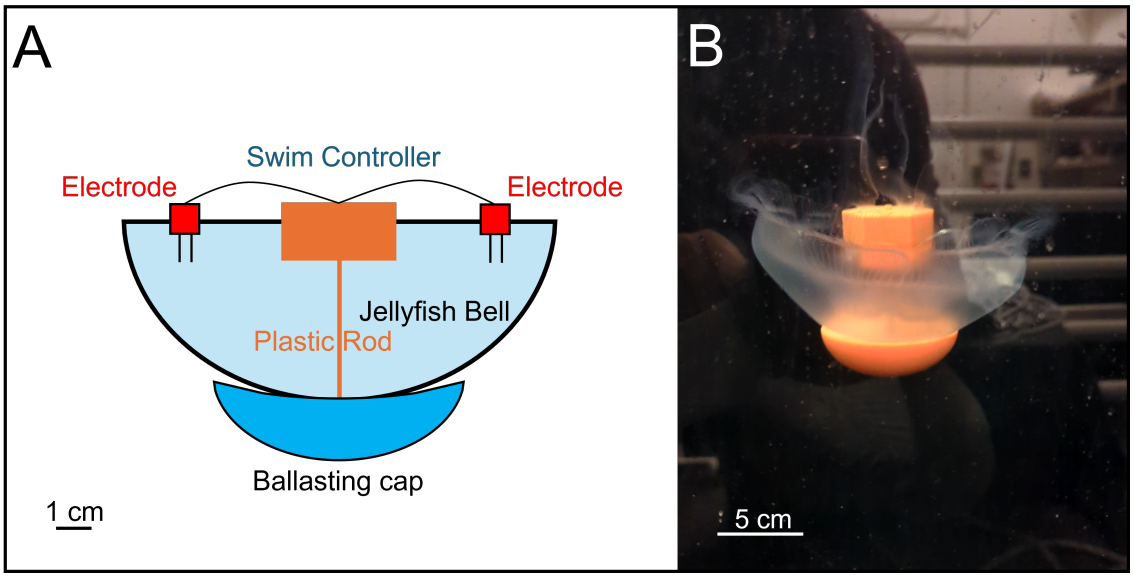

Figure 3.3: Jellyfish with embedded electronics for electrical stimulation at constant pulse rate. (A) Diagram of electronics with swim controller housing TinyLily microprocessor with 250 mAH battery, two electrodes embedded in bell margin stimulating at 0.5 Hz, plastic rod to connect components, ballasting cap to passively maintain downward vertical swimming, and 1 cm scale bar. (B) Electronics embedded in live jellyfish during continuous swimming experiment with 5 cm scale bar. This Figure was adapted from Anuszczyk and Dabiri, 2024.

sors. See previous work (Anuszczyk and John O. Dabiri, 2024) for more details on electronics and ballasting cap design and impact on swimming performance. Figure 3.3B shows the electronics stimulating a swimming jellyfish in the lab environment. The simultaneous laser scanning and respirometry experiments described in this section were additionally performed with 3 electrically stimulated animals.

Long duration stimulated free-swimming experiments

The laser scanning method was utilized to measure the free-swimming energy consumption of electrically stimulated, continuous swimming jellyfish in a 6-m tall, 13,600-liter vertical tank (Figure 3.4A). The tank was filled with artificial seawater balanced at 35 ppt and 21°C and has a continuous filtration pump, which was turned off at least 2 hours before these experiments. This tank is divided into a test section on the right, where experiments are conducted, and a recirculation region on the left with water pumps (A1200, Abyzz, Germany). This enabled continuous flow, shown with red arrows, through the test section functioning as a "flow treadmill." During long-duration swimming experiments, a jellyfish was equipped with stimulation electronics, weighted to maintain slight positive buoyancy

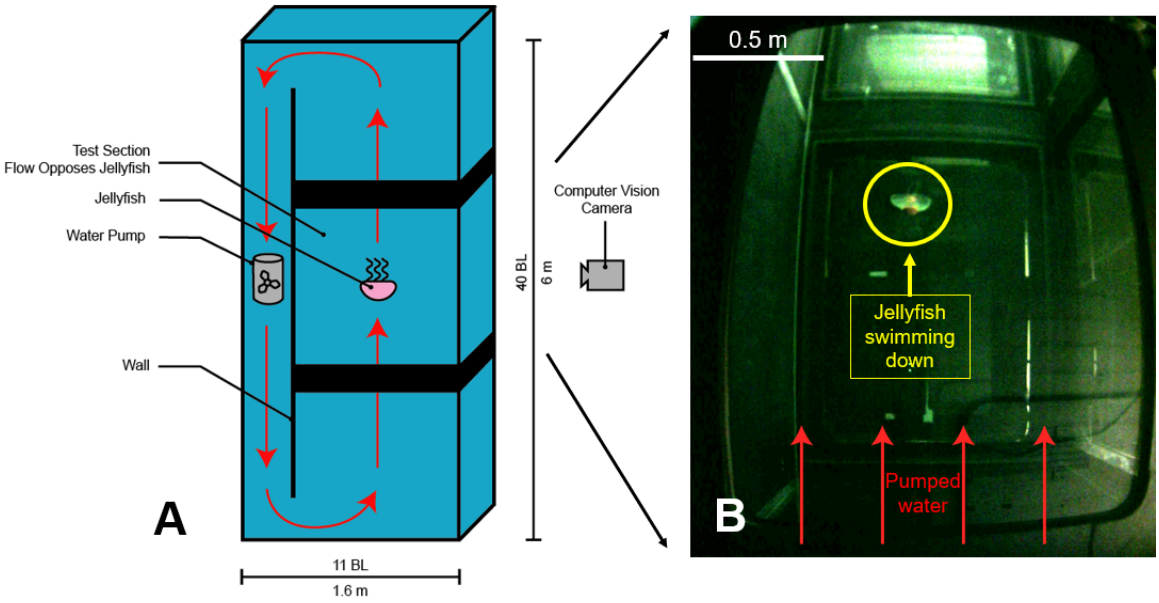

Figure 3.4: Free-swimming tank for long-duration experiments. (A) Diagram of 6 m by 1.6 m artificial seawater vertical tank facility. Water pumps in the recirculation area on the left generated flow (shown with red arrows), which opposed free-swimming jellyfish. A computer vision camera tracked the swimming animal. (B) The view from the computer vision camera of the middle section of the tank as a jellyfish, circled in yellow, swam downward. As the jellyfish descends, the camera ran a PID control loop interfacing with the water pumps to control the flow, keeping the animal in view of the camera.

with a stable downward orientation, and released at the top of the tank to swim downwards. A camera microprocessor (RT1062 Cam, OpenMV, Atlanta, GA, USA), set back 0.86 m from the tank, was programmed with a custom MicroPython computer vision algorithm. This computer vision camera tracked the animal location during continuous swimming and was programmed to interface with the water pumps while running a proportional-integral-derivative control loop. Figure 3.4B shows the view from the camera of the middle section of the tank as a jellyfish was swimming downwards. As the animal descends in the tank, the controller continuously adjusts the flow opposing the jellyfish with an optimization goal of keeping the animal within the middle section of the tank and in view of the camera. The computer vision camera was programmed to track both the animal location and the pump power. Particle Image Velocimetry (PIV) was conducted to calibrate pump power to pump flow speed and confirm flow uniformity. Animal swimming speed was found by combining the movement of the animal in the lab frame with the pump flow speed. During the course of the 50 hour experiments, the animal was occasionally out of frame for brief periods. These periods were removed when

calculating swimming metrics for speed and distance.

Basal metabolism

The total metabolism of free-swimming animals comprises both the metabolic requirements to maintain swimming and basal metabolism for other physiological processes. Additional experiments were conducted to quantify the basal metabolic component of the total metabolic measurements. To the best of our knowledge, these are the first measurements of the basal metabolism of jellyfish without animal movement. Basal metabolic experiments were performed using a 2.55 liter glass respirometry chamber and the oxygen probe and temperature sensor described in this previous section with 6 animals. Two methods were investigated successively: anesthetization with magnesium chloride ($MgCl_2$) to suppress muscle movement and excision of the nerve centers, or rhopalia, of the animal in order to arrest endogenous swimming signals. Excising rhopalia has been shown to arrest normal contractions (Romanes, 1885; Satterlie, 2002), and the animals were observed to not contract for the duration of this experiment after excision. Each animal was transferred to the respirometry chamber filled with artificial seawater, where they underwent five distinct treatments of 1 hour each. This enabled testing of both methods and comparison with natural respiration rates. First, the chamber was closed, and the normal respiration rate was measured. Next, the animal was removed and $MgCl_2$ (AC413410025, Fisher Scientific, Waltham, MA, USA) was added at a molarity of 0.3 M. The $MgCl_2$ was mixed for 5 minutes until dissolution, and the animal was added for the anesthetization test. Upon completion, the water was then exchanged for clean artificial seawater, and a second normal respiration rate was measured to ensure the animal had fully recovered from anesthetization. The same animals were then used to test the excision method. Respiratory rate was measured again for the immobilized jellyfish after excision. The animal was again removed from the tank, the water was replaced with the $MgCl_2$ solution, and respiratory rate was measured combining both anesthetization and excision methods. While both anesthetization and excision methods were tested, we report results from the excision method here due to potential confounding impacts of $MgCl_2$ with animal tissue on oxygen consumption.

Swimming metabolism model

We derived a physics-based quasi-steady swimming metabolism model based on previous work (John O. Dabiri, S. P. Colin, and Costello, 2006; Acuña, López-

Urrutia, and S. Colin, 2011). Here, we model the jellyfish energy consumption $\frac{dE}{dt}$ as the sum of the basal metabolism P_{basal}, the power expended setting the surrounding water into motion while swimming P_{wake}, and the hydrodynamic drag on the free-swimming animal P_{drag}

$$\frac{dE}{dt} = P_{basal} + P_{wake} + P_{drag} \tag{3.3}$$

We model the water motion created by the animals while swimming as primarily comprising a vortex ring. Following previous work (John O. Dabiri, S. P. Colin, and Costello, 2006), we approximate its kinetic energy as that of an equivalent oblate spheroid of water set into motion each time the jellyfish pulses and generates a vortex ring. We use the classical kinetic energy formula for the kinetic energy contained in the wake,

$$KE_{wake} = \frac{1}{2} M U_{wake}^2 \tag{3.4}$$

where M is the mass of water set in motion and U_{wake} is the speed at which this wake convects. The mass is given by $M = \rho V$ where seawater density $\rho = 1024$ kg m^{-3} at 35 PPT and 21°C, and the volume $V = \frac{4}{3}\pi R^2 h$ where R is the radius of the animal and h is the semi-minor axis of the spheroid. As the vortex ring is accelerated, it accelerates the surrounding fluid, necessitating an added mass term C_{am}. We also introduce an effective swimming efficiency term η to account for energy lost in physiological processes that convert body motion to fluid motion leading to

$$KE_{wake} = \frac{2}{3\eta} \rho \pi R^2 h (1 + C_{am}) U_{wake}^2 \tag{3.5}$$

Power is the time rate of change of kinetic energy. *Aurelia aurita* generate two vortex rings with each swimming cycle (Gemmell et al., 2013). Thus, we assume that the kinetic energy for two vortex rings is expended with each swimming cycle. Hence,

$$P_{wake} = \frac{4}{3\eta} \rho \pi R^2 h (1 + C_{am}) U_{wake}^2 f_{pulse} \tag{3.6}$$

where f_{pulse} is the pulse frequency. We model the drag on the free-swimming jellyfish as the product of the drag force and the swimming speed divided by effective swimming efficiency

$$P_{drag} = \frac{1}{2\eta} C_D \rho S U_{swim}^3 \tag{3.7}$$

with C_D the drag coefficient for the jellyfish, S the projected planform area in the direction of swimming, and U_{swim} the swimming speed of the animal. Thus, combining equations 3.6 and 3.7 into 3.3 becomes

$$\frac{dE}{dt} = P_{basal} + \frac{\rho}{\eta}[\frac{4}{3}\pi R^2 h(1 + C_{am}) U_{wake}^2 f_{pulse} + \frac{1}{2} C_D S U_{swim}^3] \tag{3.8}$$

Jellyfish geometry was measured to determine R, and h was estimated as $h = 0.4R$. The stimulated rate was set by the electronics at $f_{pulse,stim} = 0.5$ Hz, and previous work found jellyfish natural pulse rates of $f_{pulse,nat} = 0.16$ Hz (Nicole W. Xu and John O. Dabiri, 2020). While previous studies report hydrodynamic efficiencies on the order of $0.2 - 0.4$ (Acuña, López-Urrutia, and S. Colin, 2011; Sahin, Mohseni, and S. P. Colin, 2009), these values do not account for internal energy losses within the animal, including viscoelastic dissipation and muscle inefficiency. Accordingly, we use a range of $\eta = 0.1 - 0.3$ as a representative effective swimming efficiency. C_{am} was assumed to be 1, and for a flat plate $C_D = 1.12$ (Hoerner, 1967). The wake convection speed U_{wake} was approximated as the contraction velocity of the bell margin, measured by analyzing a naturally pulsing animal, and U_{swim} for the free-swimming experiments was measured as described in this section. To compare with respirometry data, we assumed 447 kilojoules per mole of oxygen consumed for protein, 12/22.4 is the weight of carbon in 1 mole of carbon dioxide (Ikeda et al., 2000), and there are 2.4×10^4 ml per mole of oxygen (Garcia and Gordon, 1992). To normalize by wet weight mass, the relation

$$WW = 0.547 R^{2.86} \tag{3.9}$$

was used (S. Uye and Shimauchi, 2005).

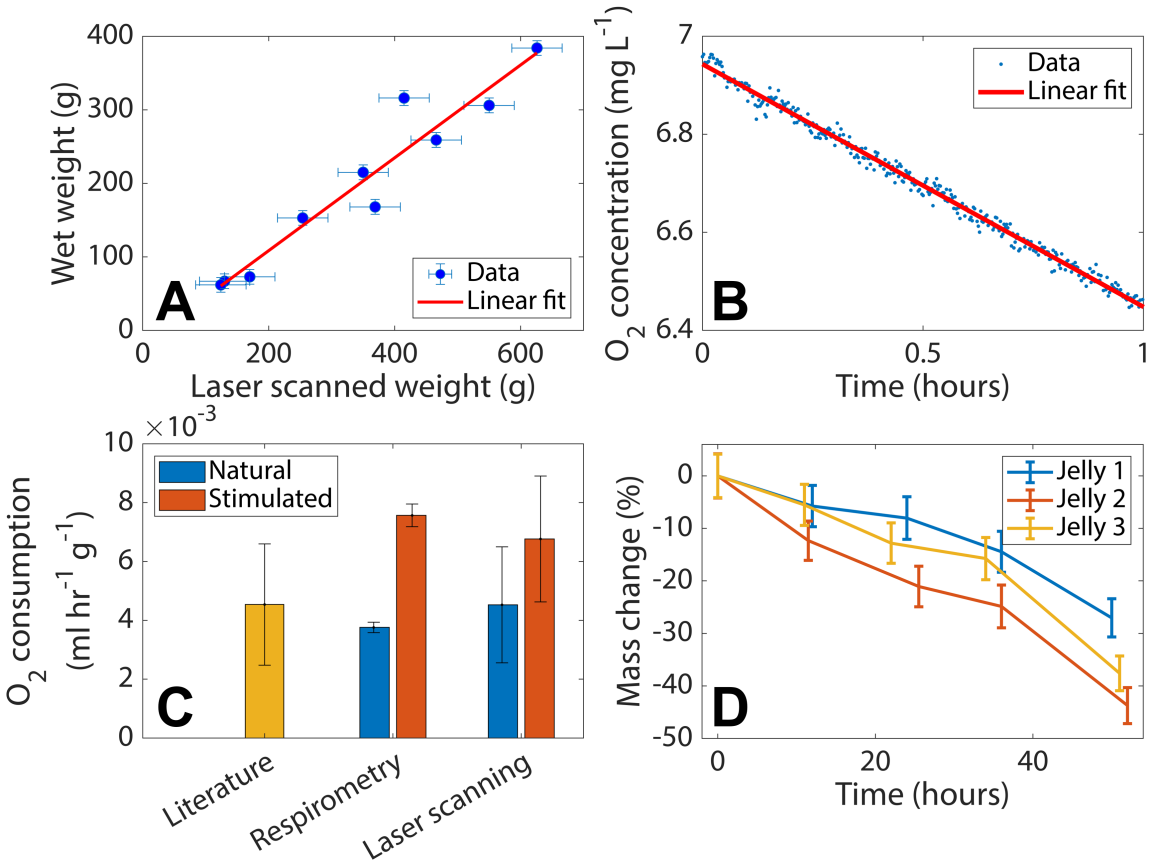

Figure 3.5: Validation of laser scanning technique for energy measurements. (A) Linear relationship between wet weight (WW) and laser scanned weight (LSW) of $WW = 0.63LSW - 17.66$ for 10 animals. (B) A sample 1 hour closed system respirometry experiment with linear fit and R-squared value of $R^2 = 0.9921$. This high R-squared value confirms the linearity of jellyfish oxygen consumption over 1 hour. (C) Literature values for natural animals compared with simultaneous closed system respirometry and laser scanning. There is no statistical difference between the oxygen consumption rates found with the two different techniques. Oxygen consumption is given in terms of ml O_2 per hour per g wet weight. (D) We deployed this technique to measure free-swimming metabolism during 50 hour experiments for 3 jellyfish. The jellyfish lost 36% ± 8.4% of their mass on average over the course of this experiment. All error bars represent 1 standard deviation.

3.3 Results

Laser scanning technique validation

We compared wet weight (WW) to laser scanned weight (LSW) to validate this technique. Figure 3.5A shows the linear relationship between the measured WW and LSW of $WW = 0.63LSW - 17.66$ with $R^2 = 0.9256$ for 10 animals of different sizes. The LSW overestimated the WW of the animal, likely due to the scattering of the laser sheet through the tissue. This well-defined relationship enabled us to

convert accurately between WW and LSW.

Simultaneous laser scanning and respirometry experiments confirmed the accuracy of this method. Figure 3.5B shows a representative 1 hour respirometry experiment. A linear fit to this data has an R-squared value of $R^2 = 0.9921$ and illustrates the linear trend in oxygen consumption over the course of these experiments. The literature bar represents the wet weight normalized oxygen consumption for an animal of the same size as those used in the respirometry and laser scanning experiments shown in Figure 3.5C. This was found using equation 3.1 with the error given as ± 1 standard deviation. The respirometry bar compares the animal's natural and electrically stimulated respiratory rate we measured in the respirometry chamber with the error given by ± 1 standard deviation of the linear fit to the respirometry data. The laser scanning bar in Figure 3.5C also compares naturally swimming animals to electrically stimulated animals measured with the laser scanning method. This error represents ± 1 standard deviation and combines the errors in scanning and equation 3.3. Electrically stimulated animals were found on average to consume 73% ± 32% more energy than naturally swimming animals in this confined configuration.

These experiments validate that the observed laser scanning respiratory rate from catabolysis, calculated using equation 3.2, corresponds to measurements from the respirometry chamber. The blue "Natural" bars have no statistically significant difference with a two-tailed t-test p-value of 0.44. Similarly, the red "Stimulated" bars have no statistically significant difference with a two-tailed t-test p-value of p=0.60. This confirms that although the laser scanning method has a higher error compared to the respirometry chamber, the two methods are in agreement and the technique is suitable for further experiments.

Long duration stimulated free-swimming experiments

We utilized this laser scanning technique to measure the free-swimming metabolism of 3 electrically stimulated, continuously swimming jellyfish in a 6-m tall vertical tank. Figure 3.5D shows the mass change of each animal as a percent of the mass at the previous timestep. The error here is found by scanning an animal multiple times and taking the mean and standard deviation of the resulting measurement. The continuously swimming animals lost a mean of 36% ± 8.4% of their mass over the course of 50 hours, which is in line with previous results on starvation (Ishii and Båmstedt, 1998). The starting masses of the animals found from scanning were $m_{jelly,1} = 470 \pm 19$ g, $m_{jelly,2} = 347 \pm 14$ g, and $m_{jelly,3} = 536 \pm 21$ g. We found

that the animals swam a mean distance of 2.55 ± 0.46 km while in view of the computer vision camera at speeds of 2.44 ± 0.60 cm s^{-1}. Previous results showed similar electrically stimulated swimming speeds over much smaller timescales on the order of minutes (Anuszczyk and John O. Dabiri, 2024).

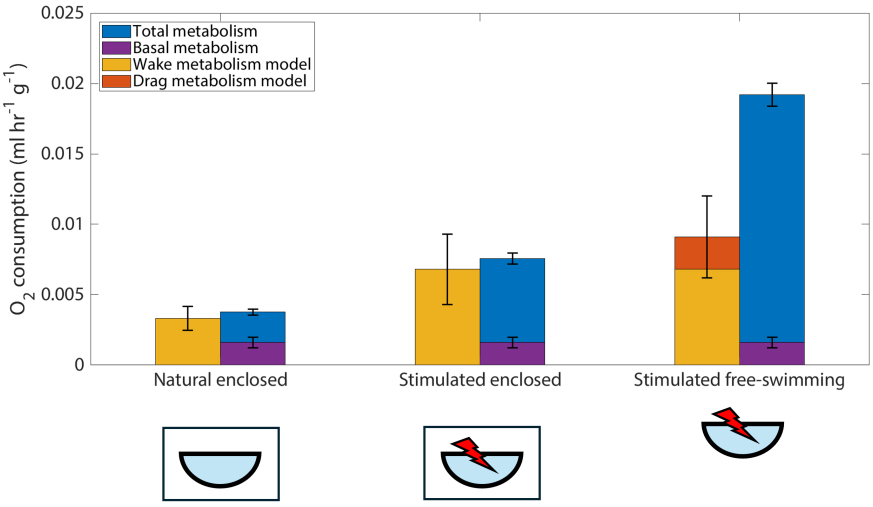

Figure 3.6: Free-swimming energy consumption and metabolism model. Total metabolism, shown in blue, in enclosed configurations here was measured using closed respirometry; free-swimming total metabolism was measured using the laser scanning technique. Stimulated free-swimming jellyfish consume 2.5 times as much energy as stimulated enclosed animals. Diagrams represent jellyfish in each configuration. We measured basal metabolism, shown in purple, by excising rhopalia as 42% ± 10% of jellyfish natural swimming energy consumption. The wake metabolism model, in yellow, representing the energy to set water in the wake into motion, underestimates energy consumption. Adding a steady drag metabolism term, in red, for the free-swimming jellyfish continues to underestimate the energy consumption. Oxygen consumption given in terms of ml O_2 per hour per g wet weight.

Free-swimming experiments showed increased energy consumption. Figure 3.6 compares the energetic costs of swimming jellyfish in the three different configurations tested. The blue bars represent the total metabolism. In the "Natural enclosed" configuration and the "Stimulated enclosed" configuration, this was measured in the respirometry chamber with the oxygen probe, and in the "Stimulated free-swimming" configuration using the laser scanning technique in the vertical tank. We found that the free-swimming animal consumes 2.5 times more energy, normalized by body mass, than the stimulated animal in the enclosed respirometry chamber. This increase in energy consumption is likely due to a combination of hy-

drodynamic effects. Because hydrodynamic power scales as the cube of swimming speed (Daniel, 1983), small increases in speed result in disproportionately higher energetic costs. The increase in swimming speed from nearly zero in the enclosed configurations to 2.44 ± 0.60 cm s^{-1} in the free-swimming configuration would thus increase the hydrodynamic power expended. In addition, recirculation in a small respirometry chamber reduces the force required to contract the bell, suggesting that the same movement might require more energy during free-swimming.

We found an average basal metabolism of $P_{basal} = (1.6 \pm 0.4) \times 10^{-3}$ ml O_2 hr^{-1} g^{-1} which constitutes 42% ± 10% of jellyfish natural swimming energy consumption based on our experiments with rhopalia excision. This is shown in Figure 3.6 in purple for each test configuration. This aligns with previous work for *Stomolophus meleagris* which found a basal metabolic rate of 50% (R. J Larson, 1987a) and as expected, this result is more efficient than some fish, e.g. tuna species *Katsuwonus pelamis*, with a basal metabolism that constitutes 58% of natural swimming total metabolism (Brill, 1987). Jellyfish are known to be among the most efficient metazoans in terms of cost of transport (COT), defined as the mass-specific energy per distance traveled (Gemmell, Costello, et al., 2013). Their low basal metabolism compared to other species suggests that their efficiency is not only due to efficient swimming as previously proposed. Instead, the low COT is also due to highly efficient essential physiological functions that make up basal metabolism, such as digestion and reproduction.

Our swimming metabolism model is shown in Figure 3.6 in orange alongside each configuration with error bars representing a range of effective swimming efficiencies. The drag term is only shown for the free-swimming animal in red, as described in Methods. This model generally captures the trends of the "Natural enclosed" and "Stimulated enclosed" configurations. However, it struggles to account for the large increase in energy consumption of the free-swimming animal, necessitating additional investigation.

3.4 Discussion

We have presented measurements of electrically stimulated free-swimming jellyfish total metabolism that we found to be 2.5 times higher than similarly stimulated animals in a closed respirometry chamber. This method of measuring metabolic rates utilizes laser scanning of jellyfish, which we calibrated and validated through additional experiments. Basal energy consumption measurements showed that jel-

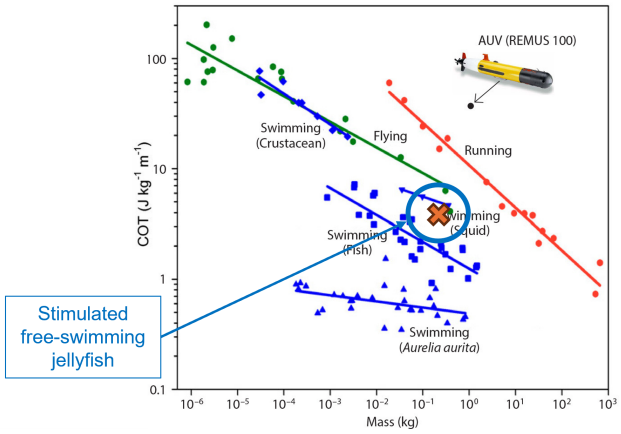

Figure 3.7: Cost of Transport of stimulated jellyfish compared to other animals. While natural jellyfish are the most efficient metazoans (Gemmell, Costello, et al., 2013), the increase in energy consumption found with the laser scanning technique increases the COT. Thus, these jellyfish have a COT comparable to swimming fish, as shown with the orange x. This COT is more than an order of magnitude smaller than a representative autonomous underwater vehicle (AUV), the REMUS 100. Figure adapted with permission from Gemmell, Costello, et al. (2013).

lyfish consume 42% ± 10% of total energy consumption for physiological functions other than swimming.

Converting the increased energy consumption into cost of transport (COT) shows that free-swimming stimulated jellyfish energy consumption is on a similar scale as swimming fish (Figure 3.7). Since this study utilized increased pulse rates, this COT suggests that one contributor to natural jellyfish efficiency is less frequent pulse rates, which often correspond to periods of coasting between pulses. Further investigation by conducting metabolic experiments with lower frequency stimulation could clarify the impact of pulse rate on COT.

Experimentally measuring the total metabolism of electrically stimulated jellyfish enables further work developing this platform for ocean exploration. Previous work found portable electrical stimulation combined with an exumbrellar ballasting cap increases animal swimming speeds by up to 4.5 times natural swimming speeds (Nicole W. Xu and John O. Dabiri, 2020; Anuszczyk and John O. Dabiri, 2024). These stimulated animals are capable of carrying scientific payloads of up to 105% of animal mass in this ballasting cap, enabling the carrying of a variety of scientific sensors to study the biogeochemistry of the ocean (Anuszczyk and John O. Dabiri, 2024). Field tests have demonstrated vertical profiling capability in oceanic conditions near the top of the water column (Nicole W. Xu, Townsend, et al. (2020b)

and Rutledge et al. (2026), in review). Our results show that stimulated animals can swim more than 2.55 km or 15,000 body lengths, which could enable deeper deployment as ocean sensors. Since these continuous swimming experiments were performed in the top 6-m of the water column, deeper deployments would be contingent upon experiments to ensure both the animal and electronics can sustain higher pressures. While the increased COT is higher than natural animals, this COT is more than an order of magnitude smaller than a representative AUV, and thus far more efficient than traditional methods of ocean exploration.

One remaining question on the feasibility of deep ocean deployments of this platform is if zooplankton distribution and animal clearing rates will provide sufficient feeding opportunities to avoid significant catabolysis. Zooplankton distribution research in the Beaufort Sea of the Arctic Ocean suggests that biovolume peaks at around 50-100 meters depth. However, some zooplankton such as *Chaetognaths* and other gelatinous zooplankton were found at high biovolume densities at 1000 m, the depth limit of this study (Forest et al., 2012). This suggests that jellyfish deployed to these depths may find different but sufficient feeding opportunities. Future work could incorporate feeding at different spatial densities into similar studies to experimentally study jellyfish ability to feed during electrical stimulation.

We developed a model that generally captures the energy consumption trends observed experimentally. After subtracting basal metabolism, the measurements of energy consumption increase by a factor of 2.8 between the natural and stimulated enclosed configurations. This closely corresponds with the increase in pulse rate $\frac{f_{pulse,stim}}{f_{pulse,nat}} = 3.1$ suggesting that energy consumption per pulse is relatively constant across pulse rates in an enclosed configuration. Therefore, this model underestimated the energetic consumption associated with each pulse, in all configurations, potentially due to the induced unsteady flow field. While the majority of the vorticity is concentrated in vortex rings, other wake energy is distributed spatially, highlighting the complicated nature of jellyfish wake flow dynamics (Gemmell, Troolin, et al., 2015). Additional work could refine this model by taking into account more detailed wake reconstructions and vortex measurements. Conducting high-resolution PIV on the wake of natural and stimulated organisms could contribute to more accurate models. Muscle inefficiency during stimulation could also lead to increased energy consumption. Previous work, using a simple drag model, has explained low energy consumption model predictions by assuming a higher basal metabolism than that measured in this study (Acuña, López-Urrutia, and S. Colin, 2011).

Although this study focused on *Aurelia aurita*, this method holds potential for application to other marine species. Recent work has achieved detailed laser scans of *Nanomia bijuga* and *Cystisoma* (Daniels, Sainz, and Katija, 2023). Our work extends these findings with automated reconstructions of larger transparent animals. Scattering and attenuation within jellyfish tissue limit laser transmission, obscuring features on the far side of the volumetric reconstruction. Reconstructions could be utilized for comparative studies of animal morphology, biomechanics, and behavior given sufficient camera frame rates to limit movement between successive laser scans. This metabolism technique could be extended to a broad range of gelatinous zooplankton but would require modification for application to more complex organisms. While jellyfish have little tissue type variation, application to some vertebrates, e.g. bony fishes, would require tracking tissue type lost through catabolysis to account for differing chemistry and carbon content.

Acknowledgments

The authors would like to thank Cabrillo Marine Aquarium and Aquarium of the Pacific for providing jellyfish used in these experiments. The authors also acknowledge helpful conversations with Lea Goentoro, Michael Dickinson, Morteza Gharib, John Costello, Sean Colin, Brad Gemmell, Emily Carrington, and Mark Denny. The authors would like to thank Marni Rosenthal for assistance in designing Figure 3.4A.

Competing Interests

No competing interests declared.

Contribution

S.R.A. and J.O.D. conceived of project, S.R.A. conducted experiments, S.R.A. and J.O.D. analyzed results and wrote paper.

Funding

This work was supported by the National Science Foundation Graduate Research Fellowship Grant Number DGE-1745301, National Science Foundation Grant 2311867, and funding from the U.S. Office of Naval Research.

Data Availability

Raw image data available upon request.

Chapter 4

WAKE DYNAMICS AND BIOMECHANICS OF ELECTRICALLY STIMULATED JELLYFISH

Abstract

Electrical stimulation of gelatinous marine invertebrates allows the study of swimming animals with prescribed motions. One key question is the effect of electrical stimulation on swimming hydrodynamics, biomechanics, and associated energy consumption. Swimmer biomechanics and energetics cannot be fully understood independently of the surrounding flow field. Here, we experimentally investigate jellyfish wake hydrodynamics using three-dimensional, full velocity field Particle Image Velocimetry. These experiments enable measurements of wake energy loss spatially across the jellyfish subumbrellar and exumbrellar surfaces. We simultaneously study animal biomechanics spatially and temporally during the contraction and relaxation phases. Conducting these experiments with both unstimulated and electrically stimulated jellyfish allows the comparison of wake energetics at different swimming stroke frequencies with natural and prescribed motions. Previous work found that electrically stimulated jellyfish consume more energy than unstimulated jellyfish, but did not identify the origin of this elevated energy consumption. We found electrical stimulation increased posterior wake energy loss by a factor of 2.9 compared to unstimulated jellyfish, primarily due to heightened pulse rates. Stimulation was also found to modify swimming biomechanics by reducing total bell margin movement and relaxation duration. By resolving three-dimensional wake energetics alongside biomechanics, we show that electrical stimulation increases energetic cost primarily through increased pulse frequency, reinforcing the speed-efficiency tradeoff in unsteady, vortex-dominated flows.

4.1 Introduction

Swimmer locomotion in fluids arises from coupled interactions between animal biomechanics and fluid dynamics. These interactions have long been proposed as a major evolutionary driver shaping the morphology and locomotion of both aquatic and aerial organisms (Thompson, 1945; Lighthill, 1997; Vogel, 1994; F. E. Fish and G. V. Lauder, 2006; J. O. Dabiri et al., 2010). Propulsive forces are generated at the solid-fluid interface, where muscular deformation of fins, bodies, and bells accelerates surrounding fluid (Vogel, 1994). By conservation of momentum, the impulse imparted to the wake balances the thrust experienced by the swimmer. Thus, animal energetics and performance cannot be understood independently of the surrounding flow field (Wu, 1971; Lighthill, 1997).

Despite the central role of wake dynamics in propulsion, most experimental measurements of swimming flows have historically been restricted to two-dimensional velocity fields (Drucker and George V. Lauder, 1999; J. O. Dabiri et al., 2010; Frank E. Fish et al., 2014; Costello, S. P. Colin, John O. Dabiri, et al., 2021; Elsinga et al., 2006). Planar Particle Image Velocimetry (PIV) captures velocity components within a single measurement plane, which can obscure out-of-plane transport of momentum and energy associated with inherently three-dimensional wake structures such as vortex rings (Willert and Gharib, 1991; Ronald J. Adrian and Westerweel, 2011). This limitation is particularly important for many medusae whose propulsion is dominated by the formation and evolution of vortex rings shed during bell contraction and relaxation (J. O. Dabiri et al., 2010; Costello, S. P. Colin, John O. Dabiri, et al., 2021). As a result, two-dimensional measurements may underrepresent the full spatial distribution of wake momentum and kinetic energy generated by swimming jellyfish.

Recent advances now enable simultaneous measurements of three-dimensional velocity fields and animal biomechanics. Multi-camera systems such as stereo PIV extend traditional 2D-2C PIV (Willert and Gharib, 1991) to enable the capture of the out-of-plane velocity component for a single two-dimensional plane (Prasad and R. J. Adrian, 1993; Wieneke, 2005; Ronald J. Adrian and Westerweel, 2011; Elsinga et al., 2006; M. K. Fu, Houghton, and John O. Dabiri, 2021). Tomographic PIV expands this system to enable the capture of full volumetric velocity fields in three dimensions. These systems can be cumbersome to set up and calibrate due to significant camera and equipment requirements, which often limit experimental volume (Elsinga et al., 2006). A similar system was previously used on *Aurelia*

aurita vortex rings with small radii of a few cm (Gemmell, Troolin, et al., 2015).

A single camera volumetric PIV scanning system was developed to improve on these limitations while recording full velocity fields in three dimensions (M. K. Fu, Houghton, and John O. Dabiri, 2021; Mohebbi et al., 2024). This technique enables direct quantification of wake dynamics, vortex structures, and kinetic energy, thus providing a more complete framework for linking kinematics to energetic cost.

Electrical stimulation

Electrical stimulation of gelatinous marine invertebrates allows the study of swimming animals with prescribed motions. Previous work has capitalized on this capability for prescribed motions by investigating the effects of stimulation of live jellyfish for use as ocean exploration robots (Nicole W. Xu and John O. Dabiri, 2020; Anuszczyk and John O. Dabiri, 2024). Nicole W. Xu and John O. Dabiri (2020) found that small electrical pulses delivered to live jellyfish cause animal contraction and increased swimming speeds. Anuszczyk and John O. Dabiri (2024) found that the bell shape could be modified to further increase swimming speeds while carrying a payload larger than the animal. Chapter 3 measured the energy consumption of unstimulated and stimulated jellyfish and found that electrical stimulation significantly increased energy consumption. Using a 13.6 m^3 water tank with flow pumps to allow continuous swimming, they showed that the addition of hydrodynamic drag increased energy consumption even further. These experiments investigated long timescales on the order of multiple days.

Here, we leverage three-dimensional PIV to quantify the changes in *Aurelia aurita* (Linnaeus, 1758) jellyfish energetics and biomechanics due to electrical stimulation. By integrating volumetric measurements with biomechanics on the order of individual pulses, we evaluate how changes in pulse actuation and frequency influence bell movement, energetic performance, and physiology.

Experimental plan

These experiments focused on measuring the flow around swimming jellyfish on the order of individual pulses. We conducted three-dimensional, three-component PIV on free-swimming jellyfish. Comparison of unstimulated and electrically stimulated animals elucidated differences between the induced flows and biomechanics of these jellyfish.

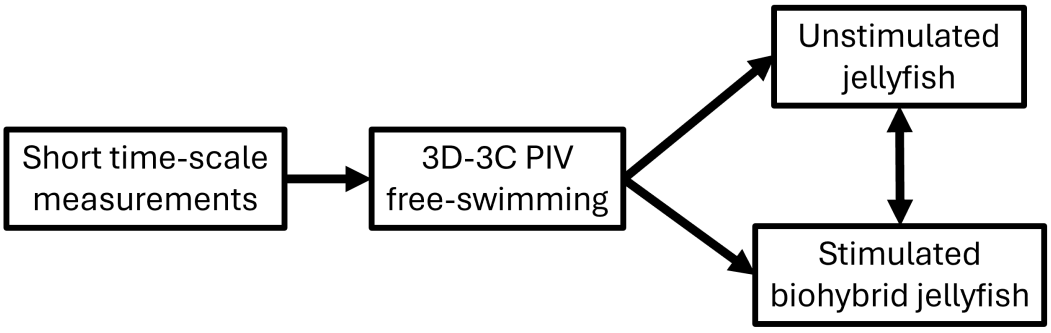

Figure 4.1: Diagram of experimental plan. This study consists of short timescale measurements of swimming jellyfish on the order of individual pulses. We will utilize three-dimensional, three-component PIV to measure and compare stimulated and unstimulated free-swimming jellyfish.

4.2 Materials and Methods

Animal husbandry

Aurelia aurita medusae were obtained from Cabrillo Marine Aquarium (San Pedro, CA, USA) and Aquarium of the Pacific (Long Beach, CA). They were housed in a 453 liter pseudokreisel tank (Jelliquarium 360, Midwater Systems, Thousand Oaks, CA, USA). The tank was filled with artificial seawater mixed with sea salt (Instant Ocean Sea Salt, Spectrum Brands, Blacksburg, VA, USA) and deionized water at 35 parts per thousand (PPT) and kept at 21°C. The jellyfish were hand-fed twice daily with frozen *Artemia franciscana* baby brine shrimp (Bio-Pure Frozen Baby Brine Shrimp, Bulk Reef Supply, Golden Valley, MN, USA).

Electrical stimulation of live jellyfish

Figure 4.2A shows the electronics for onboard electrical stimulation embedded in a model jellyfish. The system consists of a swim controller enclosed in a custom 2.50 ± 0.03 cm diameter electronics housing, two electrodes embedded in the jellyfish muscle tissue, a threaded plastic rod, and a threaded ballasting nut. The swim controller includes a small processor (TinyLily, TinyCircuits, Akron, OH, USA) and a 15 mAH lithium-polymer battery cell (PGEB181118, PowerStream Technology Inc., Orem, UT, USA). All parts of the electronics housing and ballast were fabricated via stereolithography (Form 3 Color Base Resin) on a Form 3+ resin printer (Formlabs, Somerville, Massachusetts). The swim controller housing utilized a threaded cap with an O-ring for waterproofing at high pressure. Wire coated in perfluoroalkoxy was threaded through small holes in the housing and connected to platinum rods (A-M Systems, Sequim, WA, USA) embedded in the animal muscle

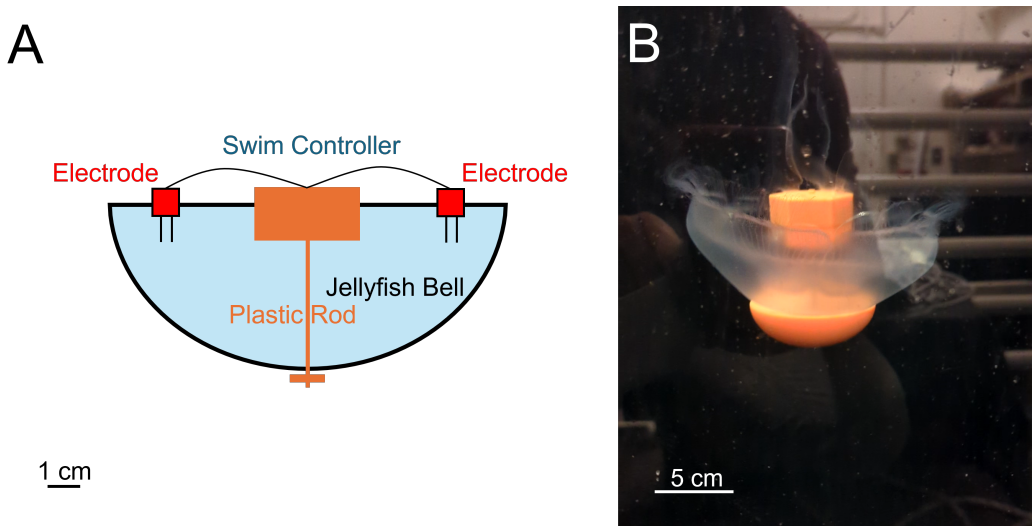

Figure 4.2: Jellyfish stimulation (A) Schematic of stimulated jellyfish with jellyfish oriented downwards. Consists of two electrodes, a swim controller containing the electronics and battery (not visible), and a plastic rod embedded in the jellyfish tissue with a small threaded nut on the exumbrellar side to keep rod secure. (B) Photo of electronics embedded in live jellyfish during swimming experiment with additional forebody for payload. Figure adapted from Chapter 3.

tissue. The pass-throughs were sealed with epoxy, and an LED was connected in series to each electrode to provide visual confirmation of stimulation. See previous work (Anuszczyk and John O. Dabiri, 2024) for more details on electronics and impact on swimming performance. Figure 3.3B shows the electronics stimulating a swimming jellyfish in the lab environment .

Laser scanning PIV

PIV data of the swimming jellyfish was taken using a three-dimensional, three-component single-camera laser scanning system developed by M. K. Fu, Houghton, and John O. Dabiri (2021) and applied to jellyfish in Chapter 3 (Fig. 4.3). This system used a 671 nm continuous laser (5 W Laserglow LRS0671 DPSS Laser System) and a series of optics to generate a scanning laser sheet. The optics consisted of a mirror mounted on a rotating galvanometer (Thorlabs GVS211/M, 10 kHz bandwidth) controlled with an arbitrary function generator (Tektronix AFG3011C) to sweep across the volume of inquiry at 10 Hz; a 25 cm diameter condenser lens to redirect the laser normal to the scanning direction; and a cylindrical, 16-mm diameter glass rod used to form the laser beam into a thin sheet. The laser sheet was set to sweep normal to its plane across a distance of 18.5 cm. A high-speed camera recording at 8000 fps (Photron FASTCAM SA-Z) thus captured 800 images

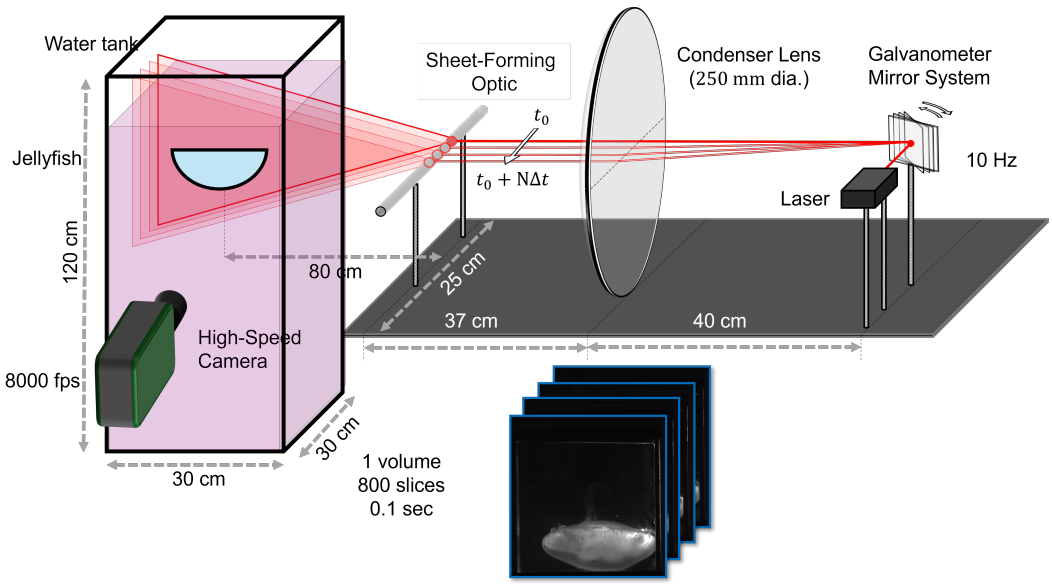

Figure 4.3: Laser scanning system for 3D-3C PIV. (A) Diagram of laser scanning system with laser, galvanometer rotating at 10 Hz, 250 mm diameter condenser lens to redirect the laser normal to the scanning direction, cylindrical glass rod to form the laser beam into a thin sheet, water tank, and jellyfish. As the laser scans across the jellyfish, a high speed camera records an image stack, or "volume", of 800 slices every 0.1 s. Figure adapted from Chapter 3.

at a resolution of 1024 x 1024 pixels, or 22.3 x 22.3 cm, for each volumetric scan. The jellyfish were manually directed downwards through the scanning volume in a 1.2 m tall x 0.3 m x 0.3 m tank filled with salt water at 35 ppt. The fluid was seeded with 20 µm neutrally-buoyant polyamide particles for flow visualization (LaVision Inc., Ypsilanti, MI). This experimental scanning setup was calibrated using a 3D-printed calibration plate with a grid of through holes spaced every 1 cm. This plate was mounted at 45 degrees to the camera. The calibration plate was scanned, reconstructed, and the hole-center to hole-center distance was measured for the entire grid. A rotational transformation was applied to these spacings, recovering the three-dimensional calibration.

Because the flow field evolves much more slowly than the temporal resolution of the measurements, the measurements across a volume can be treated as quasi-instantaneous. Volumes are recorded every 0.1 s, while the jellyfish typically swims at 1-3 cm s^{-1}. Thus, over a single sampling interval, the animal translates only 0.1-0.3 cm, which is small compared with the characteristic size of the bell and the wake structures being measured. As a result, the velocity field and associated metrics change only slightly across a measurement, allowing each volume to be

treated as an instantaneous snapshot of a slowly evolving flow (Ronald J. Adrian and Westerweel, 2011). Under these conditions, treating the measurements as such provides a reasonable approximation for this analysis.

Post-processing

A custom Python code was written to mask the three-dimensional jellyfish out of each image stack based on Chapter 3. The code identified the jellyfish and performed binarization, thresholding, and morphological opening and closing operations to create a detailed reconstruction of the animal, as shown in Figure 4.4A. After masking, the open source Python-based tool OpenPIV was used to process the image stacks and generate vectors (Liberzon et al., 2019). Velocities were computed by correlating consecutive volumetric scans, yielding one 3D velocity field per 0.1 s. Because the volume is acquired sequentially, each 3D field represents a quasi-instantaneous volume. MATLAB was used for filtering, data visualization, and analysis, and all results use the post-processed field. Velocity magnitudes exceeding $15\,\mathrm{cm/s^{-1}}$ were removed as spurious outliers, as these values are more than an order of magnitude larger than the observed swimming speeds and expected flow velocities for jellyfish pulses of these diameters.

Analytical analysis

In order to derive a relationship between the wake motion and the energy consumption of the swimming animal, we first apply the equations of motion to a control volume surrounding the jellyfish. We adapt a model from previous work on vortex propulsion (Ruiz, Whittlesey, and John O. Dabiri, 2011). Figure 4.4B illustrates a swimming jellyfish with an associated control volume J. The wake energy volume location was defined with a width of one animal diameter D and height including the animal and extending from the vertical center of the animal one radius $\frac{D}{2}$ downstream in the -Y direction. This placement was set to capture the region containing the vortex ring cores during contraction and pinch-off, which scale with bell diameter, as well as flow inside of the bell. Expressing the control volume dimensions in terms of animal diameter D ensures consistent non-dimensional scaling across animals of different morphologies while providing a balance between capturing the energetic wake structures and minimizing inclusion of bow wave and far-field background flow.

Let **u** denote fluid velocity and **n** the outward unit normal to the surface. Assuming incompressibility, the equations of conservation of mass, streamwise (along y)

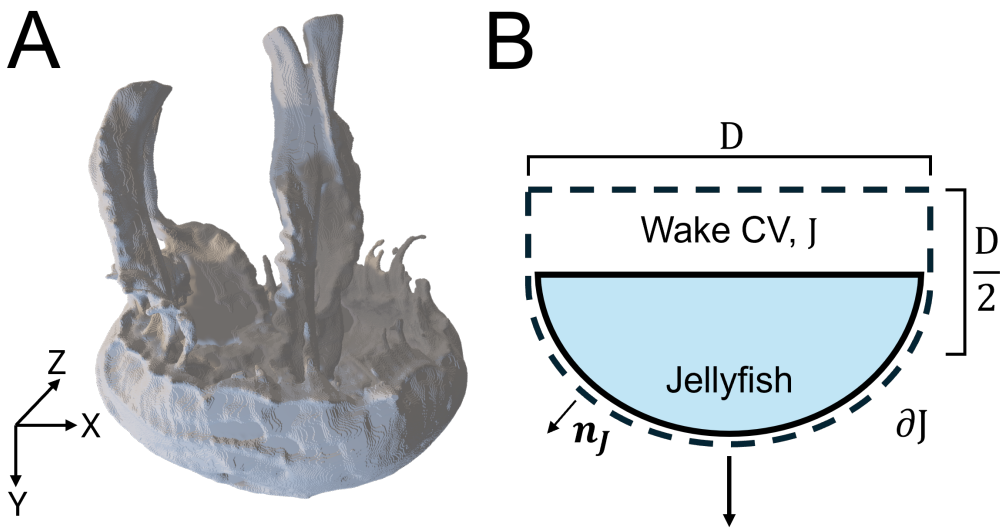

Figure 4.4: Energy volume diagram (A) Volumetric reconstruction of swimming jellyfish used to mask out pixels in the image stack before analysis. These masks were fed into the PIV code to ensure no spurious velocity vectors were generated inside swimming animal. (B) A wake energy volume was defined behind the swimming jellyfish inside which kinetic energy was analyzed. Instantaneous measurements of kinetic energy inside this volume served as a proxy measurement of energy expended into this region of the wake by the swimming animal. The dimensions of the volume were defined as a width of one diameter D and height including the entire animal as well as extending into the posterior wake by $\frac{D}{2}$ from the vertical center of the animal.

momentum, and energy are then given by

$$
\begin{aligned}
\text{mass:} \qquad & 0 = \rho \oint_{\partial J(t)} \mathbf{u} \cdot \mathbf{n}\, dA, \\
y\text{-momentum:} \qquad & F_{\text{ext},y} = \rho \left[\frac{d}{dt} \int_{J(t)} v\, dV + \oint_{\partial J(t)} v\, \mathbf{u} \cdot \mathbf{n}\, dA \right] \\
& \quad + \oint_{\partial J(t)} p\, n_y\, dA, \qquad (4.1) \\
\text{energy:} \qquad & \dot{W}_{\text{ext}} = \frac{\rho}{2} \left[\frac{d}{dt} \int_{J(t)} ||\mathbf{u}||^2\, dV + \oint_{\partial J(t)} ||\mathbf{u}||^2\, \mathbf{u} \cdot \mathbf{n}\, dA \right] \\
& \quad + \oint_{\partial J(t)} p\, \mathbf{u} \cdot \mathbf{n}\, dA.
\end{aligned}
$$

where seawater density $\rho = 1024\,\text{kg m}^{-3}$ at 35 PPT and 21°C (J. O. Dabiri et al., 2010;

Table 4.1: Volumetric PIV acquisition and processing parameters.

Acquisition	
Raw image resolution	1024×1024 pixels
Scan rate	10 Hz
Time between volumes (Δt)	0.1 s
Frames per volume	800
Volumes per trial	105
Vector fields per trial	104
Voxel spacing (x, y)	0.0217 cm
Voxel spacing (z)	0.0232 cm
PIV processing	
Interrogation window size	$32 \times 32 \times 32$ voxels
Window overlap	$16 \times 16 \times 16$ voxels
Search area size	$32 \times 32 \times 32$ voxels
Vector spacing	16 voxels (≈ 0.35 cm $\times$ 0.35 cm $\times$ 0.37 cm)
Final vector grid size	$\sim 63 \times 52 \times 49$ vectors (crop-dependent)
Subpixel peak estimation	Gaussian fit
Signal-to-noise metric	Peak-to-peak
Mask dilation	$\approx$ half interrogation window size
Vector validation and filtering	
Vector validation threshold	SNR ≥ 1
Velocity outlier cutoff	$\lvert u \rvert > 15\,\mathrm{cm\,s^{-1}}$ removed
Outlier replacement	Local interpolation (disk kernel radius 2, max 4 iterations)
Velocity smoothing	3D Gaussian filter ($\sigma = 2$ voxels)
Additional smoothing	$5 \times 5 \times 5$ mean filter

D. J. Li and Mendelson, 2023) and ∂J is the surface of the control volume. $F_{ext,y}$ is the net force exerted by the swimmer on the fluid, v is the y component of velocity vector $\mathbf{u}$, p is the pressure, and $\dot{W}_{\text{ext}}$ is the external mechanical power imparted by the swimmer to the fluid. Because pressure and viscous stresses on the control surface are not directly resolved, a full thrust estimate is not attempted. Instead, the measurable velocity-based portions of the momentum and energy balances are used. The equations of streamwise momentum and energy thus simplify to

$$\begin{aligned} y\text{-momentum:} \qquad & F_{\text{ext},y} = \rho\left[\frac{d}{dt}\int_{J(t)} v\, dV + \oint_{\partial J(t)} v\, \mathbf{u}\cdot\mathbf{n}\, dA\right] \\ \text{energy:} \qquad & \dot{W}_{\text{ext}} = \frac{\rho}{2}\left[\frac{d}{dt}\int_{J(t)} ||\mathbf{u}||^2\, dV + \oint_{\partial J(t)} ||\mathbf{u}||^2\, \mathbf{u}\cdot\mathbf{n}\, dA\right] \end{aligned} \tag{4.2}$$

We analyze the convective transport term in order to study how momentum is transported out of and around the wake control volume. We define the net streamwise (y-component) momentum transport

$$M_s(t) = \rho \oint_{\partial J(t)} v\mathbf{u}\cdot\mathbf{n} dA \tag{4.3}$$

For a pulse beginning at t_a through t_b

$$M_{\text{s, pulse}} = \int_{t_a}^{t_b} M_s(t) dt \tag{4.4}$$

This momentum transport term $M_{\text{s, pulse}}$ was evaluated across the posterior surface located downstream of the swimmer. This surface captures the directed wake momentum transport associated with propulsion as vortex rings and jet structures primarily leave the bell through the downstream wake. Lateral control surfaces instead capture refill and entrainment flows, which do not represent directed propulsion momentum exchange. This downstream control surface thus provides a direct measure of the momentum transported in the wake by each pulse. To allow comparisons across animals of different sizes, the pulse-integrated momentum was normalized by animal mass

$$I_{\text{s, pulse}} = \frac{M_{\text{s, pulse}}}{m} \tag{4.5}$$

For time-resolved comparisons across animals, we also define the instantaneous mass-specific downstream momentum flux

$$I_{\text{s}}(t) = \frac{M_{\text{s}}(t)}{m} \tag{4.6}$$

Radial momentum transport was computed from the velocity component normal to the cylindrical sidewall of the control volume and integrated over the same pulse interval. This metric enables the calculation of the momentum contribution to propulsion through the posterior control surfaces.

The momentum transport analysis above characterizes how fluid impulse is exported through the downstream wake. However, this quantity alone does not capture the energetic content of the wake. From the energy balance in Eq. 4.2, wake energetics are governed by both the temporal change in kinetic energy within the control volume and the convective transport of kinetic energy across its boundaries. Both terms contribute to the mechanical energy imparted to the wake. Here, rather than evaluating these terms separately, instantaneous kinetic energy contained within the wake control volume is used as a proxy for wake energetic output (J. O. Dabiri et al., 2010; D. J. Li and Mendelson, 2023; Ruiz, Whittlesey, and John O. Dabiri, 2011; Katija and John O. Dabiri, 2009). This approximation is justified because the control volume is small relative to the evolving wake, such that wake structures pass through the measurement region over short timescales and kinetic energy does not accumulate over long durations. Under these conditions, the kinetic energy contained within the control volume scales with the combined effects of local kinetic-energy growth and downstream kinetic-energy transport. The local kinetic energy density of the velocity field is defined as

$$e_{\text{kinetic}} = \frac{1}{2}\rho\|\mathbf{u}(\mathbf{x},\mathbf{y},\mathbf{z},\mathbf{t})\|^2 \tag{4.7}$$

and the instantaneous kinetic energy contained within the wake control volume is obtained by integrating this quantity over J leading to

$$E_{\text{J}}(t) = \int_J e_{\text{kinetic}}(x,y,z,t)\, dV \tag{4.8}$$

To characterize the cumulative wake kinetic energy over an individual pulse, the wake energy is integrated over the pulse duration

$$E_{\text{J, pulse}} = \int_{t_a}^{t_b} E_{\text{J}}(t)dt \tag{4.9}$$

To compare hydrodynamic energy loss across animals and swimming conditions, wake kinetic energy was normalized by the kinetic energy of the swimming jellyfish. This normalization yields a dimensionless measure of how strongly pulse-associated motion is exerted into the surrounding fluid relative to the motion of the animal. Because absolute wake kinetic energy increases with the overall magnitude of swimming motion, the ratio provides a more comparable metric across pulses and individuals than energy alone. These ratios should therefore be interpreted as comparative measures of resolved fluid-energy loss relative to animal motion, rather than as direct estimates of propulsive efficiency or total metabolic expenditure. We define an instantaneous energy ratio

$$E_{\text{ratio}}(t) = \frac{E_J(t)}{E_{\text{jelly}}(t)} \tag{4.10}$$

where $E_{\text{jelly}}(t)$ is the kinetic energy of the animal. The mass of each animal was found by weighing them after conducting experiments. Each animal was carefully removed from the tank, patted dry to remove excess water, and weighed on an electric balance (Eosphorus Sf-400C, 600 g range, 0.01 g precision). The three-component velocity of the swimming animal was found by tracking the movement of the bell apex. The center XY planes bisecting each animal apex were manually identified in PFV4 (Photron, San Diego, CA), and videos were exported to Matlab for analysis. The point tracking tool Dltdv8 (Hedrick, 2008) in Matlab was used to track XY apex locations over time. MATLAB was used to generate full image stack slices along the YZ planes again bisecting the animal bell apex. These were similarly tracked to find Z trajectories.

Each experimental trial captured several pulses, with stimulated trials including more pulses than unstimulated trials due to higher pulse rates. The analysis was thus manually split into individual pulses by tracking bell margin movement and identifying pulse start and end times t_a and t_b. The pulse-specific normalized wake energy ratio was defined as

$$E_{\text{ratio, pulse}} = \frac{E_{\text{J,pulse}}}{\int_{t_a}^{t_b} E_{\text{jelly}}(t)\, dt} \tag{4.11}$$

Electrical stimulation is known to increase pulse rates significantly compared to unstimulated jellyfish. While the electronics were used to stimulate at a constant

frequency of $f_{ST} = 0.5$ Hz, unstimulated *Aurelia* of similar size are known to pulse at $f_{US} = 0.16$ Hz (Nicole W. Xu and John O. Dabiri, 2020). This difference was corrected for by defining a time-specific normalized wake energy ratio to estimate the rate of energy deposition, or power, expended into the surrounding fluid

$$P_{\text{ratio, time}} = fE_{\text{ratio, pulse}} \tag{4.12}$$

This metric represents the expected energy consumption of the stimulated and unstimulated jellyfish.

We follow previous work in estimating the role of kinetic energy dissipation in these measurements (J. O. Dabiri et al., 2010). Wake vortices are known to break down on timescales of $\frac{d}{u}$ with d the vortex size and u vortex velocity (Tennekes and Lumley, 1972; Saffman, 1992). At the low Reynolds numbers observed here, this process is negligible (Rosenhead, 1963; Saffman, 1978). The time scale of viscous dissipation can be found through dimensional analysis (Rosenhead, 1963) of

$$\tau = \frac{d^2}{\nu} \tag{4.13}$$

These experiments have eddy sizes larger than 12 cm and kinematic viscosity of 10^{-2} cm^2 s^{-1} (Batchelor, 2000) leading to a dissipation timescale of τ much larger than typical pulse durations on the order of 1 second.

While these experiments focused primarily on quantifying wake energetics, additional vortex measurements were extracted from representative flow fields in each trial to characterize the vortex rings generated during contraction. Vortex properties were evaluated from a single representative time point per trial corresponding to a well-developed starting vortex ring following contraction. The out-of-plane component of vorticity was computed from the measured velocity field as

$$\omega_z = \frac{\partial v}{\partial x} - \frac{\partial u}{\partial y} \tag{4.14}$$

Circulation, impulse, and peak vorticity were calculated from the vorticity field within a region of interest surrounding the dominant vortex ring in the wake. The

vortex core was identified using a closed contour corresponding to 30% of the local peak vorticity magnitude. Circulation was calculated by integrating the vorticity over the enclosed area

$$\Gamma = \iint_A \omega_z \, dA, \tag{4.15}$$

where A denotes the area bounded by the vortex core. This circulation represents the total rotational strength of the vortex (Saffman, 1992). Assuming approximate axisymmetry, the vortex ring impulse was estimated as

$$I = \pi r_0^2 \Gamma, \tag{4.16}$$

where r_0 is the radial distance from the animal symmetry axis to the center of the vortex core. The impulse relates vortex strength to the momentum imparted to the surrounding fluid (Saffman, 1992; Morteza Gharib, Rambod, and Shariff, 1998). Peak vorticity was defined as the maximum magnitude of vorticity within the vortex core, which describes the local intensity of rotation. For each trial, a starting vortex was identified and analyzed immediately following pinch-off. Vortices were selected on the laser-illuminated side of the animal to minimize shadowing effects.

Biomechanics analysis

We conducted experiments focused on understanding the impact of electronic stimulation on the biomechanics of jellyfish. These experiments investigated both the impact of stimulation as well as the embedded electronics without stimulation. Margin movement was measured with four different treatments. The treatments were: the unstimulated animal, the unstimulated animal with passive electronics embedded, the stimulated animal, and a final repeated unstimulated animal experiment. The additional unstimulated treatment allowed the measurement of how animals might return to baseline biomechanics after stimulation experiments. Margin movement experiments were conducted with three additional animals, with one 10 second trial analyzed for each of the four treatments. While additional trials were recorded, only trials where the animal remained in the scanning volume throughout the duration of the experiment were analyzed.

The biomechanics of the swimming animals were analyzed in two dimensions at the center plane of the animal. DLTdv8 was used to track both the animal apex

and margins, enabling the calculation of biomechanics metrics across treatments. Margin movement was defined as the distance traveled by a single margin between a maximally open or relaxed bell state and maximally closed or contracted bell state. This was normalized by body length, defined as the projected maximum diameter of each animal. Contraction and relaxation duration and speed were measured from these margin-tracking trials as well as the volumetric PIV experiments, for a total of six animals. Contraction speed was additionally normalized by body length. These metrics are relevant both for measuring energy expenditure and as guides for informing optimization of electrical stimulation strategies.

Statistical Analysis

For each trial, pulse-level metrics were first calculated over manually identified pulse windows in MATLAB. Analyses were restricted to complete pulses, defined from maximum relaxation through contraction to the subsequent maximum relaxation; partial pulses were excluded prior to averaging. For each trial within each animal, the pulse-level values were averaged to obtain a single trial-level mean for that metric. Statistical comparisons between unstimulated and stimulated conditions were performed on these trial means using paired t-tests, with each unstimulated trial paired to the corresponding stimulated trial from the same animal. Thus, the unit of replication for hypothesis testing was the animal-trial pair, not the individual pulse (Sokal and Rohlf, 2013). Statistical comparisons between unstimulated and stimulated conditions for contraction duration and speed were performed on trial-averaged values using Welch's two-sample t-test to account for unequal sample sizes and variances. The first and last unstimulated treatments exhibited minimal differences and were therefore pooled into a single unstimulated group for analysis. Pulse-level points shown in Figures were included to illustrate intra-animal variability, but statistics were based on trial-level means. Statistical significance was defined as $p < 0.05$.

4.3 Results

Laser scanning PIV

We measured the 3D-3C flow induced by swimming jellyfish using the laser scanning system described above. To validate the system, we visualized the vortex rings at the center plane. Figures 4.5 and 4.6 show 2D visualizations of the flow fields for a single representative jellyfish at different points in time. Figure 4.5 illustrates the flow fields around a fully contracted jellyfish bell, whileFigure 4.6 shows a fully

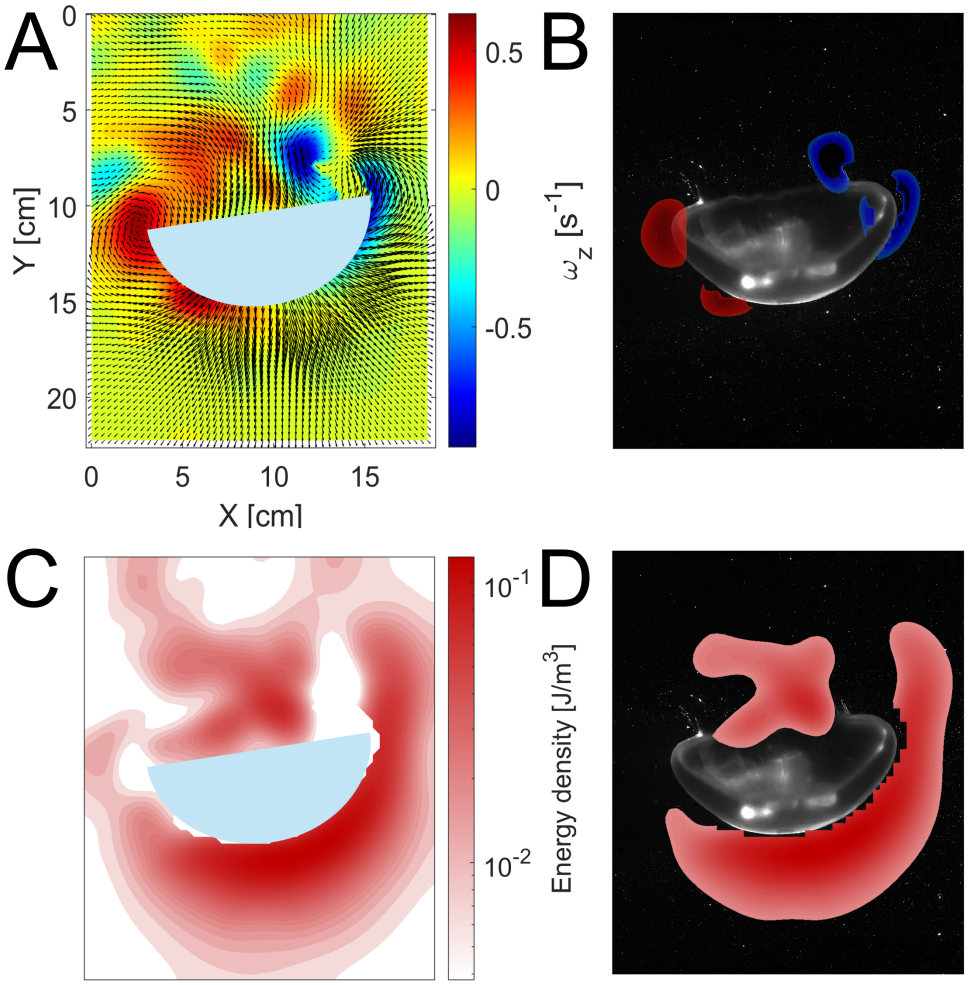

Figure 4.5: Contracted jellyfish PIV flow visualization. (A) Out-of-plane 2D vorticity visualization with overlaid velocity vector field. Jellyfish cartoon mask is shown for illustration. Color bar shows regions of positive and negative vorticity and vorticity cores are visible at margin of jellyfish bell and in the wake. (B) Vorticity with same color scale overlaid on raw image of jellyfish at center plane illuminated by laser. Regions of low magnitude vorticity are filtered out. (C) Kinetic energy density map illustrates regions of high energy in wake with fully contracted jellyfish. Energy density in units of joules/m^3. Cartoon jellyfish mask is shown for illustration and color bar is in log scale. (D) Kinetic energy density map with the same color scale overlaid on raw image of jellyfish at center plane illuminated by laser. Regions of low energy density are filtered out for visualization.

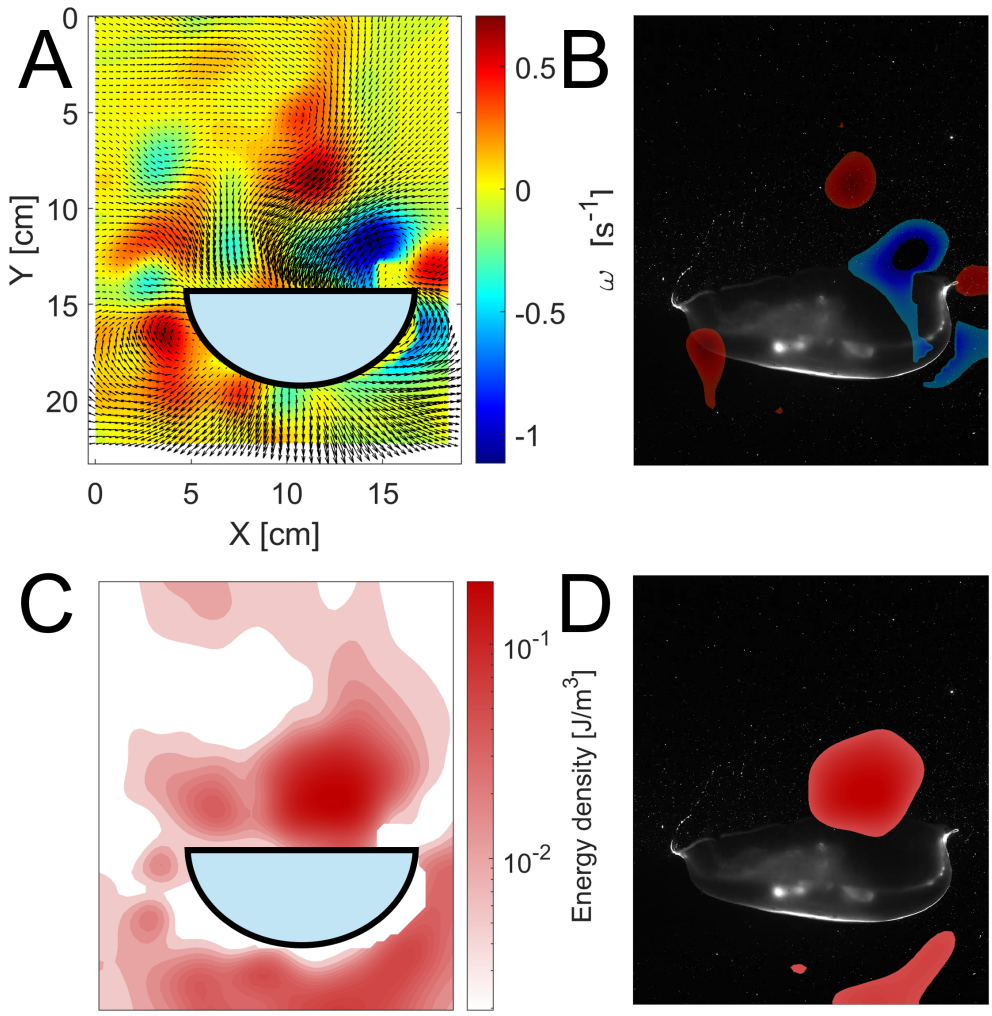

Figure 4.6: Relaxed jellyfish PIV flow visualization (A) Out-of-plane 2D vorticity visualization with overlaid velocity vector field. Jellyfish cartoon mask is shown for illustration. Color bar shows regions of positive and negative vorticity and vorticity cores are visible at margin of jellyfish bell and in the wake. (B) Vorticity with same color scale overlaid on raw image of jellyfish at center plane illuminated by laser. Regions of low magnitude vorticity are filtered out. (C) Kinetic energy density map illustrates regions of high energy in wake with fully relaxed jellyfish. Energy density in units of joules/m^3. Cartoon jellyfish mask is shown for illustration and color bar is in log scale. (D) Kinetic energy density map with the same color scale overlaid on raw image of jellyfish at center plane illuminated by laser. Regions of low energy density are filtered out for visualization.

relaxed bell. Figure 4.5A shows the 2D vorticity ω_z for a representative experiment using equation 4.14.

A cartoon jellyfish mask is shown, and opposite rotating vortex ring cores are clearly visible. Figure 4.5B shows the same vorticity field filtered and overlaid on top of the raw still image at the same location and time. As the jellyfish pulses, it releases vortex rings, and additional vorticity builds on the outside of the bell. To illustrate kinetic energy, Figure 4.5C shows the 2D kinetic energy density map in units of joules/m^3 at the same location in time and space with the cartoon jellyfish mask. Figure 4.5D shows the same energy density map filtered and overlaid on top of the raw jellyfish image. This colorbar is shown with a log scale.

Comparing the energy density in Figures 4.5C-D and 4.6C-D illustrates how these quantities vary over time. During contraction, energy density peaks in the bow wave but then falls as the animal slows during relaxation, when energy density peaks in the trailing wake behind the animal. The dominant flow structures occur in the trailing wake, therefore only the downstream wake region is analyzed here.

Figure 4.7A compares an unstimulated and stimulated trial of the same jellyfish. Here we show the wake energy within the wake energy control volume divided by the animal energy at each instant in time over the course of the 10 second experiments. The unstimulated animal energy ratio, shown here in gray, shows 2 peaks with one appearing at each pulse. The color gradient bars at the bottom of the Figure show each pulse going from light to dark, where light represents the beginning of the contraction. The stimulated animal shows 5 pulses over the same period of time due to the consistent pulse frequency of the electronics. While energy ratio peaks indicate pulses, the magnitude varies widely based on the animal speed.

We define the pulse-specific normalized energy using equation 4.11. This is shown in Figure 4.7B. These measurements were obtained from experiments with three animals. Here "US" represents the unstimulated trials, while "ST" is the stimulated trials. This shows that the pulse-specific normalized energy for unstimulated and stimulated jellyfish is not significantly different ($p = 0.91$). To correct for the different pulse frequencies observed in long term experiments, we define a time-specific normalized energy as the pulse-specific normalized energy multiplied by the pulse frequency. Figure 4.7C illustrates the increase in time specific normalized energy. These results show that stimulated animals release on average 2.9 ± 1.2 times more normalized energy per unit time into the trailing wake than unstimulated animals. This could explain earlier results from Chapter 3 that show a similar

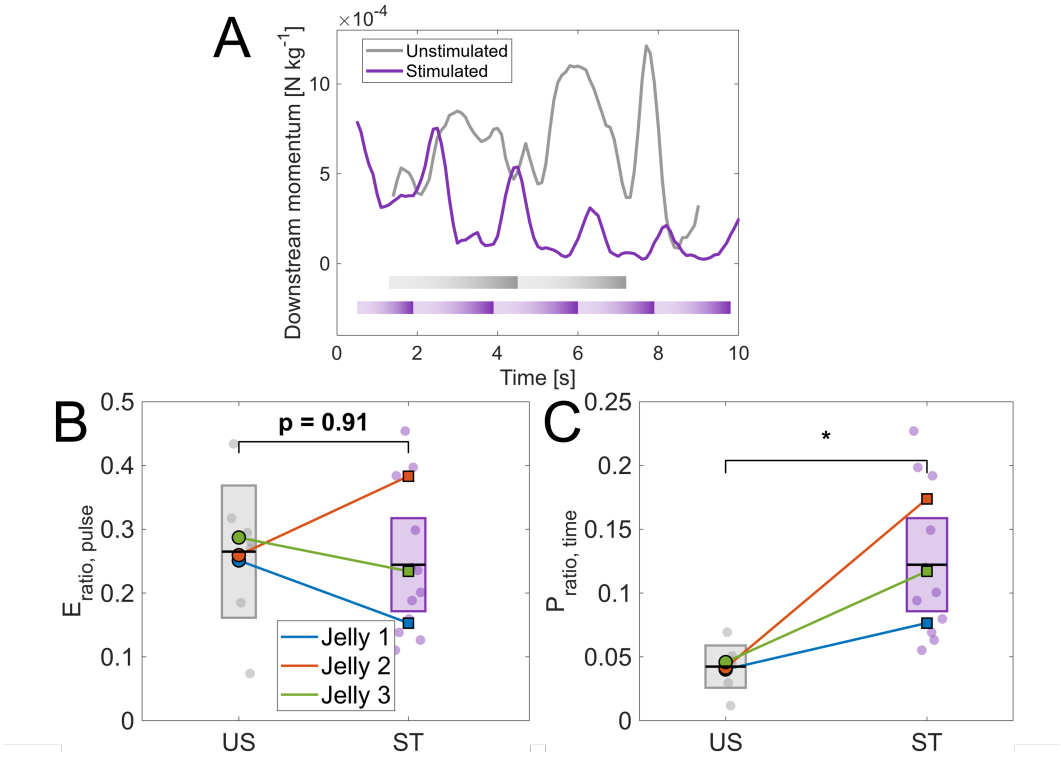

Figure 4.7: Normalized wake energy. (A) Instantaneous mass-specific net downstream momentum, equation 4.6, transported during each pulse for an unstimulated (gray) and stimulated (purple) animal over the course of 10 second experiments. This trace shows two unstimulated pulses and five stimulated pulses indicated at the bottom of the plot by the colored gradient from light to dark where light represents the beginning of the contraction. (B) Pulse-specific normalized energy $E_{\text{ratio, pulse}}$ given by eq. 4.11. Blue, red, and green points represent animal means for each condition and shaded boxes denote the 95% confidence interval of the pooled pulse mean for each condition. Gray and purple points represent individual pulses. Statistical comparisons were performed on trial-level means using paired t-tests, pairing unstimulated (US) and stimulated (ST) trials from the same animals. No significant difference in energy released per pulse was observed between conditions ($p = 0.91$). (C) Time-specific normalized energy $P_{\text{ratio, time}}$ defined by equation 4.12. Stimulated jellyfish release 2.9 ±1.2 times more energy per second to the near wake than unstimulated animals ($p = 0.047$). Points and shaded boxes are as in panel B.

increase in energy consumption.

The primary analysis used a control volume height of $H = \frac{D}{2}$. Repeating the analysis with smaller and larger control volumes ($H = \frac{D}{4}$ and $H = D$) produces similar qualitative patterns across animals and conditions (Figure 4.8). This indicates that the conclusions are not sensitive to moderate changes in control-volume height.

Having established that the wake energy estimates are robust to changes in control-volume height, we use the same control volume to examine how momentum is transported in the wake. While the preceding analysis focused on kinetic energy in the wake, the control volume analysis allows the momentum flux to be compared similarly. Figure 4.6 shows the mass-specific downstream momentum given by equation 4.6 for unstimulated (A) and stimulated (B) trials. While stimulated pulse time was fixed by electric stimulation at 2 seconds, here we normalize by pulse time for each pulse since unstimulated pulse time varies. These measurements demonstrate that in both unstimulated and stimulated cases, the pimary momentum transport occurs near the beginning of the stroke as the animal is contracting. Calculating total downstream momentum across each pulse and partitioning into downstream and radial components.provides insight into how effectively the wake from individual pulses contributes to forward propulsion compared to lateral transport of fluid. Figure 4.10A shows the downstream momentum, given by equation 4.5, between the two cases. While two animals show decreased downstream momentum transport, the third shows the opposite trend. Figure 4.10B illustrated the downstream momentum versus radial momentum as a percentage of total momentum. Stimulation generally increases the percentage of radial transport, but significant inter-animal variability is visible.

Instantaneous vortex measurements at a representative point following a complete bell contraction and creation of starting vortex are shown in Figure 4.11. Lines connect paired animals. Circulation trends downward with stimulation for all three animals. Impulse, estimated using equation 4.16, also trends downward while peak vorticity decreases for jelly 1 and 2, but increases for jelly 3, highlighting inter-animal variability.

Biomechanics Analysis

We compare swimming animals across different treatments and observe that electrical stimulation changes swimming biomechanics. Figures 4.12A-C show the margin movement between maximum relaxation and contraction states normalized by the

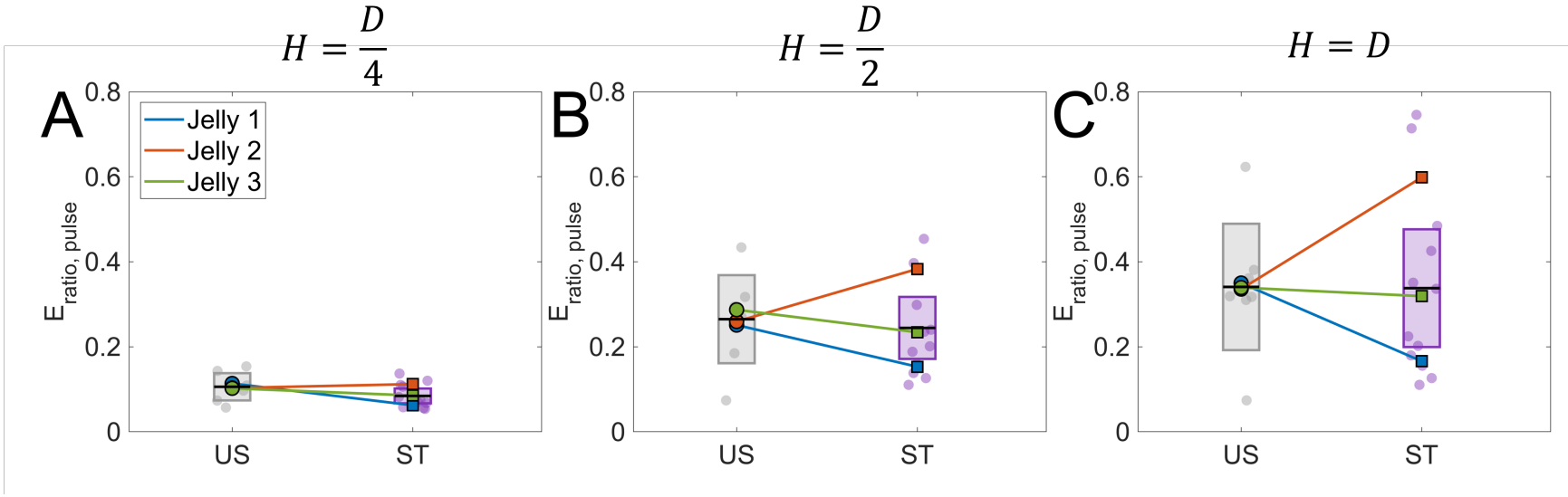

Figure 4.8: Sensitivity of normalized wake energy to control-volume height. Sensitivity of the pulse-averaged wake energy ratio to the height of the cylindrical control volume. Panels show results for control volume heights of (A) $H = \frac{D}{4}$, (B) $H = \frac{D}{2}$, and (C) $H = D$, where D is the bell diameter. Grey and purple points denote individual pulses for unstimulated (US) and stimulated (ST) trials, respectively. Colored symbols connected by lines indicate animal means. Shaded boxes show the 95% confidence interval of the pooled pulse mean for each condition. The primary analysis uses the $H = \frac{D}{2}$ control volume shown in panel (B).

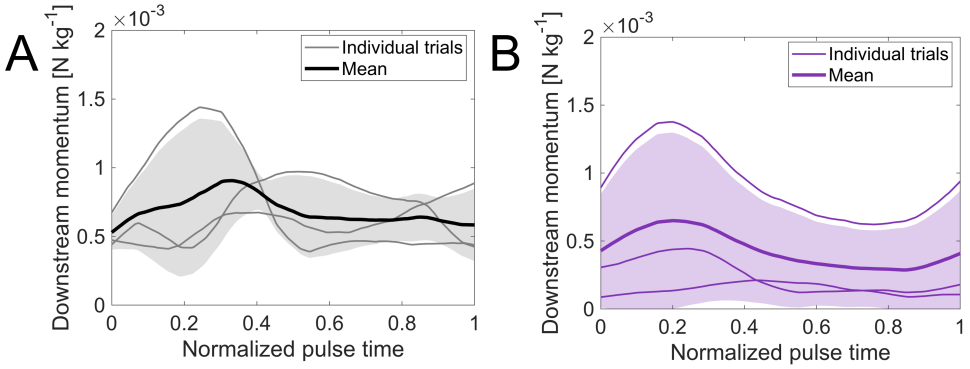

Figure 4.9: Time-resolved momentum transport (A) Unstimulated mass-specific net downstream momentum shown across a normalized pulse time starting and ending at subsequent points of maximum bell relaxation. Light gray lines represent animal average across individual trials, dark gray line represents mean average across animals, and shaded region is ± 1 standard deviation. (B) Stimulated mass-specific net downstream momentum shown across a normalized pulse time, lines defined same as in (A).

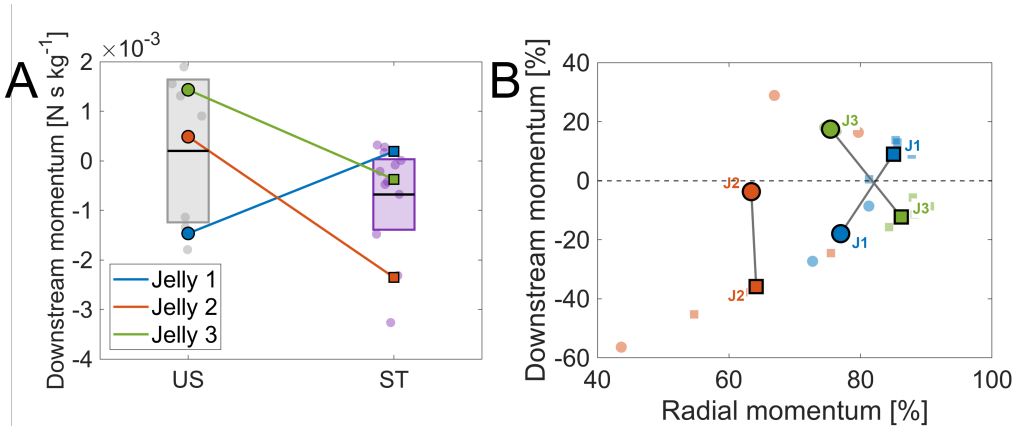

Figure 4.10: Average momentum transport in the wake (A) Mass-specific net downstream momentum, equation 4.5, transported during each pulse. Points represent individual pulses and colored markers denote animal means for unstimulated (US) and stimulated (ST) trials connected by lines for each animal. Shaded boxes indicate the 95% confidence interval of the pooled pulse mean for each condition. (B) Partitioning of momentum between downstream and radial components. Points represent individual pulses and large markers show animal means. Radial momentum is expressed as a percentage of total transported momentum magnitude, while downstream momentum is the signed fraction indicating net downstream transport.

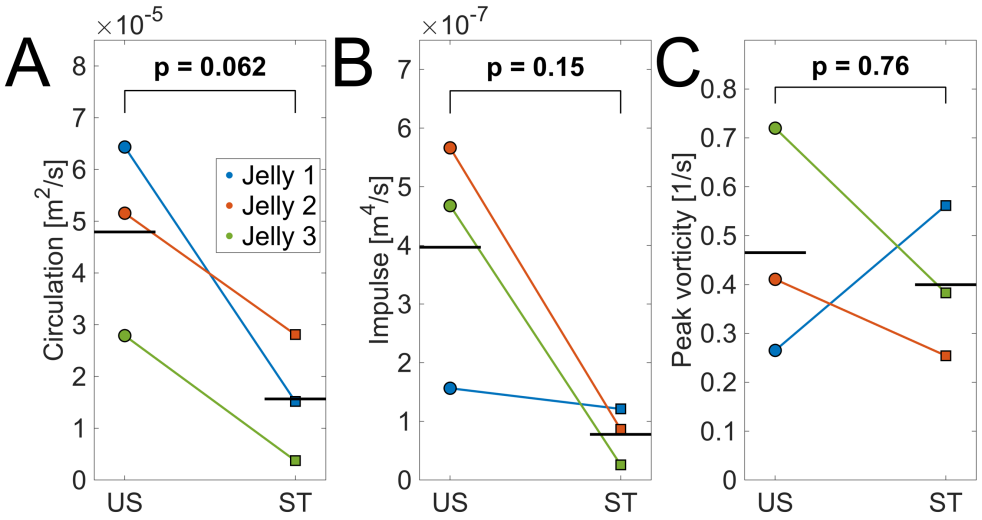

Figure 4.11: Vortex ring analysis (A) Circulation trends downward with stimulation using equation 4.15. Lines connect individual animals, black bars show mean, and statistics use paired t-test for each animal ($p = 0.062$). (B) Impulse also trends downward with stimulation using equation 4.16 ($p = 0.15$). (C) Peak vorticity measured within the vortex core measured using equation 4.14. Decreases for animals 2 and 3 but increases for animal 1, resulting in no change on average.

body diameter for three different jellyfish. These animals span a wide range of adult medusae sizes with Figures 4.12A-C having diameters measured at full relaxation of 15±0.5 cm, 19±0.5 cm, and 27±0.5 cm, respectively. As above, "US" represents the unstimulated trials and "ST" is the stimulated trials, while "PE" is measurements conducted with passive electronics embedded in the animal but without electrical stimulation. No change was observed with a final unstimulated animal experiment, so these results were combined with the initial unstimulated measurements. The "US" trials involved measuring an average of 5.7±0.5 complete pulses defined as full relaxation to full contraction, the "PE" trials involved measuring an average of 5.7±0.5 pulses, and the "ST" trials involved measuring an average of 5.3±1.2 pulses.

Figure 4.12D averages across the three animals shown in Figures 4.12A-C and shows a statistically significant decrease in margin movement with stimulation. The average of the margin movement from Figures 4.12A-C for each treatment is shown with the "US" and "ST" treatments resulting in a p-value of 0.035 measured using Welch's t-test. Comparing "US" and "PE" was not significant with a p-value of 0.31, while "PE" and "ST" have a p-value of 0.25. This shows that these embedded electronics stimulating the swimming jellyfish limit bell margin movement.

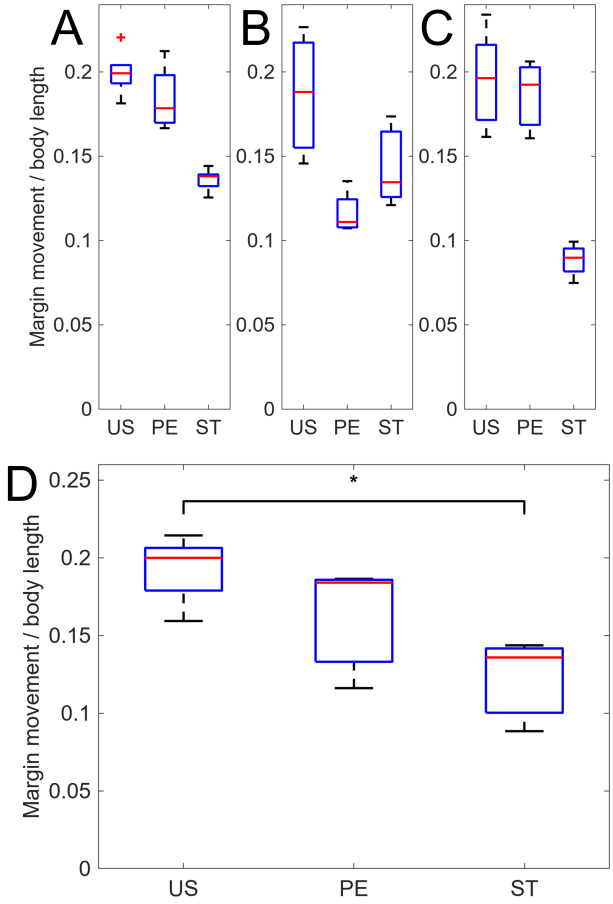

Figure 4.12: Margin movement (A)-(C) Margin movement between fully relaxed and contracted states for three jellyfish with diameters of 15±0.1 cm, 19±0.1 cm, and 27±0.1 cm respectively, measured at full relaxation. "US", "PE", and "ST" refer to unstimulated, unstimulated with embedded onboard passive electronics, and stimulated experiments. Stimulation reduces margin movement with a p-value of 0.035, while there is no statistically significant difference between the other experiments. (D) Average margin movement across (A)-(C). Stimulation reduces bell margin movement by 36.5±5.4% with a p-value of 0.035.

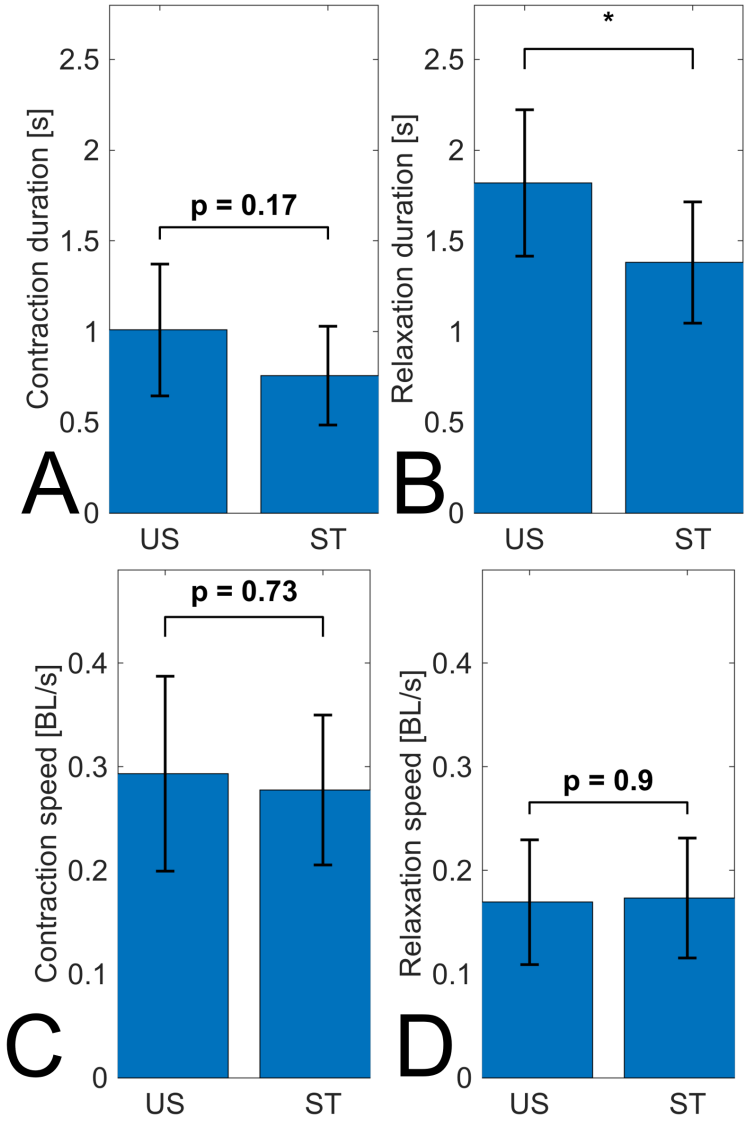

Figure 4.13: Bell kinematics. (A)-(B) Contraction and relaxation duration measurements for 6 jellyfish. Stimulation decreases relaxation duration by 24±9.7%. (C)-(D) Contraction and relaxation speed for 6 jellyfish show no statistically significant change with stimulation. Bars show mean ± SD across trials (one value per trial). P-values are from Welch's two-sample *t*-test comparing trial-level means between conditions.

We also measured contraction and relaxation duration and speed. Figures 4.13A-B show contraction and relaxation durations for six jellyfish comparing unstimulated and stimulated experiments. The relaxation duration exhibited a statistically significant decrease with a p-value of 0.042, while contraction duration was not statistically significant with a p-value of 0.17. Across experiments, relaxation duration was consistently longer than contraction duration. These measurements agree with previous observations of unstimulated jellyfish contraction and relaxation durations. In addition, animal biomechanics would predict this result, since jellyfish bell contraction is an active muscle movement while relaxation is mostly passive (Gemmell, Costello, et al., 2013; Costello, S. P. Colin, John O. Dabiri, et al., 2021). Neither contraction nor relaxation speeds changed with stimulation, suggesting that the muscular response from electrical stimulation is not different from the muscular response in an unstimulated pulse. We found p-values for contraction and relaxation speeds of 0.73 and 0.9, respectively.

4.4 Discussion and Conclusion

We used three-dimensional PIV to measure full velocity fields within the near-wake region behind free-swimming jellyfish—thus enabling the calculation of momentum and kinetic energy released to this region. We found that electrical stimulation significantly increased the normalized energy in the wake on a time-averaged basis by a factor of 2.9±1.2. Momentum analysis generally showed that stimulation increased radial momentum transport and decreased net downstream momentum. However, significant inter-animal variability makes interpreting these metrics challenging. Circulation and impulse similarly trend downwards suggesting reduced coherent vortex strength despite similar energy expenditure, while peak vorticity does not show a statistically significant change. While stimulated animals are still creating strong vortices with high peak vorticity, changes in muscle activation and swimming kinematics could lead to reduced mass entrainment.

Tracked jellyfish bell margins exhibited statistically significant reduced radial motion with stimulation. We also observed a decrease in relaxation duration. This suggests a combination of both mechanical and electrical factors affecting bell contraction. After the initial electrical bell stimulation, the jellyfish contraction speed and duration do not change. After the conclusion of the contraction phase, the relaxation begins and continues at a normal speed but does not reach full relaxation. This reduction in relaxation may arise either from the timing of electrical stimulation preventing full bell relaxation, or from mechanical effects of the embedded electrode

wires on the bell margin. Since electrical stimulation was found to be most reliable near the rhopalia at the bell margin, the electrodes were embedded at the point farthest radially from the center. As they move with the bell, the force required to bend the electrode wires could restrict animal movement. However, this effect is not fully mechanical since experiments with passive electronics showed no statistically significant decrease in margin movement. Electrical stimulation likely changes the timing of contraction relative to the development of the starting vortex, which may reduce the efficiency with which momentum is transferred to the surrounding fluid. Further work could test smaller diameter, but more fragile, wires. Lower frequency stimulation experiments could also elucidate the impact of stimulation timing on full relaxation.

The combination of higher wake energy ratios observed during stimulated swimming and decreased movement shows that externally paced contractions alter the coupling between bell kinematics and vortex formation. Combined with previous long-duration metabolic measurements in Chapter 3, these results suggest that the increased wake energy observed here provides a hydrodynamic mechanism, deriving from changes in swimming kinematics, explaining the elevated energy consumption previously measured in electrically stimulated jellyfish. Some work with other species shows that total circulation peaks early in the swim stroke (Costello, S. P. Colin, Gemmell, et al., 2019). This 'overpressure' phenomenon has been described in the vortex ring literature by Krueger and M. Gharib (2003) and Gemmell, John O. Dabiri, et al. (2021). Thus, the continued contraction follow-through lost due to changes in swimming kinematics may be important for generating directed momentum transport and higher circulation in the wake. However, previous work has consistently found stimulation increases swimming speeds, suggesting that, while potentially less directed, stimulated animals still produce significant hydrodynamic propulsion (Nicole W. Xu and John O. Dabiri, 2020; Anuszczyk and John O. Dabiri, 2024).

The present measurements are subject to several limitations. Wake energy and momentum were evaluated within a finite control volume in the near wake, which may not capture the full extent of the vortex structures as they evolve downstream. As a result, the reported energy ratios should be interpreted as relative measures within a consistent measurement domain rather than absolute estimates of total wake energetics. In addition, the limited number of animals and the observed inter-animal variability reduce the statistical power of some comparisons. These factors should

be considered when interpreting the magnitude of the reported changes. Future work extending the measurement domain and increasing sample size would help further constrain these effects.

Aurelia aurita jellyfish bells consist largely of viscoelastic transparent mesoglea (Demont and Gosline, 1988a; Megill, Gosline, and Blake, 2005). The elasticity stores energy during contraction that drives bell relaxation (Costello, S. P. Colin, John O. Dabiri, et al., 2021). A significant portion of the stored energy is dissipated in the tissue as heat and never produces motion of the animal body or surrounding fluid. This fraction has been measured to be approximately 0.42 for the hydromedusa *Polyorchis penicillatus* (Megill, Gosline, and Blake, 2005; Demont and Gosline, 1988a). This species is generally smaller than our species of inquiry, but both bells have similar stiffness values and behave as soft, viscoelastic gels (Megill, Gosline, and Blake, 2005; Gambini et al., 2012), suggesting the energy dissipated within the mesoglea is likely in a similar range of 0.4-0.5 of stored elastic energy. While the amount of elastically stored energy is unknown, estimates suggest passive energy recapture enables each swimming cycle to propel the animal 30% farther than without passive energy recapture (Gemmell, Costello, et al., 2013). Using data from Parts I and II of Demont and Gosline (1988a) and Demont and Gosline (1988b), viscoelastic dissipation is estimated to account for roughly 5-20% of the mechanical energy expended per swimming pulse in *Polyorchis penicillatus*, excluding additional hydrodynamic losses. A similar contribution of viscoelastic dissipation may therefore be expected in *Aurelia aurita*, although this has not been directly measured.

These experiments suggest a tradeoff between fast swimming and energetic efficiency. For *Aurelia aurita*, this and Chapter 3 suggest that in enclosed experiments there exists an approximately linear relationship between pulse frequency and energy consumption, after accounting for basal metabolism. Chapter 3 and Nicole W. Xu and John O. Dabiri (2020) measurements of jellyfish swimming experiments have shown energy consumption scales faster than pulse frequency. This is likely due to the changes in swimming kinematics caused by electrical stimulation documented in this work. Cost of transport (COT) therefore necessarily increases with this type of electrical stimulation. Determining the exact scaling relationship between swimming speed and energetic efficiency will require additional experiments. Measurements from Chapter 3 show that stimulation at 0.5 Hz increased free-swimming energy consumption by a factor of 5.1±0.4 with an estimated doubling of average

velocity. This corresponds to COT increasing by a factor of 2.5, bringing it closer to larger jetting jellyfish such as *Stomolophus meleagris* (R. J. Larson, 1987b), and highlighting a tradeoff that must be considered for future work.

While increased COT during short timescale experiments have little long term impact on the animals, the ability to maintain these energetic outputs over periods longer than 2 days has not been studied. Introducing food during swimming experiments could determine how stimulated jellyfish feed around the onboard electronics and measure the feasibility of maintaining high energetic states without mass loss as measured in Chapter 3. This is an important next step as we seek to deploy these stimulated jellyfish as biohybrid ocean-sensing robots.

Ocean deployments on the scale of minutes have been demonstrated by Anuszczyk, Yoder, et al. (2025), Rutledge et al. (2026), and Nicole W. Xu, Townsend, et al. (2020a). The implications of this work necessitate future ocean deployments consider increased COT when choosing electrical stimulation frequency. One option to manage energy consumption during a long-term deployment could include implementing a control loop to vary pulse frequency depending on mission scope and state. Lower pulse frequencies could be selected to conserve energy based on mission progress when decreased swimming speeds are appropriate.

Acknowledgments

The authors would like to thank Cabrillo Marine Aquarium and Aquarium of the Pacific for providing jellyfish used in these experiments. Matt Fu provided valuable assistance with the laser scanning setup.

Competing Interests

No competing interests declared.

Contribution

S.R.A. and J.O.D. conceived of project, S.R.A. and K.P. conducted experiments, S.R.A. and J.O.D. analyzed results, S.R.A. wrote initial draft and all authors edited paper.

Funding

This work was supported by the National Science Foundation Graduate Research Fellowship Grant Number DGE-1745301, National Science Foundation Grant 2311867 and funding from the U.S. Office of Naval Research.

Data Availability

Raw image data available upon request.

Chapter 5

CONCLUSION

The goals of this thesis were to further the development of biohybrid robotic jellyfish for ocean exploration by investigating the swimming dynamics, physiology, morphology, and fluid dynamics of electrically stimulated jellyfish to enable comprehensive and efficient ocean exploration.

5.1 Summary of contributions

1. **Design and implementation of 3D printed electronics housing.**
   Chapter 2 presents a waterproof, 3D resin-printed electronics housing that was later deployed to tens of meters depth with reliable sealing. This study introduces a threaded cap design to enable easy access to battery and electronics combined with modularity. Utilizing 3D printing allows easy iteration of housing designs and enables inclusion of additional sensors with minimal additional design modifications.

2. **Characterization of effects of modifying exumbrellar bell shape.**
   Chapter 2 quantifies the mechanical modification of jellyfish bell shape to decrease drag and enable significant onboard payload capacity of scientific sensors. Streamlining enhances swimming speeds while decreasing intracycle speed variability, potentially improving onboard measurement stability.

3. **Physics-based swimming kinematics model**
   A first-principles physics-based swimming kinematics model is presented in Chapter 2 to predict the performance of biohybrid jellyfish robots with various payload and animal geometries. This model generally captures the trends in both swimming speed and intracycle speed range with forebody mass.

4. **Analysis of long-distance swimming experiments.**
   Chapter 3 presents a jellyfish-tracking computer-vision system to enable continuous swimming for several days against a flow current in a vertical water treadmill. Simultaneous tracking enables analysis of jellyfish swimming over distances of several km in a 6 m tall tank.

5. **Development and validation of non-invasive metabolic technique.**
   Chapter 3 describes the development of a new non-invasive metabolic technique to measure the energy consumption of free-swimming jellyfish. A laser-scanning system enables volumetric reconstructions of live jellyfish to convert changes in morphology to energy consumption using known chemical composition. This technique was validated against conventional respirometry.

6. **Analytical swimming metabolism model.**
   An analytical physics-based swimming metabolism model is shown in chapter 3 that estimates metabolism in different environmental conditions and pulse rates. The model partitions total metabolic cost into basal, wake power, and drag power terms. This chapter also includes measurements of basal metabolic rates measured through rhopalial excision.

7. **Wake dynamics and kinematic effects of stimulation.**
   Chapter 4 quantifies the impacts of electrical stimulation on wake fluid dynamics and swimming kinematics using a single-camera, three-dimensional, three-component Particle Image Velocimetry (PIV) system. Full velocity fields enable the calculation of momentum and energy transport comparisons between unstimulated and stimulated free-swimming jellyfish.

8. **Field deployment of several species with enhanced reliability.**
   Appendix A presents field and lab tests analyzing the impact of rhopalia (nerve center) removal on electrical response reliability in *Aurelia aurita, Cassiopea xamachana,* and *Alatina alata*. Rhopalia excision prevents endogenous contractions, enabling complete electrical control of pulse timing. This technique demonstrated increased reliability and enhanced swimming speeds with all three species.

5.2 Opportunities for future work

Quantitative efficiency metrics for jellyfish

Despite substantial prior work, quantitative links between jellyfish biomechanics, hydrodynamics, and metabolism remain incomplete. This thesis addressed several of these gaps in Chapters 3 and 4, but also relied on a number of estimated or inferred parameters. In particular, direct measurements of propulsive hydrodynamic efficiency are still lacking for many species (Costello, S. P. Colin, John O. Dabiri, et al., 2021). The difficulty of maintaining consistent swimming behavior while measuring energy expenditure has limited such measurements, but the methods

presented here provide a path toward addressing this challenge. Future work should aim to quantify complete energy budgets, including mesoglea dissipation and elastic recovery, hydrodynamic losses in the wake, and the useful power contributing to propulsion. Such measurements would enable improved models of swimming efficiency and clarify how metabolism, fluid dynamics, and biomechanics interact to set performance limits.

These measurements could be accomplished by combining several methods from this thesis as well as previous work. Conducting respirometry of swimming animals could provide total energy consumption. Simultaneous 3D-3C laser scanning, as described in Chapter 4, would enable estimates of energy imparted to the fluid given sufficient resolution and scanning volume. Utilizing a flow-through system, or large tank, could enable free-swimming animals to be tracked with computer vision algorithms as described in Chapter 3. This could allow the calculation of propulsive efficiency. Finally, muscle energy dissipation could be assumed to be the remainder of the energy balance by neglecting growth, egestion, and feeding given the relatively short experimental timescales (S. Uye and Shimauchi, 2005). Additional tissue experiments, as described in Demont and Gosline (1988a), could inform *Aurelia* elasticity and resilience to quantify the fraction of energy recovered during the relaxation stroke. Together, these experiments would inform whole-system jellyfish energy budgets.

Directional control of swimming jellyfish

Expanding directional control to full three-axis locomotion is a major challenge in the deployment of this project. In this thesis, biohybrid jellyfish robots were constrained to one dimension by separating the centers of gravity and buoyancy to maintain downward swimming. Asymmetrical stimulation could prove useful, but variability of animal response and out-of-plane rotation make closed loop control difficult with this method. Another method translates a weight within the electronics housing to reorient the animal (Yoder and John O. Dabiri, 2025). This purely mechanical method could enable better control with four degrees of freedom.

Jellyfish swarm dynamics

Deployment of large swarms of jellyfish will require inter-animal coordination to maximize efficiency and spatial coverage. Most work on robotic swarms has focused on unmanned aerial vehicles, more commonly known as drones (Reynolds, 1987; Oh, M.-C. Park, and Ahn, 2015; Olfati-Saber, Fax, and Murray, 2007). More recent

work has begun to extend classical swarm principles to bioinspired and biohybrid systems, where robotic agents interact directly with biological organisms or emulate their collective behaviors to achieve distributed coordination (Ayali and Kaminka, 2023; Zhao et al., 2025). Adapting these principles to biohybrid systems will introduce new challenges related to insufficient communication between systems, reliability of animal response, and unpredictability of ocean currents.

Expanding testing to other species

This thesis focused primarily on *Aurelia aurita*, largely due to their widespread habitat, large body of literature, and relatively easy husbandry. Utilizing *Aurelia* has enabled significant advances to this platform but also places limitations on future usage. While distributed throughout the ocean, *Aurelia* are typically limited to shallow depths, with surveys documenting findings as deep as 200 m, (Han and S.-I. Uye, 2009) potentially limiting deep ocean deployment. Other species, such as *Pelagia noctiluca,* have been documented as deep as 1,400 m (Mariottini, Giacco, and Pane, 2008). While further work is needed to determine *Aurelia* resilience to the high pressures experienced at these depths (Ford, S. P. Colin, and Costello, 2026), substituting a different species could also be a viable option. Additionally, large species such as *Rhizostoma octopus*, weighing up to 35 kg, may enable the carrying of larger scientific payloads (Elliott, Hobson, and Tang, 2017). A comprehensive study of electrical stimulation on various jellyfish species could elucidate benefits of particular species for different deployments that ultimately lead to swarms of ocean-sensing biohybrid jellyfish.

Ocean exploration

This platform presents an opportunity for cheap and comprehensive ocean exploration and sensing. Jellyfish live throughout the ocean and are resilient to extremes in temperature, salinity, and depth, including in the deepest regions of the ocean (Gallo et al., 2015). As the impacts of climate change worsen, the need for better climate models increases (Benway et al., 2019). The ocean plays an outsized role in climate regulation as both a temperature and carbon sink (Levin and Le Bris, 2015). Deploying swarms of biohybrid jellyfish to measure the biogeochemistry of the ocean could inform future ocean models with additional data from previously unexplored regions and at higher resolutions. Additional work on embedded sensors, hardening of the payload for deeper depths, and directional control could enable widespread oceanic deployment.

BIBLIOGRAPHY

Acuña, José Luis, Ángel López-Urrutia, and Sean Colin (Sept. 16, 2011). "Faking Giants: The Evolution of High Prey Clearance Rates in Jellyfishes". In: *Science* 333.6049, pp. 1627–1629. ISSN: 0036-8075, 1095-9203. DOI: 10.1126/science.1205134. URL: https://www.science.org/doi/10.1126/science.1205134.

Adrian, Ronald J. and Jerry Westerweel (2011). *Particle Image Velocimetry*. Cambridge ; New York: Cambridge University Press. 586 pp. ISBN: 978-0-521-44008-0.

Anuszczyk, Simon R. and John O. Dabiri (Feb. 2024). "Electromechanical enhancement of live jellyfish for ocean exploration". In: *Bioinspiration & Biomimetics* 19.2, p. 026018. ISSN: 1748-3190. DOI: 10.1088/1748-3190/ad277f. URL: https://dx.doi.org/10.1088/1748-3190/ad277f.

Anuszczyk, Simon R., Noa Yoder, et al. (Dec. 2, 2025). "Increasing the Reliability and Versatility of Jellyfish Biohybrid Vehicles via Species Selection and Rhopalia Removal". In: *Biomimetics* 10.12. ISSN: 2313-7673. DOI: 10.3390/biomimetics10120810.

Arai, Mary Needler (1986). "Oxygen Consumption of Fed and Starved Aequorea victoria (Murbach and Shearer, 1902) (Hydromedusae)". In: *Physiological Zoology* 59.2, pp. 188–193. ISSN: 0031-935X. URL: https://www.jstor.org/stable/30156032.

Ayali, Amir and Gal A. Kaminka (July 14, 2023). "The hybrid bio-robotic swarm as a powerful tool for collective motion research: a perspective". In: *Frontiers in Neurorobotics* 17. ISSN: 1662-5218. DOI: 10.3389/fnbot.2023.1215085. URL: https://www.frontiersin.org/journals/neurorobotics/articles/10.3389/fnbot.2023.1215085/full.

Batchelor, G. K. (2000). *An Introduction to Fluid Dynamics*. Cambridge Mathematical Library. Cambridge: Cambridge University Press. ISBN: 978-0-521-66396-0. DOI: 10.1017/CBO9780511800955.

Benway, Heather M. et al. (2019). *Ocean Time Series Observations of Changing Marine Ecosystems: An Era of Integration, Synthesis, and Societal Applications*. Volume: 6. DOI: 10.3389/fmars.2019.00393. URL: https://repository.library.noaa.gov.

Bondyale-Juez, Daniel R. et al. (Mar. 10, 2022). "Wind Drifting vs. Pulsating Swimming Jellyfish: Respiratory Metabolism and Composition Differences in Physalis physalis, Velella velella, Aurelia aurita, and Pelagia noctiluca". In: *Frontiers in Marine Science* 9. ISSN: 2296-7745. DOI: 10.3389/fmars.2022.817196. URL: https://www.frontiersin.org/journals/marine-science/articles/10.3389/fmars.2022.817196/full.

Bozkurt, Alper, Robert F Gilmour, and Amit Lal (Sept. 2009). "Balloon-assisted flight of radio-controlled insect biobots". In: *IEEE transactions on bio-medical engineering* 56.9, pp. 2304–2307. ISSN: 1558-2531. DOI: 10.1109/TBME.2009.2022551.

Bradley, A.M. et al. (Oct. 2001). "Power systems for autonomous underwater vehicles". In: *IEEE Journal of Oceanic Engineering* 26.4, pp. 526–538. ISSN: 1558-1691. DOI: 10.1109/48.972089. URL: https://ieeexplore.ieee.org/document/972089.

Brill (1987). *Fishery Bulletin*. Google-Books-ID: yirB9EXef2EC. National Marine Fisheries Service. 896 pp.

Carter, Matt Ian Daniel et al. (Oct. 26, 2016). "Navigating uncertain waters: a critical review of inferring foraging behaviour from location and dive data in pinnipeds". In: *Movement Ecology* 4.1, p. 25. ISSN: 2051-3933. DOI: 10.1186/s40462-016-0090-9. URL: https://doi.org/10.1186/s40462-016-0090-9.

Charette, Matthew A. and Walter H. F. Smith (Oct. 2, 2015). "The Volume of Earth's Ocean". In: *Oceanography* 23.2, pp. 112–114. DOI: 10.5670/oceanog.2010.51. URL: https://tos.org/oceanography/article/the-volume-of-earths-ocean.

Chung, Hyunjae, Jongchan Lee, and Won Young Lee (June 1, 2021). "A Review: Marine Bio-logging of Animal Behaviour and Ocean Environments". In: *Ocean Science Journal* 56.2, pp. 117–131. ISSN: 2005-7172. DOI: 10.1007/s12601-021-00015-1. URL: https://doi.org/10.1007/s12601-021-00015-1.

Costello, John H., Sean P. Colin, John O. Dabiri, et al. (2021). "The Hydrodynamics of Jellyfish Swimming". In: *Annual Review of Marine Science* 13.1. _eprint: https://doi.org/10.1146/annurev-marine-031120-091442, pp. 375–396. DOI: 10.1146/annurev-marine-031120-091442. URL: https://doi.org/10.1146/annurev-marine-031120-091442.

Costello, John H., Sean P. Colin, Brad J. Gemmell, et al. (July 5, 2019). "Hydrodynamics of Vortex Generation during Bell Contraction by the Hydromedusa Eutonina indicans (Romanes, 1876)". In: *Biomimetics* 4.3, p. 44. ISSN: 2313-7673. DOI: 10.3390/biomimetics4030044. URL: https://pmc.ncbi.nlm.nih.gov/articles/PMC6784291/.

Cuevas, E et al. (Oct. 24, 2008). "Post-nesting migratory movements of hawksbill turtles Eretmochelys imbricata in waters adjacent to the Yucatan Peninsula, Mexico". In: *Endangered Species Research* 10, pp. 123–133. ISSN: 1863-5407, 1613-4796. DOI: 10.3354/esr00128. URL: http://www.int-res.com/abstracts/esr/v10/p123-133/.

Dabiri, J. O. et al. (Apr. 15, 2010). "A wake-based correlate of swimming performance and foraging behavior in seven co-occurring jellyfish species". In: *Journal of Experimental Biology* 213.8, pp. 1217–1225. ISSN: 0022-0949. DOI: 10.1242/jeb.034660. URL: https://doi.org/10.1242/jeb.034660.

Dabiri, John O., Sean P. Colin, and John H. Costello (June 1, 2006). "Fast-swimming hydromedusae exploit velar kinematics to form an optimal vortex wake". In: *Journal of Experimental Biology* 209.11, pp. 2025–2033. ISSN: 1477-9145, 0022-0949. DOI: 10.1242/jeb.02242. URL: https://journals.biologists.com/jeb/article/209/11/2025/16173/Fast-swimming-hydromedusae-exploit-velar.

Daniel, Thomas (1983). "Mechanics and energetics of medusan jet propulsion". In: URL: https://cdnsciencepub.com/doi/abs/10.1139/z83-190?journalCode=cjz.

Daniels, Joost, Giovanna Sainz, and Kakani Katija (Jan. 1, 2023). "New Method for Rapid 3D Reconstruction of Semi-Transparent Underwater Animals and Structures". In: *Integrative Organismal Biology* 5.1, obad023. ISSN: 2517-4843. DOI: 10.1093/iob/obad023. URL: https://doi.org/10.1093/iob/obad023.

Demont, M. Edwin and John M. Gosline (Jan. 1, 1988a). "Mechanics of Jet Propulsion in the Hydromedusan Jellyfish, Polyorchis Penicillatus: I. Mechanical Properties of the Locomotor Structure". In: *Journal of Experimental Biology* 134. ADS Bibcode: 1988JExpB.134..313D, pp. 313–332. DOI: 10.1242/jeb.134.1.313. URL: https://ui.adsabs.harvard.edu/abs/1988JExpB.134..313D.

Demont, M. Edwin and John M. Gosline (Jan. 1, 1988b). "Mechanics of Jet Propulsion in the Hydromedusan Jellyfish, Polyorchis Penicillatus:II. Energetics of the Jet Cycle". In: *Journal of Experimental Biology* 134.1, pp. 333–345. ISSN: 0022-0949. DOI: 10.1242/jeb.134.1.333. URL: https://doi.org/10.1242/jeb.134.1.333.

Dillon, T. M. (July 1, 1977). "Effects of acute changes in temperature and salinity on pulsation rates in ephyrae of the scyphozoan Aurelia aurita". In: *Marine Biology* 42.1, pp. 31–35. ISSN: 1432-1793. DOI: 10.1007/BF00392011. URL: https://doi.org/10.1007/BF00392011.

Drucker, Eliot G. and George V. Lauder (Sept. 15, 1999). "Locomotor forces on a swimming fish: three-dimensional vortex wake dynamics quantified using digital particle image velocimetry". In: *Journal of Experimental Biology* 202.18, pp. 2393–2412. ISSN: 0022-0949. DOI: 10.1242/jeb.202.18.2393. URL: https://doi.org/10.1242/jeb.202.18.2393.

Einen, Olai, Børre Waagan, and Magny S. Thomassen (July 1, 1998). "Starvation prior to slaughter in Atlantic salmon (*Salmo salar*)". In: *Aquaculture* 166.1, pp. 85–104. ISSN: 0044-8486. DOI: 10.1016/S0044-8486(98)00279-8. URL: https://www.sciencedirect.com/science/article/pii/S0044848698002798.

Elliott, Anna, Victoria Hobson, and Kam W. Tang (Jan. 1, 2017). "Balancing fishery and conservation: a case study of the barrel jellyfish Rhizostoma octopus in South Wales". In: *ICES Journal of Marine Science* 74.1, pp. 234–241. ISSN: 1054-3139. DOI: 10.1093/icesjms/fsw157. URL: https://doi.org/10.1093/icesjms/fsw157.

Elsinga, G. E. et al. (Dec. 1, 2006). "Tomographic particle image velocimetry". In: *Experiments in Fluids* 41.6, pp. 933–947. ISSN: 1432-1114. DOI: 10.1007/s00348-006-0212-z. URL: https://doi.org/10.1007/s00348-006-0212-z.

Favali, P. and L. Beranzoli (Dec. 25, 2006). "Seafloor Observatory Science: a Review". In: *Annals of Geophysics* 49.2. ISSN: 2037-416X. DOI: 10.4401/ag-3125. URL: https://www.annalsofgeophysics.eu/index.php/annals/article/view/3125.

Fish, F. E. and G. V. Lauder (Jan. 21, 2006). "PASSIVE AND ACTIVE FLOW CONTROL BY SWIMMING FISHES AND MAMMALS". In: *Annual Review of Fluid Mechanics* 38 (Volume 38, 2006), pp. 193–224. ISSN: 0066-4189, 1545-4479. DOI: 10.1146/annurev.fluid.38.050304.092201. URL: https://www.annualreviews.org/content/journals/10.1146/annurev.fluid.38.050304.092201.

Fish, Frank E. et al. (Jan. 15, 2014). "Measurement of hydrodynamic force generation by swimming dolphins using bubble DPIV". In: *Journal of Experimental Biology* 217.2, pp. 252–260. ISSN: 0022-0949. DOI: 10.1242/jeb.087924. URL: https://doi.org/10.1242/jeb.087924.

Ford, Mitchell P., Sean P. Colin, and John H. Costello (Jan. 19, 2026). "Effects of high hydrostatic pressure on the mechanical performance and behavior of shallow-water jellyfish (Aurelia aurita)". In: *Journal of Experimental Biology* 229.2, jeb251053. ISSN: 0022-0949. DOI: 10.1242/jeb.251053. URL: https://doi.org/10.1242/jeb.251053.

Forest, A. et al. (Apr. 10, 2012). "Size distribution of particles and zooplankton across the shelf-basin system in southeast Beaufort Sea: combined results from an Underwater Vision Profiler and vertical net tows". In: *Biogeosciences* 9.4, pp. 1301–1320. ISSN: 1726-4189. DOI: 10.5194/bg-9-1301-2012. URL: https://bg.copernicus.org/articles/9/1301/2012/.

Fossette, Sabrina et al. (Oct. 15, 2016). "How to tag a jellyfish? A methodological review and guidelines to successful jellyfish tagging". In: *Journal of Plankton Research* 38. DOI: 10.1093/plankt/fbw073.

Frandsen, Kristian Toft and Hans Ulrik Riisgård (Dec. 22, 1997). "Size dependent respiration and growth of jellyfish, Aurelia aurita". In: *Sarsia* 82.4. _eprint: https://doi.org/10.1080/00364827.1997.10413659, pp. 307–312. ISSN: 0036-4827. DOI: 10.1080/00364827.1997.10413659. URL: https://doi.org/10.1080/00364827.1997.10413659.

Fu, Matt K., Isabel A. Houghton, and John O. Dabiri (Aug. 2021). "A single-camera, 3D scanning velocimetry system for quantifying active particle aggregations". In: *Experiments in Fluids* 62.8, p. 168. ISSN: 0723-4864, 1432-1114. DOI: 10.1007/s00348-021-03256-x. URL: https://link.springer.com/10.1007/s00348-021-03256-x.

Fu, Zhilu et al. (Sept. 9, 2014). “Body size reduction under starvation, and the point of no return, in ephyrae of the moon jellyfish Aurelia aurita”. In: *Marine Ecology Progress Series* 510, pp. 255–263. ISSN: 0171-8630, 1616-1599. DOI: 10.3354/meps10799. URL: https://www.int-res.com/abstracts/meps/v510/p255-263/.

Gallo, Natalya et al. (May 1, 2015). “Submersible- and lander-observed community patterns in the Mariana and New Britain trenches: Influence of productivity and depth on epibenthic and scavenging communities”. In: *Deep Sea Research Part I: Oceanographic Research Papers* 99, pp. 119–133. DOI: 10.1016/j.dsr.2014.12.012.

Gambini, Camille et al. (Jan. 4, 2012). “Micro- and macrorheology of jellyfish extracellular matrix”. In: *Biophysical Journal* 102.1, pp. 1–9. ISSN: 1542-0086. DOI: 10.1016/j.bpj.2011.11.4004.

Gambino, Gaetana et al. (Mar. 2024). “Starvation resistance in planarians: multiple strategies to get a thrifty phenotype”. In: *The FEBS Journal* 291.5, pp. 965–985. ISSN: 1742-464X, 1742-4658. DOI: 10.1111/febs.17020. URL: https://febs.onlinelibrary.wiley.com/doi/10.1111/febs.17020.

Garcia, Herncin E. and Louis I. Gordon (1992). “Oxygen solubility in seawater: Better fitting equations”. In: *Limnology and Oceanography* 37.6. _eprint: https://aslopubs.onlinelibrary.wiley.com/doi/pdf/10.4319/lo.1992.37.6.1307, pp. 1307–1312. ISSN: 1939-5590. DOI: 10.4319/lo.1992.37.6.1307. URL: https://onlinelibrary.wiley.com/doi/abs/10.4319/lo.1992.37.6.1307.

Gemmell, Brad J., John H. Costello, et al. (Oct. 29, 2013). “Passive energy recapture in jellyfish contributes to propulsive advantage over other metazoans”. In: *Proceedings of the National Academy of Sciences* 110.44, pp. 17904–17909. DOI: 10.1073/pnas.1306983110. URL: https://www.pnas.org/doi/full/10.1073/pnas.1306983110.

Gemmell, Brad J., John O. Dabiri, et al. (June 17, 2021). “Cool your jets: biological jet propulsion in marine invertebrates”. In: *Journal of Experimental Biology* 224.12, jeb222083. ISSN: 0022-0949. DOI: 10.1242/jeb.222083. URL: https://doi.org/10.1242/jeb.222083.

Gemmell, Brad J., Daniel R. Troolin, et al. (July 2015). “Control of vortex rings for manoeuvrability”. In: *Journal of The Royal Society Interface* 12.108, p. 20150389. ISSN: 1742-5689, 1742-5662. DOI: 10.1098/rsif.2015.0389. URL: https://royalsocietypublishing.org/doi/10.1098/rsif.2015.0389.

Gharib, Morteza, Edmond Rambod, and Karim Shariff (Apr. 1998). “A universal time scale for vortex ring formation”. In: *Journal of Fluid Mechanics* 360, pp. 121–140. ISSN: 1469-7645, 0022-1120. DOI: 10.1017/S0022112097008410. URL: https://www.cambridge.org/core/journals/journal-of-fluid-mechanics/article/universal-time-scale-for-vortex-ring-formation/8DA34E3C7204D966AC92C5FA1E1A9BBC.

Gingerich, Andrew James, David P. Philipp, and Cory D. Suski (Mar. 2010). "Effects of nutritional status on metabolic rate, exercise and recovery in a freshwater fish". In: *Journal of Comparative Physiology. B, Biochemical, Systemic, and Environmental Physiology* 180.3, pp. 371–384. ISSN: 1432-136X. DOI: 10.1007/s00360-009-0419-4.

Groot, Valesca A de, Clive Trueman, and Amanda E Bates (Jan. 1, 2024). "Incorporating otolith-isotope inferred field metabolic rate into conservation strategies". In: *Conservation Physiology* 12.1, coae013. ISSN: 2051-1434. DOI: 10.1093/conphys/coae013. URL: https://doi.org/10.1093/conphys/coae013.

Han, Chang-Hoon and Shin-Ichi Uye (Aug. 1, 2009). "Quantification of the abundance and distribution of the common jellyfish Aurelia aurita s.l. with a Dual-frequency IDentification SONar (DIDSON)". In: *Journal of Plankton Research* 31.8, pp. 805–814. ISSN: 0142-7873. DOI: 10.1093/plankt/fbp029. URL: https://doi.org/10.1093/plankt/fbp029.

Harris, Roger (1999). *ICES zooplankton methodology manual*. San Diego, Calif. London: Academic. ISBN: 978-0-12-327645-2.

Hedrick, Tyson L (July 2008). "Software techniques for two- and three-dimensional kinematic measurements of biological and biomimetic systems". In: *Bioinspiration & Biomimetics* 3.3, p. 034001. ISSN: 1748-3190. DOI: 10.1088/1748-3182/3/3/034001. URL: https://doi.org/10.1088/1748-3182/3/3/034001.

Hoerner, Sighard F (1967). "Fluid-Dynamic Drag". In.

Ikeda, T. et al. (Feb. 14, 2000). *ICES Zooplankton Methodology Manual*. Elsevier. 455-532. ISBN: 978-0-08-049533-0.

Ishii, Haruto and Ulf Båmstedt (Jan. 1, 1998). "Food regulation of growth and maturation in a natural population of Aurelia aurita (L.)" In: *Journal of Plankton Research* 20.5, pp. 805–816. ISSN: 0142-7873. DOI: 10.1093/plankt/20.5.805. URL: https://doi.org/10.1093/plankt/20.5.805.

Katija, Kakani and John O. Dabiri (July 2009). "A viscosity-enhanced mechanism for biogenic ocean mixing". In: *Nature* 460.7255, pp. 624–626. ISSN: 1476-4687. DOI: 10.1038/nature08207. URL: https://www.nature.com/articles/nature08207.

Katzschmann, Robert et al. (Mar. 21, 2018). "Exploration of underwater life with an acoustically controlled soft robotic fish". In: *Science Robotics* 3, eaar3449. DOI: 10.1126/scirobotics.aar3449.

Kavanaugh, Maria T. et al. (Nov. 9, 2021). "Satellite Remote Sensing and the Marine Biodiversity Observation Network: Current Science and Future Steps". In: *Oceanography* 34.2, pp. 62–79. DOI: 10.5670/oceanog.2021.215. URL: https://tos.org/oceanography/article/satellite-remote-sensing-and-the-marine-biodiversity-observation-network-current-science-and-future-steps.

Keys, Ancel B. (Oct. 1930). "The measurement of the respiratory exchange of aquatic animals". In: *The Biological Bulletin* 59.2, pp. 187–198. ISSN: 0006-3185. DOI: 10.2307/1536988. URL: https://www.journals.uchicago.edu/doi/abs/10.2307/1536988.

Krueger, Paul S. and M. Gharib (May 1, 2003). "The significance of vortex ring formation to the impulse and thrust of a starting jet". In: *Physics of Fluids* 15.5, pp. 1271–1281. ISSN: 1070-6631. DOI: 10.1063/1.1564600. URL: https://doi.org/10.1063/1.1564600.

Larson, R. J (Jan. 1, 1987a). "Respiration and carbon turnover rates of medusae from the NE Pacific". In: *Comparative Biochemistry and Physiology Part A: Physiology* 87.1, pp. 93–100. ISSN: 0300-9629. DOI: 10.1016/0300-9629(87)90430-0. URL: https://www.sciencedirect.com/science/article/pii/0300962987904300.

Larson, R. J. (Nov. 1, 1987b). "Costs of transport for the scyphomedusa *Stomolophus meleagris* L. Agassiz". In: *Canadian Journal of Zoology* 65.11, pp. 2690–2695. ISSN: 0008-4301, 1480-3283. DOI: 10.1139/z87-408. URL: http://www.nrcresearchpress.com/doi/10.1139/z87-408.

Levin, Lisa A. and Nadine Le Bris (Nov. 13, 2015). "The deep ocean under climate change". In: *Science* 350.6262, pp. 766–768. ISSN: 1095-9203. DOI: 10.1126/science.aad0126.

Li, Derek J. and Leah Mendelson (Feb. 21, 2023). "Volumetric measurements of wake impulse and kinetic energy for evaluating swimming performance". In: *Experiments in Fluids* 64.3, p. 47. ISSN: 1432-1114. DOI: 10.1007/s00348-023-03586-y. URL: https://doi.org/10.1007/s00348-023-03586-y.

Li, Guorui et al. (Mar. 2021). "Self-powered soft robot in the Mariana Trench". In: *Nature* 591.7848, pp. 66–71. ISSN: 1476-4687. DOI: 10.1038/s41586-020-03153-z.

Liberzon, Alex et al. (Dec. 7, 2019). *OpenPIV/openpiv-python: fixed windows conda-forge failure with encoding*. DOI: 10.5281/zenodo.3566451. URL: https://zenodo.org/records/3566451.

Lighthill, M. J. (1997). *Mathematical biofluiddynamics*. Philadelphia, Pa: Society for Industrial and Applied Mathematics. 281 pp. ISBN: 978-0-89871-014-4.

Lilley, Martin KS et al. (2014). "Individual shrinking to enhance population survival: quantifying the reproductive and metabolic expenditures of a starving jellyfish, Pelagia noctiluca". In: *Journal of plankton research* 36.6, pp. 1585–1597. URL: https://academic.oup.com/plankt/article-abstract/36/6/1585/1480566.

Manthiram, Arumugam (Oct. 25, 2017). "An Outlook on Lithium Ion Battery Technology". In: *ACS central science* 3.10, pp. 1063–1069. ISSN: 2374-7943. DOI: 10.1021/acscentsci.7b00288.

Mariottini, Gian Luigi, Elisabetta Giacco, and Luigi Pane (Sept. 4, 2008). "The Mauve Stinger Pelagia noctiluca (Forsskål, 1775). Distribution, Ecology, Toxicity and Epidemiology of Stings. A Review". In: *Marine Drugs* 6.3, pp. 496–513. ISSN: 1660-3397. DOI: 10.3390/md20080025. URL: https://pmc.ncbi.nlm.nih.gov/articles/PMC2579739/.

Matic, Jamie J. et al. (Apr. 1, 2014). "Wireless Communication By an Autonomous Self-Powered Cyborg Insect". In: *ECS Meeting Abstracts* MA2014-01.22, p. 968. ISSN: 2151-2043. DOI: 10.1149/MA2014-01/22/968. URL: https://iopscience.iop.org/article/10.1149/MA2014-01/22/968/meta.

McHenry, Matthew J. and Jason Jed (Nov. 15, 2003). "The ontogenetic scaling of hydrodynamics and swimming performance in jellyfish (Aurelia aurita)". In: *Journal of Experimental Biology* 206.22, pp. 4125–4137. ISSN: 0022-0949. DOI: 10.1242/jeb.00649. URL: https://doi.org/10.1242/jeb.00649.

Megill, William M., John M. Gosline, and Robert W. Blake (Oct. 15, 2005). "The modulus of elasticity of fibrillin-containing elastic fibres in the mesoglea of the hydromedusa Polyorchis penicillatus". In: *Journal of Experimental Biology* 208.20, pp. 3819–3834. ISSN: 0022-0949. DOI: 10.1242/jeb.01765. URL: https://doi.org/10.1242/jeb.01765.

Mohebbi, Nina et al. (Dec. 2024). "Measurements and modelling of induced flow in collective vertical migration". In: *Journal of Fluid Mechanics* 1001, A50. ISSN: 0022-1120, 1469-7645. DOI: 10.1017/jfm.2024.1102.

Mooney, T. Aran et al. (Sept. 28, 2015). "ITAG: an eco-sensor for fine-scale behavioral measurements of soft-bodied marine invertebrates". In: *Animal Biotelemetry* 3.1, p. 31. ISSN: 2050-3385. DOI: 10.1186/s40317-015-0076-1. URL: https://doi.org/10.1186/s40317-015-0076-1.

Nawroth, Janna C. et al. (Aug. 2012). "A tissue-engineered jellyfish with biomimetic propulsion". In: *Nature Biotechnology* 30.8, pp. 792–797. ISSN: 1546-1696. DOI: 10.1038/nbt.2269.

Oh, Kwang-Kyo, Myoung-Chul Park, and Hyo-Sung Ahn (Mar. 1, 2015). "A survey of multi-agent formation control". In: *Automatica* 53, pp. 424–440. ISSN: 0005-1098. DOI: 10.1016/j.automatica.2014.10.022. URL: https://www.sciencedirect.com/science/article/pii/S0005109814004038.

Olfati-Saber, Reza, J. Alex Fax, and Richard M. Murray (Jan. 2007). "Consensus and Cooperation in Networked Multi-Agent Systems". In: *Proceedings of the IEEE* 95.1, pp. 215–233. ISSN: 1558-2256. DOI: 10.1109/JPROC.2006.887293. URL: https://ieeexplore.ieee.org/document/4118472.

Park, Sung-Jin et al. (July 8, 2016). "Phototactic guidance of a tissue-engineered soft-robotic ray". In: *Science (New York, N.Y.)* 353.6295, pp. 158–162. ISSN: 0036-8075. DOI: 10.1126/science.aaf4292. URL: https://pmc.ncbi.nlm.nih.gov/articles/PMC5526330/.

Parker, D. E., C. K. Folland, and M. Jackson (Dec. 1995). “Marine surface temperature: Observed variations and data requirements”. In: *Climatic Change* 31.2. Number: 2-4, pp. 559–600. ISSN: 1573-1480. DOI: 10.1007/bf01095162. URL: https://articles.researchsolutions.com/10.1007/bf01095162.

Picardi, G. et al. (May 13, 2020). “Bioinspired underwater legged robot for seabed exploration with low environmental disturbance”. In: *Science Robotics* 5.42, eaaz1012. ISSN: 2470-9476. DOI: 10.1126/scirobotics.aaz1012.

Prasad, A. K. and R. J. Adrian (June 1, 1993). “Stereoscopic particle image velocimetry applied to liquid flows”. In: *Experiments in Fluids* 15.1, pp. 49–60. ISSN: 1432-1114. DOI: 10.1007/BF00195595. URL: https://doi.org/10.1007/BF00195595.

Purcell, J. E. (Oct. 25, 2007). “Environmental effects on asexual reproduction rates of the scyphozoan Aurelia labiata”. In: *Marine Ecology Progress Series* 348, pp. 183–196. ISSN: 1616-1599, 0171-8630. DOI: 10.3354/meps07056. URL: https://www.int-res.com/journals/meps/articles/meps07056.

Purcell, Jennifer E. (2012). “Jellyfish and ctenophore blooms coincide with human proliferations and environmental perturbations”. In: *Annual Review of Marine Science* 4, pp. 209–235. ISSN: 1941-1405. DOI: 10.1146/annurev-marine-120709-142751.

Purcell, Jennifer E. et al. (2010). “Use of respiration rates of scyphozoan jellyfish to estimate their effects on the food web”. In: *Jellyfish Blooms: New Problems and Solutions*. Ed. by Jennifer E. Purcell and Dror L. Angel. Dordrecht: Springer Netherlands, pp. 135–152. ISBN: 978-90-481-9541-1. DOI: 10.1007/978-90-481-9541-1_11. URL: https://doi.org/10.1007/978-90-481-9541-1_11.

Ramirez-Llodra, E. et al. (Sept. 22, 2010). “Deep, diverse and definitely different: unique attributes of the world’s largest ecosystem”. In: *Biogeosciences* 7.9, pp. 2851–2899. ISSN: 1726-4170. DOI: 10.5194/bg-7-2851-2010. URL: https://bg.copernicus.org/articles/7/2851/2010/.

Reul, Nicolas et al. (Apr. 30, 2014). “Sea Surface Salinity Observations from Space with the SMOS Satellite: A New Means to Monitor the Marine Branch of the Water Cycle”. In: *Surveys In Geophysics* 35.3, pp. 681–722. ISSN: 0169-3298. DOI: 10.1007/s10712-013-9244-0. URL: https://archimer.ifremer.fr/doc/00152/26334/.

Reynolds, Craig W. (Aug. 1, 1987). “Flocks, herds and schools: A distributed behavioral model”. In: *Proceedings of the 14th annual conference on Computer graphics and interactive techniques*. SIGGRAPH ’87. New York, NY, USA: Association for Computing Machinery, pp. 25–34. ISBN: 978-0-89791-227-3. DOI: 10.1145/37401.37406. URL: https://dl.acm.org/doi/10.1145/37401.37406.

Romanes, George John (1885). *Jelly-Fish, Star-Fish, and Sea-Urchins: Being a Research on Primitive Nervous Systems*. https://www.gutenberg.org/files/46607/46607-h/46607-h.htm. Last Modified: 2025-05-18T22:26:16.586699+00:00. URL: https://www.gutenberg.org/cache/epub/46607/pg46607-images.html.

Romano, Donato (Mar. 22, 2023). "The beehive of the future is a robot socially interacting with honeybees". In: *Science Robotics* 8.76, eadh1824. DOI: 10.1126/scirobotics.adh1824. URL: https://www.science.org/doi/10.1126/scirobotics.adh1824.

Romano, Donato et al. (June 1, 2019). "A review on animal–robot interaction: from bio-hybrid organisms to mixed societies". In: *Biological Cybernetics* 113.3, pp. 201–225. ISSN: 1432-0770. DOI: 10.1007/s00422-018-0787-5. URL: https://doi.org/10.1007/s00422-018-0787-5.

Rosenhead, Louis (1963). *Laminar boundary layers; an account of the development, structure, and stability of laminar boundary layers in incompressible fluids, together with a description of the associated experimental techniques*. In collab. with Internet Archive. Oxford [Eng.] Clarendon Press. 742 pp. URL: http://archive.org/details/laminarboundaryl0000rose.

Rudnick, Daniel L. (Jan. 3, 2016). "Ocean Research Enabled by Underwater Gliders". In: *Annual Review of Marine Science* 8 (Volume 8, 2016), pp. 519–541. ISSN: 1941-1405, 1941-0611. DOI: 10.1146/annurev-marine-122414-033913. URL: https://www.annualreviews.org/content/journals/10.1146/annurev-marine-122414-033913.

Ruiz, Lydia A., Robert W. Whittlesey, and John O. Dabiri (Feb. 10, 2011). "Vortex-enhanced propulsion". In: *Journal of Fluid Mechanics* 668, pp. 5–32. ISSN: 0022-1120, 1469-7645. DOI: 10.1017/S0022112010004908. URL: https://www.cambridge.org/core/product/identifier/S0022112010004908/type/journal_article.

Rutledge, Kelsi M. et al. (2026). "Biohybrid robotic jellyfish for swimming-enhanced vertical ocean profiling". In.

Ryabinin, Vladimir et al. (July 31, 2019). "The UN Decade of Ocean Science for Sustainable Development". In: *Frontiers in Marine Science* 6. DOI: 10.3389/fmars.2019.00470.

Saffman, P. G. (Feb. 1978). "The number of waves on unstable vortex rings". In: *Journal of Fluid Mechanics* 84.4, pp. 625–639. ISSN: 1469-7645, 0022-1120. DOI: 10.1017/S0022112078000385.

Saffman, P. G. (1992). *Vortex Dynamics*. Cambridge Monographs on Mechanics. Cambridge: Cambridge University Press. ISBN: 978-0-521-47739-0. DOI: 10.1017/CBO9780511624063. URL: https://www.cambridge.org/core/books/vortex-dynamics/2F33335617172249253B949EA3406F89.

Sahin, Mehmet, Kamran Mohseni, and Sean P. Colin (Aug. 15, 2009). "The numerical comparison of flow patterns and propulsive performances for the hydromedusae Sarsia tubulosa and Aequorea victoria". In: *Journal of Experimental Biology* 212.16, pp. 2656–2667. ISSN: 0022-0949. DOI: 10.1242/jeb.025536. URL: https://doi.org/10.1242/jeb.025536.

Sahoo, Avilash, Santosha K. Dwivedy, and P. S. Robi (June 1, 2019). "Advancements in the field of autonomous underwater vehicle". In: *Ocean Engineering* 181, pp. 145–160. ISSN: 0029-8018. DOI: 10.1016/j.oceaneng.2019.04.011. URL: https://www.sciencedirect.com/science/article/pii/S0029801819301623.

Sanchez, Carlos J. et al. (Apr. 6, 2015). "Locomotion control of hybrid cockroach robots". In: *Journal of The Royal Society Interface* 12.105, p. 20141363. ISSN: 1742-5689. DOI: 10.1098/rsif.2014.1363. URL: https://doi.org/10.1098/rsif.2014.1363.

Sato, Hirotaka et al. (Oct. 5, 2009). "Remote radio control of insect flight". In: *Frontiers in Integrative Neuroscience* 3. ISSN: 1662-5145. DOI: 10.3389/neuro.07.024.2009. URL: https://www.frontiersin.org/journals/integrative-neuroscience/articles/10.3389/neuro.07.024.2009/full.

Satterlie, Richard A (Oct. 2002). "Neuronal control of swimming in jellyfish: a comparative story". In: *Canadian Journal of Zoology* 80.10, pp. 1654–1669. ISSN: 0008-4301. DOI: 10.1139/z02-132. URL: https://cdnsciencepub.com/doi/abs/10.1139/z02-132.

Shoji, Kan et al. (Aug. 2016). "Autonomous environmental monitoring by self-powered biohybrid robot". In: *2016 IEEE International Conference on Mechatronics and Automation*. 2016 IEEE International Conference on Mechatronics and Automation. ISSN: 2152-744X, pp. 629–634. DOI: 10.1109/ICMA.2016.7558636. URL: https://ieeexplore.ieee.org/document/7558636.

Simpkins, Darin G. et al. (2003). "Physiological responses of juvenile rainbow trout to fasting and swimming activity: effects on body composition and condition indices". In: *Transactions of the American Fisheries Society* 132.3, pp. 576–589. URL: https://academic.oup.com/tafs/article-abstract/132/3/576/7891049.

Smith, Ewan St John and Gary R. Lewin (Dec. 2009). "Nociceptors: a phylogenetic view". In: *Journal of Comparative Physiology. A, Neuroethology, Sensory, Neural, and Behavioral Physiology* 195.12, pp. 1089–1106. ISSN: 1432-1351. DOI: 10.1007/s00359-009-0482-z.

Sokal, Robert and F. Rohlf (Apr. 27, 2013). *Biometry : the principles and practice of statistics in biological research / Robert R. Sokal and F. James Rohlf*. Journal Abbreviation: SERBIULA (sistema Librum 2.0) Publication Title: SERBIULA (sistema Librum 2.0).

Svendsen, M. B. S., P. G. Bushnell, and J. F. Steffensen (2016). "Design and setup of intermittent-flow respirometry system for aquatic organisms". In: *Journal of Fish Biology* 88.1. _eprint: https://onlinelibrary.wiley.com/doi/pdf/10.1111/jfb.12797, pp. 26–50. ISSN: 1095-8649. DOI: 10.1111/jfb.12797. URL: https://onlinelibrary.wiley.com/doi/abs/10.1111/jfb.12797.

Tennekes, Hendrik and John Leask Lumley (1972). *A First Course in Turbulence*. MIT Press. 320 pp. ISBN: 978-0-262-20019-6.

Thompson, D'Arcy Wentworth (1945). *On growth and form*. In collab. with MBLWHOI Library. Cambridge : University Press ; New York : Macmillan. 1140 pp. URL: http://archive.org/details/ongrowthform00thom.

Tills, O. et al. (July 1, 2016). "Reduced pH affects pulsing behaviour and body size in ephyrae of the moon jellyfish, *Aurelia aurita*". In: *Journal of Experimental Marine Biology and Ecology* 480, pp. 54–61. ISSN: 0022-0981. DOI: 10.1016/j.jembe.2016.03.014. URL: https://www.sciencedirect.com/science/article/pii/S0022098116300491.

Treberg, Jason R. et al. (Dec. 1, 2016). "Estimates of metabolic rate and major constituents of metabolic demand in fishes under field conditions: Methods, proxies, and new perspectives". In: *Comparative Biochemistry and Physiology Part A: Molecular & Integrative Physiology*. Ecophysiology methods: refining the old, validating the new and developing for the future 202, pp. 10–22. ISSN: 1095-6433. DOI: 10.1016/j.cbpa.2016.04.022. URL: https://www.sciencedirect.com/science/article/pii/S109564331630099X.

Uye, S. and H. Shimauchi (Mar. 1, 2005). "Population biomass, feeding, respiration and growth rates, and carbon budget of the scyphomedusa Aurelia aurita in the Inland Sea of Japan". In: *Journal of Plankton Research* 27.3, pp. 237–248. ISSN: 0142-7873. DOI: 10.1093/plankt/fbh172. URL: https://doi.org/10.1093/plankt/fbh172.

Ventura, Daniele et al. (Aug. 20, 2018). "Mapping and Classification of Ecologically Sensitive Marine Habitats Using Unmanned Aerial Vehicle (UAV) Imagery and Object-Based Image Analysis (OBIA)". In: *Remote Sensing* 10.9. ISSN: 2072-4292. DOI: 10.3390/rs10091331. URL: https://www.mdpi.com/2072-4292/10/9/1331.

Vogel, Steven (1994). *Life in Moving Fluids: The Physical Biology of Flow - Revised and Expanded Second Edition*. NED - New edition. Princeton University Press. ISBN: 978-0-691-03485-0. DOI: 10.2307/j.ctvzsmfc6. URL: https://www.jstor.org/stable/j.ctvzsmfc6.

Wieneke, B. (Aug. 1, 2005). "Stereo-PIV using self-calibration on particle images". In: *Experiments in Fluids* 39.2, pp. 267–280. ISSN: 1432-1114. DOI: 10.1007/s00348-005-0962-z. URL: https://doi.org/10.1007/s00348-005-0962-z.

Willert, C E and M Gharib (1991). "Digital particle image velocimetry". In: *Experiments in Fluids*.

Wölfl, Anne-Cathrin et al. (2019). *Seafloor Mapping – The Challenge of a Truly Global Ocean Bathymetry*. Volume: 6. DOI: 10.3389/fmars.2019.00283. URL: https://repository.library.noaa.gov.

Wu, T. Yao-Tsu (Mar. 1971). "Hydromechanics of swimming propulsion. Part 1. Swimming of a two-dimensional flexible plate at variable forward speeds in an inviscid fluid". In: *Journal of Fluid Mechanics* 46.2, pp. 337–355. ISSN: 1469-7645, 0022-1120. DOI: 10.1017/S0022112071000570. URL: https://www.cambridge.org/core/journals/journal-of-fluid-mechanics/article/hydromechanics-of-swimming-propulsion-part-1-swimming-of-a-twodimensional-flexible-plate-at-variable-forward-speeds-in-an-inviscid-fluid/9B79F3BC80D992328A6021BE69269AE2.

Xu, Nicole W and John O Dabiri (2024). *The creation of an augmented jellyfish: Ethical considerations from a scientific perspective,* 127-139.

Xu, Nicole W, Olga Lenczewska, Sarah Wieten, et al. (Oct. 1, 2020). *Ethics of Biohybrid Robotic Jellyfish Modification and Invertebrate Research*. DOI: 10.20944/preprints202010.0008.v1. URL: https://www.preprints.org/manuscript/202010.0008/v1.

Xu, Nicole W, Olga Lenczewska, Sarah E Wieten, et al. (May 30, 2025). "Ethics of biohybrid robotics and invertebrate research: biohybrid robotic jellyfish as a case study". In: *Bioinspiration & Biomimetics* 20.3, p. 033001. ISSN: 1748-3182, 1748-3190. DOI: 10.1088/1748-3190/adc0d4. URL: https://iopscience.iop.org/article/10.1088/1748-3190/adc0d4.

Xu, Nicole W. and John O. Dabiri (Jan. 29, 2020). "Low-power microelectronics embedded in live jellyfish enhance propulsion". In: *Science Advances* 6.5, eaaz3194. DOI: 10.1126/sciadv.aaz3194. URL: https://www.science.org/doi/10.1126/sciadv.aaz3194.

Xu, Nicole W., James P. Townsend, et al. (Nov. 21, 2020a). "Field Testing of Biohybrid Robotic Jellyfish to Demonstrate Enhanced Swimming Speeds". In: *Biomimetics* 5.4, p. 64. ISSN: 2313-7673. DOI: 10.3390/biomimetics5040064. URL: https://www.ncbi.nlm.nih.gov/pmc/articles/PMC7709697/.

Xu, Nicole W., James P. Townsend, et al. (Nov. 20, 2020b). "Field Testing of Biohybrid Robotic Jellyfish to Demonstrate Enhanced Swimming Speeds". In: *Biomimetics* 5.4. ISSN: 2313-7673. DOI: 10.3390/biomimetics5040064. URL: https://www.mdpi.com/2313-7673/5/4/64.

Yoder, Noa and John O. Dabiri (Nov. 25, 2025). "Swimming performance of robotically controlled jellyfish in three dimensional trajectories". In: 78th Annual Meeting of the Division of Fluid Dynamics. URL: https://archive.aps.org/dfd/2025/z05/5/.

Yuh, J., Giacomo Marani, and D. Richard Blidberg (Oct. 1, 2011). “Applications of marine robotic vehicles”. In: *Intelligent Service Robotics* 4.4, pp. 221–231. ISSN: 1861-2784. DOI: 10.1007/s11370-011-0096-5. URL: https://doi.org/10.1007/s11370-011-0096-5.

Zereik, Enrica et al. (Jan. 1, 2018). “Challenges and future trends in marine robotics”. In: *Annual Reviews in Control* 46, pp. 350–368. ISSN: 1367-5788. DOI: 10.1016/j.arcontrol.2018.10.002. URL: https://www.sciencedirect.com/science/article/pii/S1367578818300038.

Zhao, Qiang et al. (June 2025). “Bio-inspired swarm of underwater robots: a review”. In: *Bioinspiration & Biomimetics* 20.4, p. 041002. ISSN: 1748-3190. DOI: 10.1088/1748-3190/ade215. URL: https://doi.org/10.1088/1748-3190/ade215.

Appendix A

INCREASING THE RELIABILITY AND VERSATILITY OF JELLYFISH BIOHYBRID VEHICLES VIA SPECIES SELECTION AND RHOPALIA REMOVAL

The contents of this appendix have been adapted from Anuszczyk et al. (2025), published in the journal Biomimetics under the title "Increasing the reliability and versatility of jellyfish biohybrid vehicles via species selection and rhopalia removal". As the first author, Simon Anuszczyk made the primary contributions towards the experiment design and data acquisition. Co-author Sean Colin conducted primary analysis and drafted the manuscript. All co-authors contributed to experimental design, data acquisition, and helped edit and review the manuscript.

Abstract

Jellyfish biohybrid robots have been demonstrated to be successfully programmed to perform vertical sampling profiles of the ocean water column. However, the jellyfish's endogenous swimming behavior can interfere with the controlled swim cycles decreasing performance. Further, the model animal used to date, Aurelia aurita, is a rela-tively slow, weakly swimming species. To enhance the performance of the biohybrid vehicles we tested whether removing the swimming pacemaker of the jellyfish, the rhopalia, eliminated endogenous movements and enhanced responsiveness of the jellyfish to the swim controller. Further, we tested the responsiveness of two fast swim-ming jellyfish species, the rhizostome Cassiopea spp. and the cubomedusae Alatina alata. We found in field trials, where the jellyfish swam controlled vertical profiles in the ocean, that removal of rhopalia eliminated all endogenous behaviors and greatly im-proved the responsiveness of the jellyfish to the swim controller. This was especially true for species with strong endogenous behaviors that prevented the controller from manipulating swim pulses. Further, we found that both Cassiopea spp. and A. alata were highly responsive to the swim controller and that these faster swimming jellyfish spe-cies greatly increased the speed that the biohybrid vehicle could traverse vertical pro-files in the water column. These enhancements greatly increase the reliability and ver-satility of jellyfish biohybrid robot vehicles.

Keywords: cyborg jellyfish, robotic vehicle, ocean sampling, swimming kinematics, medusa, box jellyfish

A.1 Introduction

Ocean monitoring and observation is central to understanding our impact on climatic and biological systems. Models used to predict how oceans may impact, and are impacted by, climate and how the use of ocean resources, such as fish and minerals, affect ocean ecosystems are only as reliable as the data they are based on [1]. However, ocean observation is most often limited by access to remote habitats and the funding needed to deploy sensors [2]. Autonomous vehicles (AUVs) equipped with sensors are often seen as the best solution to ocean observation challenges. AUVs enable access to remote habitats and can be deployed for extended sampling missions [2–4]. However, they are too expensive to scale to the full ocean and the data they can collect is often limited by battery power and the habitats that they can operate in [5,6]. Biohybrid robots are robotic systems that incorporate biological components or control entire organisms to serve as autonomous vehicles. Integrating biological organisms into robotics has been seen as a solution to many of the biggest challenges in AUV robotics including power consumption, cost, and adaptability to complex habitats [7]. Within the family of biohybrid robots are those which robotically manipulate an entire animal and rely on the animal's natural propulsion to transport the vehicle. As potential low-cost options, biohybrid vehicles equipped with sensors may facilitate ocean observation by enabling researchers to deploy large numbers of vehicles throughout different habitats. And because they are made primarily from living material, they can biodegrade, limiting their impact on ecosystems [8]. There have only been a few successful attempts at biohybrid robots based on whole animal manipulation. Goldfish and lamprey have been stimulated using electrical or optogenetic stimulation, respectively, to make controlled movements of fins [9–11]. Using electrical stimulation along the lateral line, eels have been controlled to perform short bouts of forward and reverse swimming at increased swimming speeds [12]. However, fish have complex neuro-muscular systems that are difficult to control and to override the fish's natural behavior. Further, habituation to the stimulus can decrease the responsiveness of the fish. Jellyfish have also been manipulated to function as biohybrid vehicles [13–16] and Rutledge et al., In review). Having much simpler neuro-muscular systems, jellyfish can be electronically stimulated to swim for long durations at enhanced swimming speeds without damaging the jellyfish [15,16]. Jellyfish also require the lowest level of electrical power per unit mass to control their swimming [13]. However, similar to biohybrid fish, the natural swimming behavior of jellyfish interferes with the stimulated bell contractions which can reduce control and performance of the biohybrid jellyfish [13]. The scyphozoan

jellyfish Aurelia aurita is the only jellyfish species that has been used as biohybrid robot platform. A. aurita and other scyphozoans use rowing propulsion to swim and their propulsion has been shown to be the most efficient mode of swimming among all animals [17–19]. A. aurita, and other scyphozoans, swim by rhythmically contracting and relaxing their mesoglea bells to generate large vortex rings in their wake. The bell contractions are initiated by rhopalial pacemakers that are distributed around the bell margin of the jellyfish [20]. Jellyfish typically have about 8 rhopalia but some species can have 16 or more. To initiate a contraction, a rhopalium sends an electrical impulse that is conducted to the other pacemakers through the nerve-net. This suppresses the other rhopalia and stimulates the jellyfish muscles to contract the bell [20]. During contraction, collagen fibers in the mesoglea are stretched. After contraction, the muscles relax and, due to relaxation of the elastic strain stored in mesogleal collogen fibers, the bell recoils to its resting size and shape. The high swimming efficiency and relatively simple neuro-muscular system that controls swimming make scyphozoan jellyfish ideal animal models for biohybrid vehicles [13]. However, compared to other scyphozoan species, A. aurita is a slow, weak swimmer making it a less than optimal animal model for applications that require faster moving biohybrid robots. The basic circuitry of the scyphozoan neural system allows jellyfish to be stimulated to swim by activating an electrode that has been inserted into their sub-umbrellar surface. A 5mV electrical impulse is sufficient to initiate bell contraction, however, unlike the natural signals from the rhopalia, the external electrical impulse does not suppress the rhopalia from also initiating pulses [13]. The endogenous bell contractions initiated by the rhopalia interfere with externally stimulated bell contractions and can affect swimming performance. In addition, scyphozoan jellyfish swim nearly continuously which can prevent the biohybrid robot from stopping or maneuvering on command. These endogenous behaviors have been cited as some of the major challenges with jellyfish biohybrid robots. In fact, endogenous animal behaviors have been cited as one of the main obstacles to whole-animal biohybrid robots [7]. The goal of this study was to advance jellyfish biohybrid vehicle design by enhancing the control and speed of biohybrid vehicle. While other studies have improved the engineering to increase the reliability and versatility of jellyfish biohybrid robots – e.g, improving the swim controller, the connection to the jellyfish and the ballasting of the controller payload – no other studies to date have tried to leverage jellyfish biology to enhance the performance of these robot systems. In this study, we evaluated how leveraging two biological traits – the natural rhopalia pacemakers and the natural swimming performance of different

species – can improve the reliability and versatility of jellyfish biohybrid robots. Using biological traits to improve biohybrid robots takes advantage of the evolution of these animals that has already optimized animal performance. To enhance the control of swimming, we tested whether removing the rhopalial pacemakers around the bell margin eliminated endogenous bell contractions of the jellyfish. To enhance the speed of biohybrid vehicles we tested the ability to control the swimming of two different fast swimming jellyfish species. First, we tested another scyphozoan jellyfish, Cassiopea spp. (Fig. 1 c and d). Cassiopea is a rhizostome which are typically stronger, faster swimmers than semaeostomes like A. aurita (Fig. 1 a and b). We also tested a cubomedusae, Alatina alata, which uses jet-propulsion to swim instead of the rowing propulsion described above that is used by scyphozoan jellyfish (Fig. 1 e and f). Specifically, we compared the responsiveness and swimming speed of Cassiopea spp. and A. alata to A. aurita by using a swim controller to stimulate them to swim for 6 meter vertical transects in natural ocean waters. For Cassiopea spp. and A. aurita we also conducted experiments comparing the responsiveness of animals with intact rhopalia to animals whose rhopalia were all removed to determine if the jellyfish will be equally responsive to the swim controller if we remove the endogenous swimming of the jellyfish.

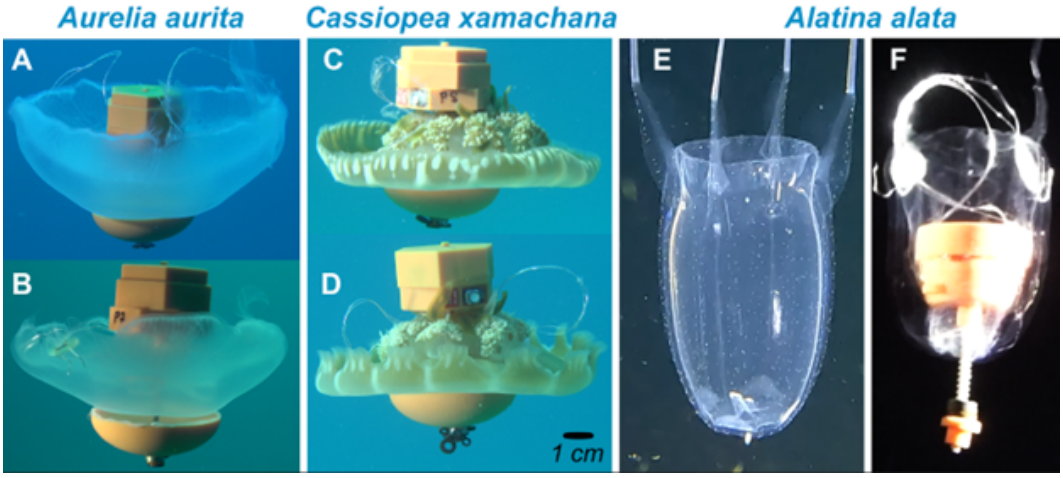

Figure A.1: Fig. 1. Jellyfish species used for biohybrid robots swimming in the natural water column. A) Non-excised and B) excised Aurelia aurita. C) Non-excised and D) excised Cassiopea xamachana. E) Cubomedusa Alatina alata without swim controller. F) A. alata with swim controller.

A.2 Materials and Methods

Animals and care

In situ experiments were done with the scyphozoan jellyfish Cassiopea xamachana and Aurelia aurita offshore from Long Key, FL and with the cubomedusa Alatina alata offshore from Kona, HI. C. xamachana individuals were collected by hand from the waters adjacent to the Keys Marine Laboratory (KML) Long Key, FL, USA and A. aurita individuals were supplied by the Cabrillo Aquarium and Aquarium of the Pacific and shipped to the KML. Medusae were kept in large (>100L) tanks supplied with filtered seawater at ambient temperature (same temperature as the dive site) and fed natural plankton. All experiments were conducted within three days of animals being collected or arriving to the lab.

Biohybrid robotic system

We modified the robotic system described in Anuszczyk and Dabiri (2024) for our field experiments. The swim controller comprised a mini processor (TinyLily, TinyCircuits, Akron, OH, USA) and 10 mAh lithium polymer cell (GM201212, PowerStream Technology Inc., Orem, UT, USA) in plastic housing made entirely from polypropylene pieces sealed with hot melt adhesives. The housing was ballasted with stainless steel washers to keep the system neutrally buoyant in seawater. Two electrodes were assembled using perfluoroalkoxy-coated silver wires and platinum rod tips (A-M Systems, Sequim, WA, USA) connected in series to red light-emitting diodes (LEDs); (TinyLily 0402, TinyCircuits, Akron, OH, USA) as a visualization tool to identify when impulses were sent to the jellyfish (Supplementary Fig. 1). Platinum wire tips were hooked to improve attachment to the subumbrellar surface of the jellyfish. The robotic system was attached to the jellyfish bell in three locations: a plastic threaded pin connected to the housing was inserted into the center of the manubrium from the subumbrellar surface, and 2 electrodes were inserted into the subumbrellar tissue. The other end of the plastic threaded pin was attached to a plastic forebody similar to Anuszczyk and Dabiri (2024).

Field experiments

To examine the effects of jellyfish species type on the responsiveness and swimming speeds of biohybrid robots we conducted field experiments where the different robot treatments swam from the surface down to 6 m depth. Five different treatments were compared (C. xamachana with and without rhopalia, A. aurita with and without rhopalia, A. alata with rhopalia) with 2 replicate individuals of each treatment. For

the experiments, the swim controllers were programmed to start sending impulses at 0.5 Hz at the surface and to stop sending impulses at 6 m depth. All the robot treatments were neutrally buoyant. SCUBA divers videoed descending jellyfish at 30 fps using SONY camcorders (SONY AX700) in Gates underwater housings. The red LED signals on the swim controller were visible in the video recordings and indicated when electrical impulses were sent. Rhopalia were excised using surgical scissors by cutting small v-shaped grooves into the bell margin that removed the rhopalia (Supplementary Fig. 1). The jellyfish were unharmed by the procedure and were able to be maintained in good condition, in fact, rhopalia are known to be able to be regenerated by scyphozoan and cubozoan jellyfish within 2-weeks. All the experiments were conducted within 2 days of the rhopalial excision to ensure the pacemakers had not regenerated.

Laboratory experiments

In the laboratory, we performed additional tests to evaluate the relationship between stimulation frequency and jellyfish pulse frequency. These experiments were conducted in Kona, HI with A. alata and Cassiopea andromeda. C. andromeda were supplied by the Waikiki Aquarium. For these experiments individual jellyfish were placed into tanks with the swim controller connected to their bells. They were video recorded using a GoPro camera at 30 fps (Supplementary Fig. 2). The swim controller was set to different frequencies ranging from 0.5 Hz to 2.5 Hz.

Data and statistical analysis

Videos of descending biohybrid jellyfish were analyzed to quantify the correspondence between electrical impulses and bell contractions. The timing of electrical impulses were identified by the flashing of the red LED attached to the inserted electrode. The bell contractions were quantified by measuring the bell diameter and height and calculating the fineness ratio (height/diameter). The videos were scaled by measuring the diameter of the swim controller which was known to be 4 cm diameter. This enabled us to ensure diameter did not change due to a change in the distance the animal was from the camera. Minimum and maximum bell contraction correspond to minimum and maximum fineness ratios, respectively. Both field and laboratory videos were analyzed by hand to determine the pulse frequencies of the jellyfish. Pulse frequencies were measured manually where contractions were noted to start at the first frame when the bell diameter began to decrease. From this analysis we calculated the time delay between the impulse and the onset of bell

contraction, the contraction frequency and the impulse frequency (which was set to 0.5 Hz). Descent speed was measured by changes in pressure over time quantified by pressure sensors in the swim control unit. To quantify an average descent speed, the depth of the jellyfish was plotted versus time and the slope of that line was used to estimate an average descent rate.

A.3 Results

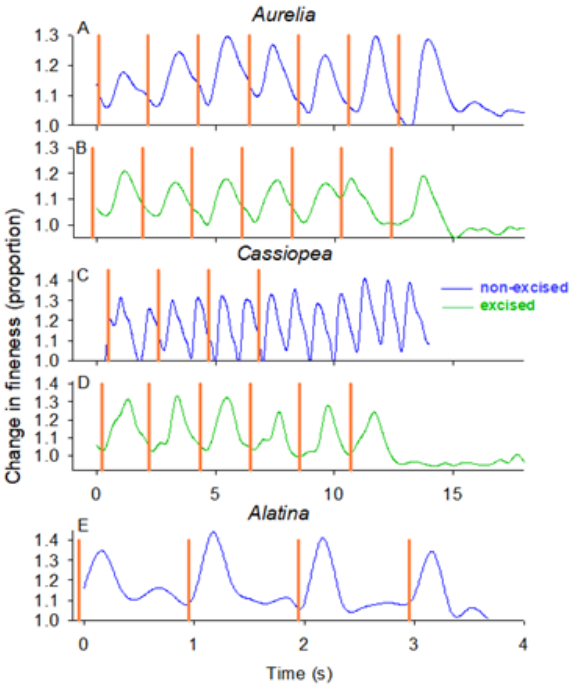

Figure A.2: Fig. 2. Timing of bell contractions versus stimulation signals from the swim controller for individual jelly-fish. The fineness ratio (or aspect ratio) illustrates when the jellyfish bells are in their completely re-laxed, expanded state (minimum fineness ratio) or in their contracted state (maximum fineness ratio). A swim cycle begins when the jellyfish in the relaxed state initiates muscle contractions that cause the bell to contract thus increasing the fineness ratio. The orange vertical lines indicate the timing of the stimulation from the swim controller.

Control of bell contraction for excised versus non-excised

In the field, we evaluated the ability of the swim controller unit to control bell contractions by comparing the timing of bell contractions of Cassiopea xamachana and Aurelia aurita, with and without rhopalia, to the timing of the electrical impulses from the control unit. Fig. 2 visualizes the timing of the stimulation impulse (orange lines) and the timing of the bell contractions (changes in fineness ratio where peak fineness occurs at peak contraction and minimum fineness at bell relaxation). The

controller reliably initiated bell contractions for both non-excised and excised A. aurita (Fig. 2 a and b; Fig. S3) where the pulsation frequency was the same as the stimulation frequency (Fig. 3a and b). In contrast, the bell contractions of the non-excised C. xamachana (with rhopalia pacemakers), did not correspond with the impulse signals from the controller (Fig. 2c). In fact, the non-excised C. xamachana swam with a contraction frequency that was twice the frequency of the electrical impulses (Fig. 3c) and after the electrical impulses stopped, the medusae continued pulsing at that same inherent frequency. In contrast, the excised C. xamachana contracted their bells synchronously with the electrical impulse at a frequency equal to the electrical impulse at 0.47 Hz (Fig. 2d, 3b and S4; *t*-test, $P > 0.05$). Further, as soon as the electrical impulse stopped the medusae stopped contracting their bells. Of note, the excised bells of the two species reacted to the stimulus at different speeds where C. xamachana initiated bell contractions in less than half the time of A. aurita, contracting 0.16 s after the stimulus vs 0.41s for A. aurita (Fig. 3e).

Control of cubomedusa Alatina alata

We were able to collect 2 individuals of Alatina alata, an oceanic epipelagic cubomedusae, and evaluate if this class of medusae responds to the stimulus as well as scyphozoan medusae. We found that the controller also reliably initiated bell contractions for excised A. alata (Fig. 2E and S5) with the bell contracting at the same frequency as the stimulus (*t*-test, $P > 0.05$). In fact, the bell contractions of A. alata were initiated just as quickly as C. xamachana after the stimulus, contracting 0.17 s after the stimulus.

Comparison of descent rates

The speed that the medusae descended in the water column was directly related to contraction rate (Fig. 4a and b, Regression analysis, $P < 0.0002$). Medusan species did not seem to strongly vary descent rate with both C. xamachana and A. alata descending at the same rate when pulsing at the same frequency. However, C. xamachana did swim significantly faster than A. aurita when pulsing at 0.5 Hz (*t*-test, $P < 0.05$). A doubling of the contraction rate (0.5 vs. 1 Hz) almost doubled the descent speed of the medusae (3.7 vs. 6.5 cm s-1).

Contraction frequency limits

In the laboratory, we stimulated C. andromeda and A. alata at different rates to determine how rapidly each species could potentially contract their bells. We found

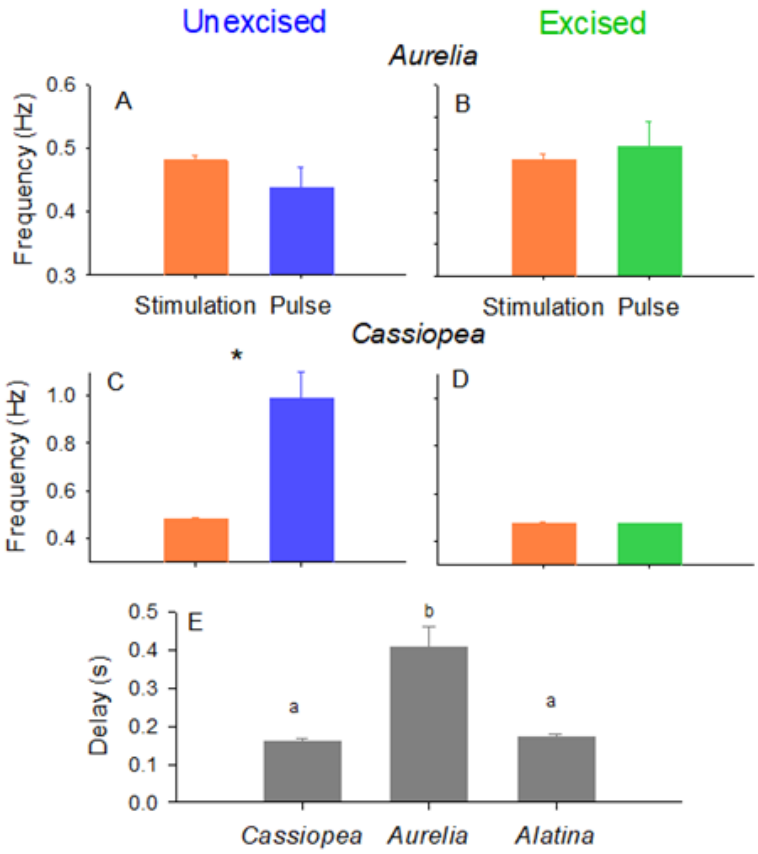

Figure A.3: Fig. 3. Comparison of stimulation frequency to jellyfish pulse frequency and delay. When the swim control-ler was able to manipulate pulses, the stimulation and pulse frequencies were the same. Asterisk indicates when the stimulation and the pulse frequencies were significantly different (*t*-test, $p < 0.05$). E) Time delay between when the jellyfish received the stimulation and the bell began to contract to start a swim cycle. Species with the same letters were not significantly different from each other while species with different delay times were indicated with different letter (Student-Newman-Keuls Pair-wise comparison, $P < 0.05$).

a very tight correlation between stimulus and contraction frequencies for excised C. andromeda (Fig. 5) and non-excised A. alata (Fig. 5). There was no correspondence for non-excised C. andromeda (Fig. 5). A. alata pulsed at rates as high as 2.5 Hz. However, C. andromeda was not able to contract its bell at rates greater than 1.67 Hz (Fig. 5).

A.4 Discussion

Laboratory and field studies with the moon jellyfish, Aurelia aurita, demonstrate that scyphozoan swimming can be externally controlled using simple electrical impulses due to their relatively simple neuromuscular systems [13,15,16] Rutledge et al., In

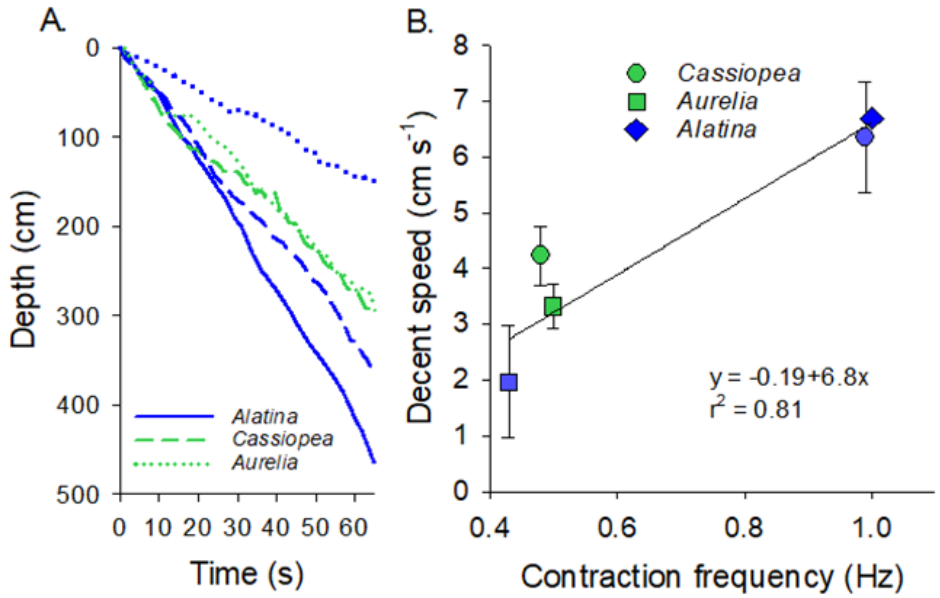

Figure A.4: Fig. 4. Swimming speeds of the different species. A) Depth versus time for the different species. For Cassiopea spp. and Aurelia aurita we had profiles for animals with their rhopalia intact (unexcised, blue) and with their rhopalia removed (excised, green). B) Relationship between jellyfish bell contraction frequency and the speed that the jellyfish descended.

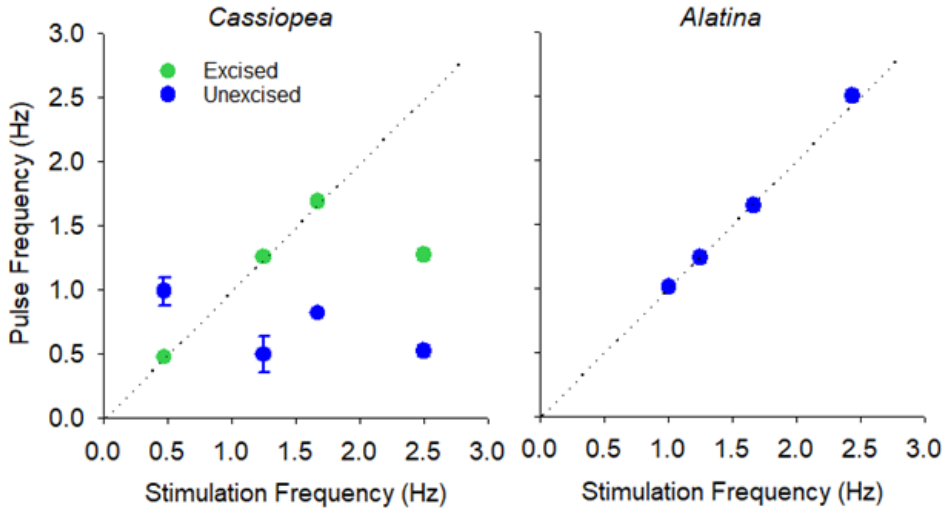

Figure A.5: Fig. 5. Relationship between stimulation frequency and jellyfish bell pulse frequency. Dotted line shows where the 1:1 relationship falls on the plot.

review). This feature makes jellyfish a promising platform for biohybrid robots capable of large-scale ocean sampling. However, A. aurita exhibits inherently low pulsation frequencies and slow swimming speeds, constraining applications such

as deep vertical profiling. Moreover, inter-individual variability in responsiveness reduces reliability – some individuals fail to initiate swimming under stimulation, while others exhibit natural contractions that interfere with induced pulses [13]. These limitations restrict the operational versatility of jellyfish biohybrid robots. To enhance the versatility of jellyfish biohybrid robots, we evaluated the ability of the swim controller to regulate swimming in multiple jellyfish species. Swimming in two distantly related medusae—the rhizostome Cassiopea spp. and the cubomedusa Alatina alata—was successfully controlled. Both taxa are stronger swimmers than Aurelia aurita, enabling faster vertical profiling. However, in Cassiopea, endogenous bell pulsations interfered with controller-driven pulses. Removal of the rhopalia, which initiate and coordinate natural contractions, eliminated this interference and rendered Cassiopea consistently responsive to the swim controller. In contrast, both A. aurita and A. alata remained responsive even with intact rhopalia. Thus, controller responsiveness is species- and potentially individual-specific, introducing uncertainty in performance. Nevertheless, rhopalia removal eliminates natural endogenous pulsations while preserving responsiveness, markedly improving control and reliability. Furthermore, the capacity to employ species with distinct swimming behaviors and physiological traits broadens the operational versatility of jellyfish biohybrid robots. Jellyfish swimming is governed by rhopalia, pacemaker structures that generate electrical impulses to initiate bell contractions [20]. Typically, eight or more rhopalia are distributed around the bell margin; when one fires, it suppresses the others, ensuring a single pacemaker controls each pulse [20–22]. In contrast, impulses from the swim controller do not inhibit rhopalial activity, allowing natural signals to interfere with controller-driven pulses. This can disrupt swimming kinematics or, as observed in Cassiopea spp., render the controller ineffective. Cassiopea exhibits a higher intrinsic pulse frequency than Aurelia aurita and exceeded the stimulation frequency of the controller. Previous studies have shown that in some medusae the fastest pacemaker dominates swimming activity [20–22]. Consequently, with intact rhopalia, Cassiopea's endogenous pacemakers overrode the controller. Rhopalia removal eliminated pacemaker activity and endogenous contractions, leaving the swim controller as the sole driver of bell pulsations. Under these conditions, contractions occurred reliably, independent of the jellyfish's natural pacemaker frequency. Demonstrating that different jellyfish taxa are responsive to the swim controller increases the versatility of jellyfish biohybrid robots. The pacemaker system that controls swimming is similar among all scyphozoan jellyfish such as A. aurita and Cassiopea spp. Likewise, cubomedusae, or box-jellyfish, also

share a very similar pacemaker system [20]. Therefore, we expect that most, if not all, scyphozoan and cubozoan jellyfish will respond well to removal of their rhopalia and to the swim controller. However, the neuromuscular organization of hydromedusae is fundamentally different [20]. The pacemakers in hydromedusae are not localized to rhopalia, rather, they are integrated directly into a marginal nerve ring the encircles the bell [23,24]. In fact, the entire bell margin of hydromedusae needs to be removed to stop their swim pulsations [20]. Additionally, hydromedusae are much smaller than most scyphomedusae and cubomedusae, limiting the size of the payload that they can transport and their utility as biohybrid robots. Nevertheless, the taxonomic diversity of scyphozoans and cubozoans provides substantial opportunities for tailoring jellyfish biohybrid robots to distinct applications. Medusan species exhibit considerable variation in size, swimming behavior, and physiology. Across the taxa examined, pulsation rate emerged as the primary determinant of swimming speed. For instance, Cassiopea and A. alata achieved similar speeds when pulsing at equivalent frequencies, consistent with their classification as fast-swimming rhizostomes and cubomedusae. Doubling Cassiopea's pulsation rate nearly doubled its swimming speed; however, even at identical frequencies, A. aurita swam significantly slower (t-test, $P < 0.05$). Further, not all species are capable of pulsing at high pulsation rates. We found that while A. alata was capable of pulsing reliably at 2.5 Hz, Cassiopea was not able to pulse faster than 1.7 Hz. This is due to the fact that bell relaxation is a passive process controlled by the elastic properties and shape of the medusan bell rather than muscles. Therefore, the time it takes the bell to relax will limit the fastest pulse frequency. Cubomedusae like A. alata are jet propelled – rather than rowing propelled like the scyphomedusae – and jetting jellyfish are generally capable of faster bell kinematics. These species-specific biomechanical traits may be influential variables when selecting jellyfish for biohybrid robotic applications. Additional species-specific traits, such as body size and swimming efficiency, may further expand the utility of jellyfish biohybrid robots. A. aurita has been reported as the most efficient swimmer among both aquatic and terrestrial animals [25], and although all scyphozoans exhibit high efficiency via rowing propulsion, A. aurita is nearly twice as efficient as the rhizostome Stomolophus meleagris. Whether this efficiency translates to swim-controller–driven propulsion remains unknown, and future work is needed to quantify battery consumption relative to swimming efficiency. Size also varies substantially among medusae: while the species tested here were <20 cm in diameter, the rhizostome Rhizostoma pulmo can exceed 100 cm. Increased bell size directly increases potential payload capacity, including the swim

controller and additional sensors. Substantial additional research will be necessary to fully evaluate the potential versatility of diverse jellyfish as biohybrid robots.

A.5 Conclusions

Our findings show that multiple different types of jellyfish can be developed as biohybrid robots and that reliability can be improved when endogenous pulses are eliminated by the removal of rhopalia. But performance depends on species-specific traits such as swimming mechanics, efficiency, and body size. These factors influence reliability, speed, and payload capacity, making species choice critical for optimizing function. Together, these findings highlight the importance of species selection in optimizing jellyfish biohybrid robots for distinct oceanographic applications, while also underscoring the need for further investigation into efficiency, control reliability, and scalability.

Supplementary Materials

The following supporting information can be downloaded at: https://www.mdpi.com/article/doi/s1, Fig. S1, S2 and S3. Author Contributions: Conceptualization, S.A., N.Y., J.C., J.D., B.G., K.R., S.C.; methodology, S.A., N.Y., J.C., J.D., B.G., K.R., S.C.; software, S.A., J.D. ; formal analysis, S.C.; investigation, S.A., N.Y., J.C., J.D., B.G., K.R., S.C.; data curation, S.C.; writing—original draft preparation, S.C.; writing—review and editing, S.A., N.Y., J.C., J.D., B.G., K.R., S.C.; visualization, S.C.; project administration, J.D.; funding acquisition, J.D., J.C., S.C., B.G. All authors have read and agreed to the published version of the manuscript.

Funding

This research was funded by the Office of Naval Research (ONR MURI Award #N00014-23-1-2754 awarded to J.C.) and the National Science Foundation (NSF-OCE 2529199 to S.C., NSF-OCE 2529198 to J.D., NSF-OCE 2529201 to B.G., NSF-OCE 2529200 to J.C, NSF DGE-2146755 to S.A., and NSF DGE-2146755 to N.Y.).

Data Availability Statement

Data from this project can be downloaded from
https://submit.bco-dmo.org/project/r0LV5WK8wqzu1wQ7.

Acknowledgments

The authors would like to thank the Cabrillo Aquarium and Aquarium of the Pacific for supplying jellyfish for this study.

Conflicts of Interest

The authors declare no conflicts of interest.

BIBLIOGRAPHY

1. Räisänen, J. How Reliable Are Climate Models? *Tellus, Series A: Dynamic Meteorology and Oceanography* **2007**, 59, 2–29.

2. Breier, J.A.; Jakuba, M.V.; Saito, M.A.; Dick, G.J.; Grim, S.L.; Chan, E.W.; McIlvin, M.R.; Moran, D.M.; Alanis, B.A.; Allen, A.E.; et al. Revealing Ocean-Scale Biochemical Structure with a Deep-Diving Vertical Profiling Autonomous Vehicle. *Science Robotics* **2020**, 5, eabc7104, doi:10.1126/scirobotics.abc7104.

3. Dodd, P.A.; Price, M.R.; Heywood, K.J.; Pebody, M. Collection of Water Samples from an Autonomous Underwater Vehicle for Tracer Analysis; **2006**.

4. Das, J.; Py, F.; Maughan, T.; O'Reilly, T.; Messié, M.; Ryan, J.; Sukhatme, G.S.; Rajan, K. Coordinated Sampling of Dynamic Oceanographic Features with Underwater Vehicles and Drifters. In *Proceedings of the International Journal of Robotics Research*; April **2012**; Vol. 31, pp. 626–646.

5. Bradley, A.M.; Feezor, M.D.; Singh, H.; Yates Sorrell, F. Power Systems for Autonomous Underwater Vehicles; **2001**; Vol. 26.

6. Fan, S.; Bose, N.; Liang, Z. Polar AUV Challenges and Applications: A Review. *Drones* **2024**, 8.

7. Webster-Wood, V.A.; Guix, M.; Xu, N.W.; Behkam, B.; Sato, H.; Sarkar, D.; Sanchez, S.; Shimizu, M.; Parker, K.K. Biohybrid Robots: Recent Progress, Challenges, and Perspectives. *Bioinspiration & Biomimetics* **2023**, 18, doi:10.1088/1748-3190/ac9c3b.

8. Xu, N.W.; Lenczewska, O.; Wieten, S.E.; Federico, C.A.; Dabiri, J.O. Ethics of Biohybrid Robotics and Invertebrate Research: Biohybrid Robotic Jellyfish as a Case Study. *Bioinspiration & Biomimetics* **2025**, 20, doi:10.1088/1748-3190/adc0d4.

9. Sirota, M.G.; Viana, G.; Prisco, D.; Dubuc, R.Â. Stimulation of the Mesencephalic Locomotor Region Elicits Controlled Swimming in Semi-Intact Lampreys. *European Journal of Neuroscience* **2000**, 12, 4081–4092.

10. Kobayashi, N.; Yoshida, M.; Matsumoto, N.; Uematsu, K. Artificial Control of Swimming in Goldfish by Brain Stimulation: Confirmation of the Midbrain Nuclei as the Swimming Center. *Neuroscience Letters* **2009**, 452, 42–46, doi:10.1016/j.neulet.2009.01.035.

11. Fetcho, J.R.; Svoboda, K.R. Fictive Swimming Elicited by Electrical Stimulation of the Midbrain in Goldfish. *Journal of Neurophysiology* **1993**, 70.

12. Yu, L.; Lai, J.; Huang, J.; Liu, H.; Pi, X. Wireless Motion Control of a Swimming Eel-Machine Hybrid Robot. *Bioinspiration & Biomimetics* **2025**, 20, doi:10.1088/1748-3190/adbeac.

13. Xu, N.W.; Dabiri, J.O. Low-Power Microelectronics Embedded in Live Jellyfish Enhance Propulsion. *Science Advances* **2020**, 6, 1–11, doi:10.1126/sciadv.aaz3194.

14. Xu, N.W.; Townsend, J.P.; Costello, J.H.; Colin, S.P.; Gemmell, B.J.; Dabiri, J.O. Developing Biohybrid Robotic Jellyfish (*Aurelia aurita*) for Free-Swimming Tests in the Laboratory and in the Field. *Bio-Protocol* **2021**, 11, doi:10.21769/BioProtoc.3974.

15. Xu, N.W.; Townsend, J.P.; Costello, J.H.; Colin, S.P.; Gemmell, B.J.; Dabiri, J.O. Field Testing of Biohybrid Robotic Jellyfish to Demonstrate Enhanced Swimming Speeds. *Biomimetics* **2020**, 5, 1–17, doi:10.3390/biomimetics5040064.

16. Anuszczyk, S.R.; Dabiri, J.O. Electromechanical Enhancement of Live Jellyfish for Ocean Exploration. *Bioinspiration & Biomimetics* **2024**, 19, doi:10.1088/1748-3190/ad277f.

17. Colin, S.P.; Costello, J.H. Morphology, Swimming Performance and Propulsive Mode of Six Co-Occurring Hydromedusae. *Journal of Experimental Biology* **2002**, 205, 427–437.

18. Gemmell, B.J.; Costello, J.H.; Colin, S.P.; Stewart, C.J.; Dabiri, J.O.; Tafti, D.; Priya, S. Passive Energy Recapture in Jellyfish Contributes to Propulsive Advantage over Other Metazoans. *Proceedings of the National Academy of Sciences USA* **2013**, 110, 17904–17909, doi:10.1073/pnas.1306983110.

19. Costello, J.H.; Colin, S.P.; Dabiri, J.O.; Gemmell, B.J.; Lucas, K.N.; Sutherland, K.R. The Hydrodynamics of Jellyfish Swimming. *Annual Review of Marine Science* **2021**, 13, 375–396, doi:10.1146/annurev-marine-031120-091442.

20. Satterlie, R.A. Neuronal Control of Swimming in Jellyfish: A Comparative Story. *Canadian Journal of Zoology* **2002**, 80, 1654–1669, doi:10.1139/Z02-132.

21. Pantin, C.F.A.; Dias, M.V. Rhythm and Afterdischarge in Medusae. Serviço Gráfico do Instituto Brasileiro de Geografia e Estatistica, **1952**.

22. Horridge, G.A. The Nerves and Muscles of Medusae VI. The Rhythm. *Journal of Experimental Biology* **1959**, 36, 72–91.

23. Anderson, P.A.V.; Mackie, G.O. Electrically Coupled, Photosensitive Neurons Control Swimming in a Jellyfish; **1977**; Vol. 197.

24. Romanes, G.J. *Jellyfish, Starfish and Sea Urchins, Being a Research on Primitive Nervous Systems*; D. Appleton, New York, **1885**.

25. Gemmell, B.J.; Colin, S.P.; Costello, J.H. Widespread Utilization of Passive Energy Recapture in Swimming Medusae. *Journal of Experimental Biology* **2018**, 1–5, doi:10.1242/jeb.168575.

Appendix B

SUPPLEMENTARY MATERIAL FOR CHAPTER 4

We define a bow wave energy ratio equivalent to 4.11 for the bow wave

$$E_{\text{bow ratio, pulse}} = \frac{\int_{t_a}^{t_b} \left(\int_{V_{\text{wake}}} E_{\text{bow wave}}(x, y, z, t)\, dV \right) dt}{\int_{t_a}^{t_b} E_{\text{jelly}}(t)\, dt} \tag{B.1}$$

where $E_{\text{bow wave}}(x, y, z, t)$ is defined over a region of the same size as that in 4.4A but extending into the bow wave as shown in B.1A. We also define an analogue for $E_{\text{bow ratio, time}}$. These measurements are shown in B.1B-C. While the bow wave contains significant energy, the time-energy trace changes little over the course of each pulse and does not contain coherent flow structures such as those observed in the trailing wake.

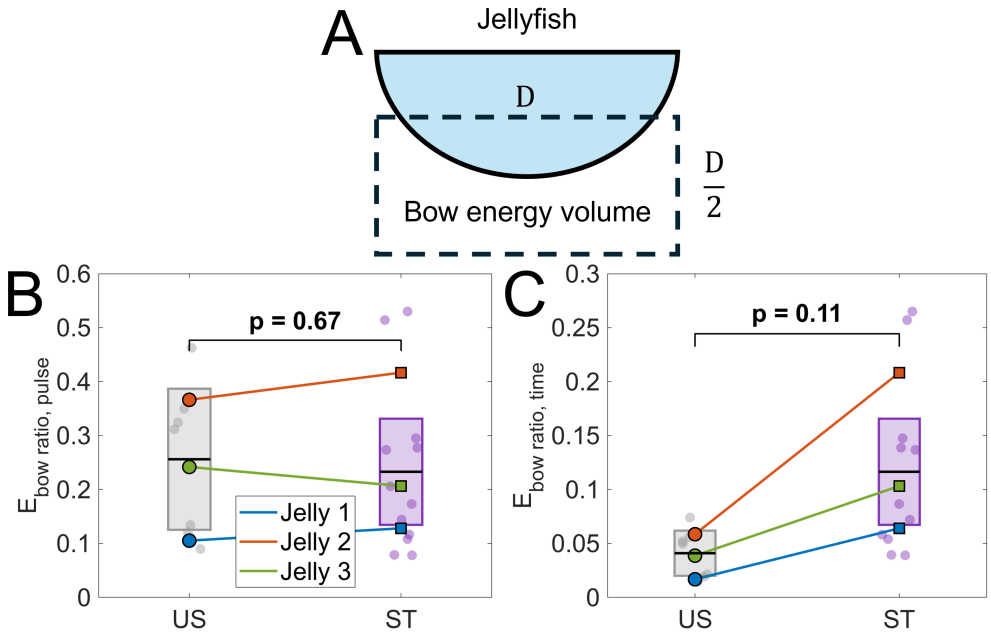

Figure B.1: Normalized bow wave energy. (A) A bow-wave control volume defined ahead of the swimming jellyfish within which kinetic energy was analyzed. Instantaneous measurements of kinetic energy inside this volume served as a proxy for energy transferred into the bow-wave region of the wake by the swimming animal. The dimensions of the volume were defined as a width of one bell diameter D and a height of $\frac{D}{2}$. (B) Pulse-specific normalized energy $E_{\text{bow ratio, pulse}}$ given by eq. B.1. Blue, red, and green points represent animal means for each condition and shaded boxes denote the 95% confidence interval of the pooled pulse mean for each condition. Gray and purple points represent individual pulses. Statistical comparisons were performed on trial-level means using paired t-tests, pairing unstimulated (US) and stimulated (ST) trials from the same animals. No statistically significant difference in energy released per pulse was observed between conditions ($p = 0.67$). (C) Time-specific normalized energy $E_{\text{bow ratio, time}}$. Points and shaded boxes are as in panel B. While stimulated jellyfish animal-level means increased, the increase in time-normalized bow-wave energy was not statistically significant ($p = 0.11$).